

CHEMICAL VAPOR DEPOSITION OF BORON CARBIDE

A THESIS SUBMITTED TO
THE GRADUATE SCHOOL OF NATURAL AND APPLIED SCIENCES
OF
THE MIDDLE EAST TECHNICAL UNIVERSITY

BY

MUSTAFA KARAMAN

IN PARTIAL FULFILLMENT OF THE REQUIREMENTS
FOR THE DEGREE OF DOCTOR OF PHILOSOPHY
IN
CHEMICAL ENGINEERING

SEPTEMBER 2007

Approval of the thesis:

“CHEMICAL VAPOR DEPOSITION OF BORON CARBIDE ”

submitted by **MUSTAFA KARAMAN** in partial fulfillment of the requirements for the degree of **Doctor of Philosophy** in **Chemical Engineering Department, Middle East Technical University** by,

Prof. Dr. Canan Özgen
Dean, Graduate School of **Natural and Applied Sciences**

Prof. Dr. Nurcan Baç
Head of Department, **Chemical Engineering**

Prof. Dr. Hilmi Önder Özbelge
Supervisor, **Chemical Engineering, METU**

Assoc. Prof. Dr. Naime Aslı Sezgi
Co-Supervisor, **Chemical Engineering, METU**

Examining Committee Members:

Prof. Dr. Timur Doğu
METU, ChE

Prof. Dr. H. Önder Özbelge
METU, ChE

Prof. Dr. Naci Sevinç
METU, METE

Assoc. Prof. Dr. Burhanettin Çiçek
Ankara Üniv., ChE

Assoc. Prof. Dr. Ahmet Gülce
Selçuk Üniv., ChE

Date: 07.09.2007

I hereby declare that all information in this document has been obtained and presented in accordance with academic rules and ethical conduct. I also declare that, as required by these rules and conduct, I have fully cited and referenced all material and results that are not original to this work.

Name, Last name : Mustafa Karaman

Signature : _____

ABSTRACT

CHEMICAL VAPOR DEPOSITION OF BORON CARBIDE

Karaman, Mustafa

Ph.D., Department of Chemical Engineering

Supervisor: Prof. Dr. H. Önder Özbelge

Co-Supervisor: Assoc. Prof. Dr. N. Aslı Sezgi

September 2007, 164 pages

Boron carbide was produced on tungsten substrate in a dual impinging-jet CVD reactor from a gas mixture of BCl_3 , CH_4 , and H_2 . The experimental set-up was designed to minimise the effect of mass transfer on reaction kinetics, which, together with the on-line analysis of the reactor effluent by FTIR, allowed a detailed kinetic investigation possible.

The phase and morphology studies of the products were made by XPS, XRD, micro hardness and SEM methods. XPS analysis showed the existence of chemical states attributed to the boron carbide phase, together with the existence of oxy-boron carbide species. SEM pictures revealed the formation of 5-fold icosahedral boron carbide crystals up to 30 micron sizes for the samples produced at 1300°C . Microhardness tests showed change of boron carbide hardness with the temperature of tungsten substrate. The hardness

values (Vickers Hardness) observed were between 3850 kg/mm² and 4750 kg/mm² corresponding to substrate temperatures of 1100 and 1300°C, respectively.

The FTIR analysis of the reaction products proved the formation of reaction intermediate BHC₂, which is proposed to occur mainly in the gaseous boundary layer next to the substrate surface. The experimental parameters are the temperature of the substrate, and the molar fractions of methane and borontrichloride at the reactor inlet. The effects of those parameters on the reaction rates, conversions and selectivities were analysed and such analyses were used in mechanism determination studies. An Arrhenius type of a rate expression was obtained for rate of formation of boron carbide with an energy of activation 56.1 kJoule/mol and the exponents of methane and boron trichloride in the reaction rate expression were 0.64 and 0.34, respectively, implying complexity of reaction. In all of the experiments conducted, the rate of formation of boron carbide was less than that of dichloroborane.

Among a large number of reaction mechanisms proposed only the ones considering the molecular adsorption of boron trichloride on the substrate surface and formation of dichloroborane in the gaseous phase gave reasonable fits to the experimental data. Multiple non-linear regression analysis was carried out to predict the deposition rate of boron carbide as well as formation rate of dichloroborane simultaneously.

Keywords: CVD, Reaction Mechanism, Kinetics, Reaction Engineering, Adsorption, Chemical Reactors

ÖZ

KİMYASAL BUHAR BİRİKTİRME YÖNTEMİ İLE BOR KARBÜR ÜRETİMİ

Karaman, Mustafa

Doktora, Kimya Mühendisliği Bölümü

Tez Yöneticisi: Prof. Dr. H. Önder Özbelge

Ortak Tez Yöneticisi: Doç. Dr. N. Aslı Sezgi

Eylül 2007, 164 sayfa

Bu çalışmada, bor karbür BCl_3 , CH_4 , ve H_2 , gaz karışımı kullanılarak tungsten folyo yüzeyinde kimyasal buhar biriktirme yöntemi ile üretilmiştir. Bu süreçteki kütle transferi adımının önemi kullanılan çift taraflı çarpan-jet reaktör konfigürasyonu ile en aza indirilmiş ve reaktör çıkışına bağlanan FTIR spektrofotometresi detaylı kinetik araştırmayı mümkün kılmıştır.

Üretilen malzemelerin faz ve morfoloji çalışmaları XPS, XRD, mikro sertlik ve SEM metodları ile yapılmıştır. XPS analizi ile bor karbür fazına ait olan kimyasal verilerin yanı sıra, oksijen-bor karbürlerin varlığı da ispatlanmıştır. SEM analizi neticesinde boyutları 30 mikrometreye varan beşgen tabanlı piramit şeklindeki bor karbür kristallerinin varlığı gözlemlenmiştir. Mikrosertlik analizi sonucunda tungsten folyo sıcaklığının bor karbür sertliğini

önemli ölçüde etkilediği gözlemlenmiştir. Ölçülen bor karbür Vickers sertlik değerleri 1100 ve 1300 °C tungsten folyo sıcaklık aralığında 3850 kg/mm² ve 4750 kg/mm² arasında değişiklik göstermiştir.

Reaksiyon ürünlerinin FTIR analizi sonucunda yüzeyde bor karbürü oluşturan reaksiyona ek olarak, gaz fazındaki bir başka reaksiyon sonucunda diklorobor (BHCl₂)'un oluştuğu kanıtlanmıştır. Deneysel parametreler folyo sıcaklığı ile reaktör girişindeki metan ve bor triklorürün mol oranları olup, bu parametrelerin iki ana reaksiyonun hızlarına, dönüşümlerine ve seçiciliklerine etkileri irdelenmiş ve bunlar mekanizma önerme çalışmalarında kullanılmıştır. Bütün deneysel veriler, Arrhenius tipi bir hız denklemine uyarlanmıştır. Doğrusal dışı eğri uyarlama prosedürü uygulanarak, bor karbür oluşum reaksiyonunun aktivasyon enerjisi 56,1 kJoule/mol olarak bulunmuştur. Bor karbür oluşum hızı, reaktör girişindeki bor triklorürün mol oranının 0,34, metanın mol oranının 0,64'üncü kuvvetleri ile orantılıdır. Bu sonuçlar karmaşık bir reaksiyon mekanizması olduğunu işaret etmektedir. Yapılan bütün deneylerde bor karbür oluşum hızının diklorobor oluşum hızından düşük olduğu açığa çıkmıştır.

Bir çok reaksiyon mekanizması modellenmiş ve bu modellerin deneyler sonucunda gözlenen hız verilerine uyumluluğu istatistiksel olarak denenmiştir. Bu modeller arasında bor triklorürün taban (subtrat) yüzeyine ayrışmasız olarak tutunduğu durumlar en iyi sonucu vermiştir. Önerilen mekanizmada diklorobor gazının sadece gaz fazındaki reaksiyon ile oluştuğu varsayılmıştır. Diğer taraftan, bor karbür kompleks bir yüzey mekanizma serisi sonucu oluşmaktadır.

Anahtar Kelimeler: CVD, Reaksiyon Mekanizması, Kinetik, Reaksiyon Mühendisliği, Adsorpsiyon, Kimyasal Reaktörler

To My Family

ACKNOWLEDGEMENTS

I would like to express my deepest appreciation to my supervisor Prof. Dr. Hilmi Önder Özbelge. His enthusiasm, inspiration, and encouragement helped me in all stages of my thesis research. His guidance will continue to be my source of inspiration for my future career.

I would like to thank to my co-supervisor Assoc. Prof. Dr. N. Aslı Sezgi for her invaluable help and guidance for almost all of the stages of this study.

I am also very greatfull to my thesis commitee members, Prof. Timur Doğu and Prof. Naci Sevinç for their insightfull comments and suggestions on this research.

I wish to thank The Scientific and Technological Research Council of Turkey (TUBITAK) (project no: MISAG-217) and State Planning Organization of Turkey (project no: BAP-08-11-DPT2002K120510-IM-5) for their financial supports of this project.

I greatly appreciate the help of Mr. Fatih Fırat for the preparation of the experimental set-up, and Mr. Engin Özkol, for his help in computer programming.

I would also want to thank the staff of the Chemical Engineering Department of METU for their support.

Finally, I would like to express my deepest gratitude to my family for their support and encouragement throughout my whole life.

TABLE OF CONTENTS

| | |
|--|------|
| ABSTRACT | iv |
| ÖZ..... | vi |
| DEDICATION..... | viii |
| ACKNOWLEDGEMENTS | ix |
| TABLE OF CONTENTS | x |
| LIST OF TABLES | xiii |
| LIST OF FIGURES | xv |
| LIST OF SYMBOLS | xxii |
| CHAPTER | |
| 1. INTRODUCTION | 1 |
| 1.1. Literature Survey on CVD of Boron Carbide | 9 |
| 1.2. Objective of the Present Work..... | 12 |
| 2. EXPERIMENTAL | 13 |
| 2.1 Experimental Set-up..... | 16 |
| 2.2 Experimental Procedure | 18 |
| 3. RESULTS AND DISCUSSIONS..... | 21 |
| 3.1. Spectrophotometric Analysis of the Reactor Effluent..... | 21 |
| 3.2. Analysis of the Reactions Occuring in the Deposition Process..... | 24 |
| 3.2.1. Reaction Rate Calculations | 27 |
| 3.2.2. Conversion Calculations:..... | 30 |
| 3.2.3. Selectivity Calculations: | 31 |
| 3.3. Analysis of the Effects of Various Experimental Parameters on the Reaction Kinetics..... | 31 |

| | |
|---|-----|
| 3.3.1. Effects of Experimental Parameters on Selectivities..... | 38 |
| 3.3.2. Effects of Experimental Parameters on Boron Carbide Yield..... | 42 |
| 3.4. Mechanism Studies on CVD of Boron Carbide from BCl ₃ , CH ₄ and H ₂ Gas Mixture in a Dual Impinging Jet Reactor | 46 |
| 3.5. Morphological Investigations of the Deposits | 111 |
| 3.5.1. X-Ray Photoelectron Spectroscopy Results | 111 |
| 3.5.2. X-Ray Diffraction Results | 115 |
| 3.5.3. Scanning Electron Microscopy (SEM) Results..... | 117 |
| 3.5.4 Effect of Deposition Temperature on the Hardness of Boron Carbide ... | 118 |
| 4. CONCLUSIONS AND RECOMMENDATIONS..... | 123 |
| REFERENCES | 126 |
| APPENDIX | |
| A. FTIR CALIBRATION METHODS | 129 |
| A.1 Calibration of Methane | 129 |
| A.2 Calibration of Boron Trichloride..... | 131 |
| A.3 Calibration of Hydrogen Chloride..... | 133 |
| B. X-RAY DIFFRACTION DATA | 135 |
| C. DERIVATIONS OF RATE LAWS FROM PROPOSED MECHANISMS..... | 139 |
| D. RAW DATA | 142 |
| E. HEAT AND MASS TRANSFER CALCULATIONS AROUND THE TUNGSTEN FILAMENT..... | 160 |
| E.1 Calculation of Heat Dissipated From the Substrate Surface | 160 |
| E.2 Temperature profile around the filament | 164 |
| E.3 Comparison of Diffusion Effects Over the Substrate Surface Between the Impinging Jet and Parallel Flow Conditions | 168 |
| F. REPRODUCIBILITY CALCULATIONS..... | 170 |

| | |
|---|-----|
| G. COMPARISON BETWEEN EQUILIBRIUM AND THE EXPERIMENTALLY OBSERVED CONVERSIONS..... | 172 |
| CIRRICULUM VITAE..... | 176 |

LIST OF TABLES

| | |
|---|-----|
| Table 1.1 Physical Properties of Boron Carbide [1]..... | 2 |
| Table 1.2 Boron Carbide Fiber Properties in Comparison with Some Other Refractory Materials [1]..... | 3 |
| Table 2.1 Experimental Conditions in the Applied Runs | 20 |
| Table 3.1 Characteristic wavenumber ranges for the FTIR peaks for the reaction constituents | 24 |
| Table 3.2 Stoichiometric Table | 26 |
| Table 3.3. Some of the probable surface reactions considered for CVD of boron carbide | 48 |
| Table 3.4 Model Parameters and Correlation Coefficients..... | 107 |
| Table 3.4 Model Parameters and Correlation Coefficients (cont'd)..... | 108 |
| Table 3.4 Model Parameters and Correlation Coefficients (cont'd)..... | 109 |
| Table 3.4 Model Parameters and Correlation Coefficients (cont'd)..... | 110 |
| Table 3.5. Effect of temperature on Vickers Hardness of Boron Carbide..... | 122 |
| Table B.1 XRD Data for Boron Carbide[17] | 135 |
| Table B.2 XRD Data for Boron [17] | 135 |
| Table B.3 XRD Data for α -Tungstan Carbide [17] | 136 |
| Table B.4 XRD Data for Tungstan Carbide [17]..... | 136 |
| Table B.5 XRD Data for Tungstan [17]..... | 136 |
| Table B.6 XRD Data for α -Tungstan Carbide [17] | 136 |
| Table B.7 XRD Data for Carbon (Diamond) [17]..... | 137 |
| Table B.8 XRD Data for Carbon (Graphite) [17]..... | 137 |
| Table B.9 XRD Data for Silicon Oxide [17]..... | 137 |
| Table B.10 XRD Data for Silicon Carbide [17]..... | 138 |
| Table B.11 XRD Data for α -Silicon Carbide [17]..... | 138 |
| Table D.1 Raw Data for the Experiment BCL3B..... | 143 |
| Table D.2 Raw Data for the Experiment BCL3D..... | 144 |

| | |
|---|-----|
| Table D.3 Raw Data for Experiment BCl3F | 145 |
| Table D.4 Raw Data for Experiment BCl3C..... | 146 |
| Table D.5 Raw Data for Experiment BCl3G | 147 |
| Table D.6 Raw Data for Experiment BCl3E..... | 148 |
| Table D.7 Raw Data for Experiment CH4D | 149 |
| Table D.8 Raw Data for Experiment CH4B..... | 150 |
| Table D.9 Raw Data for the Experiment CH4E | 151 |
| Table D.10 Raw Data for the Experiment CH4F | 152 |
| Table D.11 Raw Data for the Experiment CH4A..... | 153 |
| Table D.12 Raw Data for the Experiment TEA | 154 |
| Table D.13 Raw Data for the Experiment TEB | 155 |
| Table D.14 Raw Data for the Experiment TEC | 156 |
| Table D.15 Raw Data for the Experiment TED | 157 |
| Table D.16 Raw Data for the Experiment TEE..... | 158 |
| Table D.17 Raw Data for the Experiment TEF..... | 159 |
| Table F.1 Experimental Conditions for the Reproducibility Experiments | 171 |
| Table G.1 Thermodynamic Properties of Reactants and Products..... | 173 |

LIST OF FIGURES

| | |
|--|----|
| Figure 1.1 The rhombohedral crystal structure of boron carbides. Atoms are placed at the vertices of the icosahedra and within the three-atom intericosahedral chain | 4 |
| Figure 1.2 Schematic drawing of the chemical vapor deposition (CVD) process | 6 |
| Figure 1.3 Various fundamental steps involved in a chemical vapor deposition process | 8 |
| Figure 2.1 Dual Impinging-Jet Chemical Vapor Deposition Reactor | 14 |
| Figure 2.2 Experimental Set-Up | 15 |
| Figure 3.1 Typical FTIR Spectrum of the Reactor Effluent Before Heating the Substrate | 22 |
| Figure 3.2 Typical FTIR Spectrum of the Reactor Effluent After Heating the Substrate | 23 |
| Figure 3.3 Change of mole fractions of reaction constituents with time ($T=1150^{\circ}\text{C}$, $y_{\text{BCl}_3_0}=0.089$, $y_{\text{CH}_4_0}=0.02$, $y_{\text{BCl}_3_0}/y_{\text{CH}_4_0}=4.45$, $y_{\text{H}_2_0}=0.891$) | 28 |
| Figure 3.4 Comparison of the calculated B_4C deposit weight (w) with the actual B_4C deposit weight (w^*) | 30 |
| Figure 3.5 Effect of initial BCl_3 mole fraction on the B_4C and BHCl_2 formation rates with the standard deviations indicated by the error bars ($y_{\text{CH}_4_0}=0.02$ in hydrogen, $y_{\text{BCl}_3_0}/y_{\text{CH}_4_0}=1.5-5.5$, $T=1150^{\circ}\text{C}$) | 33 |
| Figure 3.6 Effect of substrate temperature on B_4C and BHCl_2 formation rates with the standard deviations indicated by the error bars ($y_{\text{BCl}_3_0}=0.081$, $y_{\text{CH}_4_0}=0.02$, in hydrogen) | 34 |
| Figure 3.7 Effect of initial CH_4 mole fraction on B_4C and BHCl_2 formation rates with the standard deviations indicated by the error bars ($T=1150^{\circ}\text{C}$, $y_{\text{BCl}_3_0}=0.084$ in hydrogen) $y_{\text{BCl}_3_0}/y_{\text{CH}_4_0}=2-4.5$) | 36 |

| | |
|---|----|
| Figure 3.8 Effect of initial BCl_3 ($y_{\text{CH}_4}=0.02$, in hydrogen, $T=1150^\circ\text{C}$) (a) and CH_4 ($y_{\text{BCl}_3}=0.084$, in hydrogen, $T=1150^\circ\text{C}$) (b) mole fractions and temperature ($y_{\text{BCl}_3}=0.081$, $y_{\text{CH}_4}=0.02$, in hydrogen) (c) on B_4C formation rate with the standard deviations indicated by the error bars and model predictions indicated by the dashed lines | 37 |
| Figure 3.9 Effect of initial BCl_3 mole fraction on B_4C and BHCl_2 selectivities ($y_{\text{CH}_4}=0.02$ in hydrogen, $y_{\text{BCl}_3}/y_{\text{CH}_4}=1.5-5.5$, $T=1150^\circ\text{C}$)..... | 39 |
| Figure 3.10 Effect of initial CH_4 mole fraction on B_4C and BHCl_2 selectivities ($T=1150^\circ\text{C}$, $y_{\text{BCl}_3} = 0.084$ in hydrogen) | 40 |
| Figure 3.11 Effect of temperature on B_4C and BHCl_2 selectivities ($y_{\text{BCl}_3}=0.081$, $y_{\text{CH}_4}=0.02$, in hydrogen)..... | 41 |
| Figure 3.12 Effect of initial BCl_3 mole fraction on B_4C yield ($y_{\text{CH}_4}=0.02$ in hydrogen, $y_{\text{BCl}_3}/y_{\text{CH}_4}=1.5-5.5$, $T=1150^\circ\text{C}$)..... | 43 |
| Figure 3.13 Effect of initial CH_4 mole fraction on B_4C yield ($T=1150^\circ\text{C}$, $y_{\text{BCl}_3} = 0.084$ in hydrogen)..... | 44 |
| Figure 3.14 Effect of temperature on B_4C yield ($y_{\text{BCl}_3}=0.081$, $y_{\text{CH}_4}=0.02$, in hydrogen) | 45 |
| Figure 3.15 Comparison of the effect of BCl_3 inlet mole fractions on the observed and Model 1 predicted formation rates of B_4C ($T=1150^\circ\text{C}$, $y_{\text{CH}_4}=0.02$ in hydrogen, $y_{\text{BCl}_3}/y_{\text{CH}_4}= 1.5- 5.5$, simultaneous analysis)..... | 54 |
| Figure 3.16 Comparison of the effect of CH_4 inlet mole fractions on the observed and Model 1 predicted formation rates of B_4C ($T=1150^\circ\text{C}$, $y_{\text{BCl}_3}=0.084$ in hydrogen, $y_{\text{BCl}_3}/y_{\text{CH}_4}=2-4.5$, simultaneous analysis)..... | 55 |
| Figure 3.17 Comparison of the effect of BCl_3 inlet mole fractions on the observed and Model 1 predicted formation rates of BHCl_2 ($T=1150^\circ\text{C}$, $y_{\text{CH}_4}=0.02$ in hydrogen, $y_{\text{BCl}_3}/y_{\text{CH}_4}= 1.5- 5.5$, simultaneous analysis) | 56 |
| Figure 3.18 Comparison of the effect of CH_4 inlet mole fractions on the observed and Model 1 predicted formation rates of BHCl_2 ($T=1150^\circ\text{C}$, $y_{\text{BCl}_3}=0.084$ in hydrogen, $y_{\text{BCl}_3}/y_{\text{CH}_4}=2-4.5$, simultaneous analysis)..... | 57 |

| | |
|---|----|
| Figure 3.19 Comparison of the effect of BCl_3 inlet mole fractions on the observed and Model 2 predicted formation rates of B_4C ($T=1150^\circ\text{C}$, $y_{\text{CH}_4}=0.02$ in hydrogen, $y_{\text{BCl}_3}/y_{\text{CH}_4}=1.5-5.5$, simultaneous analysis)..... | 59 |
| Figure 3.20 Comparison of the effect of CH_4 inlet mole fractions on the observed and Model 2 predicted formation rates of B_4C ($T=1150^\circ\text{C}$, $y_{\text{BCl}_3}=0.084$ in hydrogen, $y_{\text{BCl}_3}/y_{\text{CH}_4}=2-4.5$, simultaneous analysis)..... | 60 |
| Figure 3.21 Comparison of the effect of BCl_3 inlet mole fractions on the observed and Model 2 predicted formation rates of BHCl_2 ($T=1150^\circ\text{C}$, $y_{\text{CH}_4}=0.02$ in hydrogen, $y_{\text{BCl}_3}/y_{\text{CH}_4}=1.5-5.5$, simultaneous analysis) | 61 |
| Figure 3.22 Comparison of the effect of CH_4 inlet mole fractions on the observed and Model 2 predicted formation rates of BHCl_2 ($T=1150^\circ\text{C}$, $y_{\text{BCl}_3}=0.084$ in hydrogen, $y_{\text{BCl}_3}/y_{\text{CH}_4}=2-4.5$, simultaneous analysis)..... | 62 |
| Figure 3.23 Comparison of the effect of BCl_3 inlet mole fractions on the observed and Model 3 predicted formation rates of B_4C ($T=1150^\circ\text{C}$, $y_{\text{CH}_4}=0.02$ in hydrogen, $y_{\text{BCl}_3}/y_{\text{CH}_4}=1.5-5.5$, simultaneous analysis)..... | 64 |
| Figure 3.24 Comparison of the effect of CH_4 inlet mole fractions on the observed and Model 3 predicted formation rates of B_4C ($T=1150^\circ\text{C}$, $y_{\text{BCl}_3}=0.084$ in hydrogen, $y_{\text{BCl}_3}/y_{\text{CH}_4}=2-4.5$, simultaneous analysis)..... | 65 |
| Figure 3.25 Comparison of the effect of BCl_3 inlet mole fractions on the observed and Model 3 predicted formation rates of BHCl_2 ($T=1150^\circ\text{C}$, $y_{\text{CH}_4}=0.02$ in hydrogen, $y_{\text{BCl}_3}/y_{\text{CH}_4}=1.5-5.5$, simultaneous analysis) | 66 |
| Figure 3.26 Comparison of the effect of CH_4 inlet mole fractions on the observed and Model 3 predicted formation rates of BHCl_2 ($T=1150^\circ\text{C}$, $y_{\text{BCl}_3}=0.084$ in hydrogen, $y_{\text{BCl}_3}/y_{\text{CH}_4}=2-4.5$, simultaneous analysis)..... | 67 |
| Figure 3.27 Comparison of the effect of BCl_3 inlet mole fractions on the observed and Model 4 predicted formation rates of B_4C ($T=1150^\circ\text{C}$, $y_{\text{CH}_4}=0.02$ in hydrogen, $y_{\text{BCl}_3}/y_{\text{CH}_4}=1.5-5.5$, simultaneous analysis)..... | 70 |
| Figure 3.28 Comparison of the effect of CH_4 inlet mole fractions on the observed and Model 4 predicted formation rates of B_4C ($T=1150^\circ\text{C}$, $y_{\text{BCl}_3}=0.084$ in hydrogen, $y_{\text{BCl}_3}/y_{\text{CH}_4}=2-4.5$, simultaneous analysis)..... | 71 |

| | |
|---|----|
| Figure 3.29 Comparison of the effect of BCl_3 inlet mole fractions on the observed and Model 4 predicted formation rates of BHCl_2 ($T=1150^\circ\text{C}$, $y_{\text{CH}_4}=0.02$ in hydrogen, $y_{\text{BCl}_3}/y_{\text{CH}_4}=1.5-5.5$, simultaneous analysis) | 72 |
| Figure 3.30 Comparison of the effect of CH_4 inlet mole fractions on the observed and Model 4 predicted formation rates of BHCl_2 ($T=1150^\circ\text{C}$, $y_{\text{BCl}_3}=0.084$ in hydrogen, $y_{\text{BCl}_3}/y_{\text{CH}_4}=2-4.5$, simultaneous analysis)..... | 73 |
| Figure 3.31 Comparison of the effect of BCl_3 inlet mole fractions on the observed and Model 5 predicted formation rates of B_4C ($T=1150^\circ\text{C}$, $y_{\text{CH}_4}=0.02$ in hydrogen, $y_{\text{BCl}_3}/y_{\text{CH}_4}=1.5-5.5$, simultaneous analysis)..... | 76 |
| Figure 3.32 Comparison of the effect of CH_4 inlet mole fractions on the observed and Model 5 predicted formation rates of B_4C ($T=1150^\circ\text{C}$, $y_{\text{BCl}_3}=0.084$ in hydrogen, $y_{\text{BCl}_3}/y_{\text{CH}_4}=2-4.5$, simultaneous analysis)..... | 77 |
| Figure 3.33 Comparison of the effect of BCl_3 inlet mole fractions on the observed and Model 5 predicted formation rates of BHCl_2 ($T=1150^\circ\text{C}$, $y_{\text{CH}_4}=0.02$ in hydrogen, $y_{\text{BCl}_3}/y_{\text{CH}_4}=1.5-5.5$, simultaneous analysis) | 78 |
| Figure 3.34 Comparison of the effect of CH_4 inlet mole fractions on the observed and Model 5 predicted formation rates of BHCl_2 ($T=1150^\circ\text{C}$, $y_{\text{BCl}_3}=0.084$ in hydrogen, $y_{\text{BCl}_3}/y_{\text{CH}_4}=2-4.5$, simultaneous analysis)..... | 79 |
| Figure 3.35 Comparison of the effect of BCl_3 inlet mole fractions on the observed and Model 6 predicted formation rates of B_4C ($T=1150^\circ\text{C}$, $y_{\text{CH}_4}=0.02$ in hydrogen, $y_{\text{BCl}_3}/y_{\text{CH}_4}=1.5-5.5$, simultaneous analysis)..... | 81 |
| Figure 3.36 Comparison of the effect of CH_4 inlet mole fractions on the observed and Model 6 predicted formation rates of B_4C ($T=1150^\circ\text{C}$, $y_{\text{BCl}_3}=0.084$ in hydrogen, $y_{\text{BCl}_3}/y_{\text{CH}_4}=2-4.5$, simultaneous analysis)..... | 82 |
| Figure 3.37 Comparison of the effect of BCl_3 inlet mole fractions on the observed and Model 6 predicted formation rates of BHCl_2 ($T=1150^\circ\text{C}$, $y_{\text{CH}_4}=0.02$ in hydrogen, $y_{\text{BCl}_3}/y_{\text{CH}_4}=1.5-5.5$, simultaneous analysis) | 83 |
| Figure 3.38 Comparison of the effect of CH_4 inlet mole fractions on the observed and Model 6 predicted formation rates of BHCl_2 ($T=1150^\circ\text{C}$, $y_{\text{BCl}_3}=0.084$ in hydrogen, $y_{\text{BCl}_3}/y_{\text{CH}_4}=2-4.5$, simultaneous analysis)..... | 84 |

| | |
|---|----|
| Figure 3.39 Comparison of the effect of BCl_3 inlet mole fractions on the observed and Model 7 predicted formation rates of B_4C ($T=1150^\circ\text{C}$, $y_{\text{CH}_4}=0.02$ in hydrogen, $y_{\text{BCl}_3}/y_{\text{CH}_4}=1.5-5.5$, simultaneous analysis)..... | 86 |
| Figure 3.40 Comparison of the effect of CH_4 inlet mole fractions on the observed and Model 7 predicted formation rates of B_4C ($T=1150^\circ\text{C}$, $y_{\text{BCl}_3}=0.084$ in hydrogen, $y_{\text{BCl}_3}/y_{\text{CH}_4}=2-4.5$, simultaneous analysis)..... | 87 |
| Figure 3.41 Comparison of the effect of BCl_3 inlet mole fractions on the observed and Model 7 predicted formation rates of BHCl_2 ($T=1150^\circ\text{C}$, $y_{\text{CH}_4}=0.02$ in hydrogen, $y_{\text{BCl}_3}/y_{\text{CH}_4}=1.5-5.5$, simultaneous analysis) | 88 |
| Figure 3.42 Comparison of the effect of CH_4 inlet mole fractions on the observed and Model 7 predicted formation rates of BHCl_2 ($T=1150^\circ\text{C}$, $y_{\text{BCl}_3}=0.084$ in hydrogen, $y_{\text{BCl}_3}/y_{\text{CH}_4}=2-4.5$, simultaneous analysis)..... | 89 |
| Figure 3.43 Comparison of the effect of BCl_3 inlet mole fractions on the observed and Model 8 predicted formation rates of B_4C ($T=1150^\circ\text{C}$, $y_{\text{CH}_4}=0.02$ in hydrogen, $y_{\text{BCl}_3}/y_{\text{CH}_4}=1.5-5.5$, simultaneous analysis)..... | 92 |
| Figure 3.44 Comparison of the effect of CH_4 inlet mole fractions on the observed and Model 8 predicted formation rates of B_4C ($T=1150^\circ\text{C}$, $y_{\text{BCl}_3}=0.084$ in hydrogen, $y_{\text{BCl}_3}/y_{\text{CH}_4}=2-4.5$, simultaneous analysis)..... | 93 |
| Figure 3.45 Comparison of the effect of BCl_3 inlet mole fractions on the observed and Model 8 predicted formation rates of BHCl_2 ($T=1150^\circ\text{C}$, $y_{\text{CH}_4}=0.02$ in hydrogen, $y_{\text{BCl}_3}/y_{\text{CH}_4}=1.5-5.5$, simultaneous analysis) | 94 |
| Figure 3.46 Comparison of the effect of CH_4 inlet mole fractions on the observed and Model 8 predicted formation rates of BHCl_2 ($T=1150^\circ\text{C}$, $y_{\text{BCl}_3}=0.084$ in hydrogen, $y_{\text{BCl}_3}/y_{\text{CH}_4}=2-4.5$, simultaneous analysis)..... | 95 |
| Figure 3.47 Comparison of the effect of BCl_3 inlet mole fractions on the observed and Model 9 predicted formation rates of B_4C ($T=1150^\circ\text{C}$, $y_{\text{CH}_4}=0.02$ in hydrogen, $y_{\text{BCl}_3}/y_{\text{CH}_4}=1.5-5.5$, simultaneous analysis)..... | 97 |
| Figure 3.48 Comparison of the effect of CH_4 inlet mole fractions on the observed and Model 9 predicted formation rates of B_4C ($T=1150^\circ\text{C}$, $y_{\text{BCl}_3}=0.084$ in hydrogen, $y_{\text{BCl}_3}/y_{\text{CH}_4}=2-4.5$, simultaneous analysis)..... | 98 |

| | |
|---|-----|
| Figure 3.49 Comparison of the effect of BCl_3 inlet mole fractions on the observed and Model 9 predicted formation rates of BHCl_2 ($T=1150^\circ\text{C}$, $y_{\text{CH}_4}=0.02$ in hydrogen, $y_{\text{BCl}_3}/y_{\text{CH}_4}=1.5-5.5$, simultaneous analysis) | 99 |
| Figure 3.50 Comparison of the effect of CH_4 inlet mole fractions on the observed and Model 9 predicted formation rates of BHCl_2 ($T=1150^\circ\text{C}$, $y_{\text{BCl}_3}=0.084$ in hydrogen, $y_{\text{BCl}_3}/y_{\text{CH}_4}=2-4.5$, simultaneous analysis)..... | 100 |
| Figure 3.51 Comparison of the effect of BCl_3 inlet mole fractions on the observed and Model 10 predicted formation rates of B_4C ($T=1150^\circ\text{C}$, $y_{\text{CH}_4}=0.02$ in hydrogen, $y_{\text{BCl}_3}/y_{\text{CH}_4}=1.5-5.5$, simultaneous analysis) | 102 |
| Figure 3.52 Comparison of the effect of CH_4 inlet mole fractions on the observed and Model 10 predicted formation rates of B_4C ($T=1150^\circ\text{C}$, $y_{\text{BCl}_3}=0.084$ in hydrogen, $y_{\text{BCl}_3}/y_{\text{CH}_4}=2-4.5$, simultaneous analysis)..... | 103 |
| Figure 3.53 Comparison of the effect of BCl_3 inlet mole fractions on the observed and Model 10 predicted formation rates of BHCl_2 ($T=1150^\circ\text{C}$, $y_{\text{CH}_4}=0.02$ in hydrogen, $y_{\text{BCl}_3}/y_{\text{CH}_4}=1.5-5.5$, simultaneous analysis) | 104 |
| Figure 3.54 Comparison of the effect of CH_4 inlet mole fractions on the observed and Model 10 predicted formation rates of BHCl_2 ($T=1150^\circ\text{C}$, $y_{\text{BCl}_3}=0.084$ in hydrogen, $y_{\text{BCl}_3}/y_{\text{CH}_4}=2-4.5$, simultaneous analysis)..... | 105 |
| Figure 3.55 Comparison of reaction rates predicted by reaction mechanism model 10 and Arrhenius equation with the experimental data | 111 |
| Figure 3.56 XPS survey scan for boron carbide produced at 1150°C with initial boron trichloride to methane molar ratio of 4.0 in hydrogen..... | 113 |
| Figure 3.57 XPS spectra of the produced solid phase before (circles) and after (dots) the sputtering process and spectrum deconvolutions (deconvoluted components (dashed lines), fitted results (solid lines)) ($T=1150^\circ\text{C}$, $y_{\text{BCl}_3}/y_{\text{CH}_4}=4.0$ in hydrogen) | 114 |
| Figure 3.58 X-ray diffraction patterns of the samples produced at different substrate temperatures under atmospheric conditions with initial boron trichloride to methane molar ratio of 4.0 and with a temperature of; a) 1300°C , b) 1200°C , c) 1100°C | 116 |

| | |
|---|-----|
| Figure 3.59 SEM images of the samples produced at different temperatures (P=1 atm., $y_{\text{CH}_4}/y_{\text{BCl}_3}=0.25$ in hydrogen at reactor inlet) a) 1100°C; b) 1200°C; c) 1300°C | 119 |
| Figure 3.60 Vickers Hardness Test..... | 121 |
| Figure A-1 FTIR Calibration Curve for Methane (Wavenumber: 3183 cm^{-1})..... | 130 |
| Figure A-2 FTIR Calibration Curve for Boron Trichloride (Wavenumber: $1040\text{-}920\text{ cm}^{-1}$) | 132 |
| Figure A-3 FTIR Calibration Curve for Hydrochloric Acid (Wavenumber: 2789 cm^{-1})..... | 134 |
| Figure E.1 Schematic representation of jet impingement on the flat surface | 161 |
| Figure E.2 Temperature profile in the vicinity of the heated substrate surface at 1150 °C (x: distance along the surface;z: distance from the surface)..... | 168 |
| Figure G.1 Temperature dependence of chemical equilibrium constants for boron carbide and dichloroborane formation reactions | 175 |

LIST OF SYMBOLS

| | |
|-------|--|
| A | Substrate surface area |
| A_c | Crosssectional area of the nozzle |
| c_p | Specific heat (kJ/kg-K) |
| d | Distance between the crystallographic planes |
| D | The edge length of indentation in mm |
| D_h | Hydraulic diameter of the nozzle |
| E_a | Activation energy (kjoule/mol) |
| F | Force applied in kilograms-force |
| F_i | Molar flow rate of species i to the reactor (mol/min) |
| f_i | Fraction of adsorption sites occupied by species i |
| h | Convection heat transfer coefficient |
| H | FTIR Peak Height |
| H | Distance between nozzle and the substrate surface in the reactor (m) |
| HV | Vickers number |
| k | Thermal conductivity (W/m-K) |
| k_i | Rate constant of reaction i |
| K_i | Adsorption equilibrium constant of reaction i |
| k_o | Frequency factor |
| K_p | Chemical equilibrium constant |
| M_i | Molecular weight of species i (grams/mol) |
| N | Number |
| Nu | Nusselt number |
| P_i | Partial pressure of species i |
| Pr | Prandtl number |
| q'' | Heat flux |

| | |
|------------|---|
| q | Heat transfer rate |
| R | Reaction rate (g-mole/min) |
| R | Correlation Coefficient |
| Re | Reynolds number |
| s | Adsorption site |
| S | Sample standard deviation |
| S_i | Selectivity of the of species i |
| t | Time (min) |
| t | Student's t |
| T_m | Mean temperature |
| V_i | Velocity in the i direction |
| V_T | Volumetric flow rate (cm^3/min) |
| w | Weight (grams) |
| x | Conversion |
| \bar{X} | Sample mean |
| y_i | Mole fraction of a species i |
| z_k | The core length |
| α | Thermal diffusivity (m^2/s) |
| δ | Boundary layer thickness |
| ΔH | Heat of formation (J/mole) |
| Θ | Bragg angle (Half the Diffraction Angle) |
| μ | Viscosity (Ns/m^2) |
| ω | confidence interval |
| ρ | Density (kg/m^3) |
| v | Degrees of freedom |
| ν | Kinematic viscosity (m^2/s) |

CHAPTER 1

INTRODUCTION

Boron carbide is an important non-metallic material with useful physical and chemical properties. After the cubic boron nitride, it is the hardest boron containing compound. Its high melting point, high modulus of elasticity, large neutron capture section, low density, chemical inertness, outstanding thermal and electrical properties make boron carbide a strong candidate for high technology applications. In comparison with other refractory materials, such as diamond, silicon carbide, boron nitride, alumina, relatively little effort has been put into studying and developing boron carbide deposition methods. This has started to change in recent years due to the need of high quality boron carbide based materials especially in microelectronics, nuclear military, space and medical industries [1].

The physical properties of boron carbide are given in Table 1.1. The fiber properties of boron carbide in comparison with some other refractory materials are given in Table 1.2. As can be seen in Table 1.2, boron carbide is the third hardest material at room temperature suppressed only by diamond and cubic boron nitride. However, the

hardness of diamond and cubic boron nitride gradually decreases at high temperatures.

Boron carbide is characterized by its high thermal stability. In fact, above 1100°C, it keeps its hardness [2]. B₄C is the most stable compound in the B-C system.

Table 1.1 Physical Properties of Boron Carbide [1]

| | |
|--|---|
| Colour | :Dark Grey |
| Crystal Forms | : Tetragonal Orthorombic β-Rhombohedral |
| Molecular Weight | :55.25 |
| Density (g/cm³) | :2.52 |
| Melting Point (°C) | :2400 |
| Oxidation Temperature (°C) | :600 |
| Heat of Formation @ 298 K (kcal/mol) | :13.8 |
| Specific Heat @ 298 K (cal/°C mol) | :12.55 |
| Shear Modulus (GPa) | :158-188 |
| Thermal Conductivity (W/mK) | :29-67 |
| Thermal Expansion Coefficient @ 298 K (1/K) | :4x10 ⁻⁶ |
| Compressive Strength (psi) | :414,000 |
| Knoop Hardness (100 gr load) | :3900 |
| Electrical Resistivity (ohm-cm) | :5 |

Table 1.2 Boron Carbide Fiber Properties in Comparison with Some Other Refractory Materials [1]

| Property | B ₄ C | Steel | Diamond | SiC | c-BN |
|--|------------------|-------|---------|------|------|
| Density (g/cm ³) | 2.46-2.52 | 7.84 | 3.5 | 3.2 | 2.2 |
| Knoop Hardness (kg/mm ²) | 2800 | | 7000 | 2500 | 4700 |
| Tensile Strength (Gpa) | 13.8 | 0.615 | 27.2 | 20 | |
| Shear Modulus (GPa) | 158-188 | 83 | 478 | 50.9 | |
| Thermal conductivity (W/cm-K) | 0.35 | 4800 | 20 | 5 | 13 |
| Thermal expansion coefficient (x10 ⁻⁶) (1/K) | 4 | 11 | 0.8 | 4.7 | 1.15 |
| Electrical Resistivity (ohm-cm) | 5 | | 106 | 1 | -- |

Structurally, it is a rhombohedral phase composed of icosahedral clusters which are linked by direct covalent bonds and through three-atom icosahedral chains along the main diagonal of the rhombohedron. The most widely accepted structural model for B₄C considers B₁₁C icosahedra with C-B-C chains and the stoichiometric composition B₁₂C₃, [3]. The boron carbides, illustrated in in Figure 1.1, have a three-atom chain along the longest diagonal of the rhombohedral cell. They are degenerate semiconductors with near-term applications as high-temperature thermoelectric materials. They

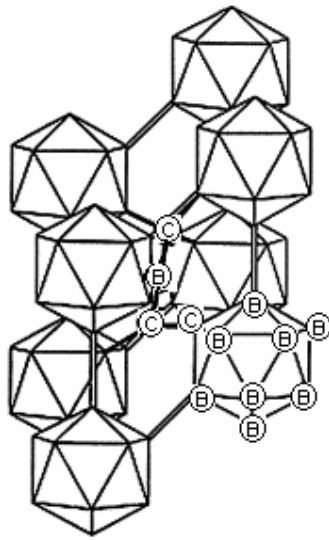


Figure 1.1 The rhombohedral crystal structure of boron carbides. Atoms are placed at the vertices of the icosahedra and within the three-atom intericosahedral chain

exist as a single-phase material from about 8 to 20 percent atomic carbon.

This large range of carbon composition is due to replacement of boron atoms with carbon atoms within the icosahedral chains and the icosahedra. However, there persists uncertainty as to the location of the carbon atoms within the unit cell of any given composition [4].

Boron carbide was first prepared by Joly in 1883, but the stoichiometric composition, known as ‘technical boron carbide’, was not assigned until 1934. The interest in boron carbide microelectronic devices and high temperature thermoelectronic conversion devices

started in the 1950's. In almost all early attempts to fabricate electronic quality boron carbides, the materials exhibited low resistivity and therefore their use in microelectronic applications was limited. It is produced in industrial quantities by reduction of boron anhydrides, hot pressing, and pressureless sintering. Pyrolysis of organics, physical vapor deposition (PVD), and the chemical vapor deposition (CVD) are frequently used to prepare boron carbides in the laboratory. The PVD methods are often expensive and boron carbide targets difficult to work with. On the other hand, CVD offers the advantage of better controlled deposition of well-defined, high purity single phase boron carbides [1].

Chemical vapor deposition processes are widely used in industry due to their versatility for depositing a very large variety of elements and compounds covering a wide range from amorphous deposits to epitaxial layers having a high degree of perfection and purity [5].

CVD can be defined as a process in which the gaseous chemical reactants are transported to the reaction chamber, activated thermally (conventional CVD) or by other than thermal means (plasma activated CVD or laser induced CVD), in the vicinity of the substrate, and made to react to form a solid deposit on the substrate surface. It is possible to deposit films of uniform thickness and low porosity even on substrates of complicated shape in this process. A major area for utility of CVD is in microelectronic applications, such as insulating layers, passivation layers, oxidation barriers, doped epitaxial layers of silicon etc. CVD techniques are also extensively employed for protective coatings for a variety of operating environments where

protection is required against wear, erosion, and high temperature oxidation [5].

In conventional CVD, which is the technique that is being used in this study, the gaseous reactants are activated thermally in the vicinity of the heated substrate, and react to form a film on the substrate. A simple schematic representation of CVD is shown in Figure 1.2. In this figure, the reactant gases enter the reactor and react to form a solid deposit onto a heated surface. The reaction by-product, which is in the gas form, is then removed from the reactor.

The various heating sources are used in CVD:

1. Hot plate: The substrate is in direct contact with the hot plate which is either resistively or inductively heated
2. Radiant heat: The substrate is heated by thermal radiation technique or optical technique (tungsten filament lamp or laser)

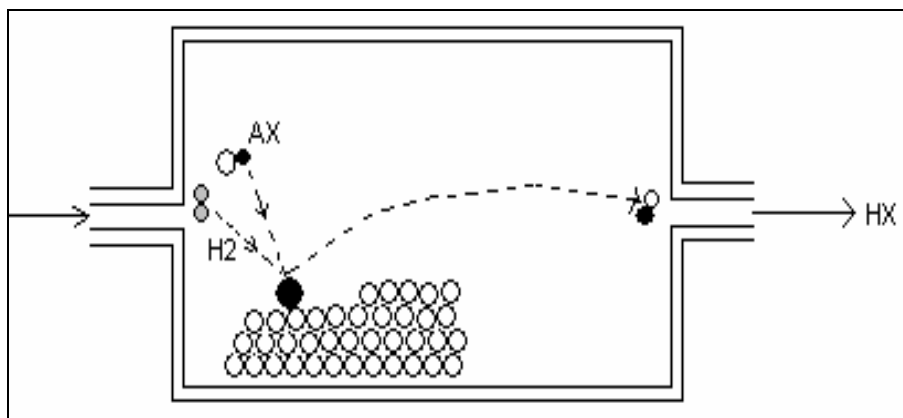


Figure 1.2 Schematic drawing of the chemical vapor deposition (CVD) process

3. Heating of a conductive substrate: Conductive substrates can be heated resistively or by RF induction.

The logical approach to the development of a CVD coating is to first determine the feasibility of a particular coating system. The process itself is basically governed by the following two important mechanisms:

- Thermodynamics which determines driving force and
- Kinetics which determines the rate control of the chemical reactions

The fundamental steps involved in a chemical vapor deposition process are shown in Figure 1.3.

The sequence of events in a CVD process is as follows:

1. Diffusion of reactants to the surface
2. Adsorption of reactants at the surface
3. Surface kinetics such as chemical reaction, diffusion, etc.
4. Desorption of products from the surface
5. Diffusion of products away from the surface

Among these steps, the slowest one is the rate-determining step. The rate limiting step is mainly determined by the process parameters. The most important rate limiting steps in the CVD process are mass transport, and surface kinetics. If one wants to study surface kinetics, an experimental method must be found which minimises the effect of mass transport.

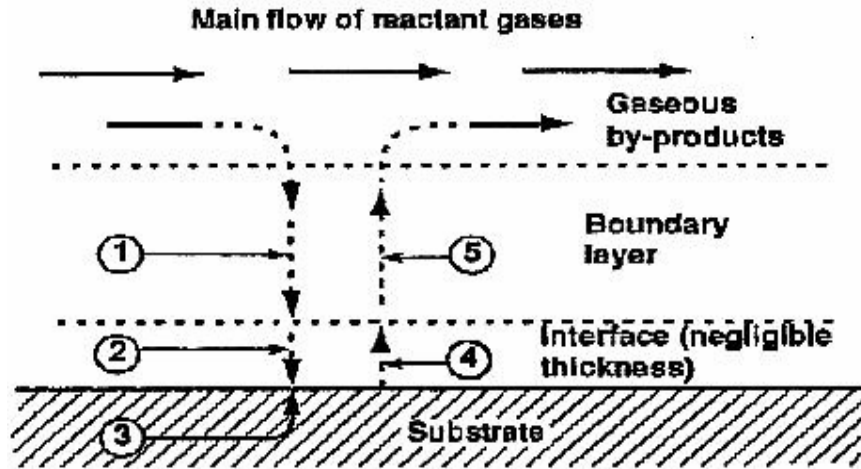


Figure 1.3 Various fundamental steps involved in a chemical vapor deposition process

Because of the need for high quality and pure products and a well controlled process, chemical vapor deposition was selected to be the best method to produce boron carbide. Some other production methods are thermal decomposition of boronyl pyridine ($\text{BOC}_5\text{H}_5\text{N}$), reduction of boron anhydride (B_2O_3) and reduction of boric acid (H_3BO_3) with lamp black. In all of these methods, boron carbide is produced in powder form and contains excess amount of carbon. Such methods are followed by hot pressing of the produced boron carbide powder. These high temperature and complex processes result in impure and mechanically poor products.

CVD studies made so far showed that high rates of deposition results in non-uniform surfaces with possible cracks. It must be noted that slow production rates are not desirable in industry. Therefore an optimum deposition rate must be found for uniform deposits. That can

be achieved by finding out the dependence of deposition rates on the process parameters.

In chemical vapor deposition process, various reactant gas mixtures containing boron, hydrogen, carbon and halogen gases can be used to deposit boron carbide on various substrates. Several reaction gas mixtures are $\text{BI}_3\text{-CH}_4$, $\text{BCl}_3\text{-CH}_4\text{-H}_2$, $\text{BBr}_3\text{-CH}_4\text{-H}_2$, and $\text{BCl}_3\text{-CCl}_4\text{-H}_2$. The rhombohedral boron carbide can be deposited from these reaction gas mixtures over broad temperature and vapour composition ranges [6].

1.1. Literature Survey on CVD of Boron Carbide

Due to its outstanding properties, boron carbide has been the subject of many investigations. The necessity for producing such a high quality material with a well controlled process resulted in the application of chemical vapor deposition in this area.

Cochran et al. [7] deposited boron carbide on to a variety of substrates at 1300°C by using methane, boron trichloride and hydrogen as feed gases. When stoichiometric amounts of CH_4 and BCl_3 were reacted with an excess of H_2 at 1300°C , B_4C deposits were obtained. The excess CH_4 in the reaction mixture resulted in free carbon. Also tungsten and graphite was found to be the best substrates considering the adherence of the deposits formed. No reaction between tungsten and boron deposit were detected either spectroscopically or visually, tungsten was the most desirable substrate tested.

Ploog [8] deposited boron carbide on tantalum and boron nitride substrates by CVD method in a non-flow reactor from BBr_3 , CH_4 , and H_2 . Tetragonal, orthorombic and rhombohedral boron carbides were obtained at different temperature, pressure and reactant gas compositions. The lattice parameters and crystal structures of the formed crystal phases were investigated in detail.

Jansson [9] studied CVD of boron carbide in a temperature range of 1300-1500 K at a total pressure of 50 torr, using boron trichloride, methane and hydrogen as reactant gases in a cold wall reactor. CVD phase diagram of the produced B-C system was obtained and using X-ray powder diffraction analysis, cell parameters for the produced phases were determined. It was observed that the carbon content in the coatings increased with an increase in temperature.

Vandenbulcke [10] deposited boron carbide from a BCl_3 - CH_4 - H_2 mixture by using a stagnation flow technique in a cold wall reactor. The deposition rates and the solid compositions are compared with a mass transfer equilibrium model. Also deposition domains of the various structures as a function of reaction parameters (temperature and partial pressures of reaction precursors) were obtained. At various combinations of methane and borontrichloride within an excess hydrogen, single phase boron carbide was obtained through a wide range of temperature(1400-1900 K).

Grigorev et al. [11] studied the deposition of B_4C from a BCl_3 - C_7H_8 - H_2 mixture on to a heated tungsten filament in a non-flow reactor at a total pressure of 0.33 atm. The experimental results were compared with the thermodynamic calculations, which were based on Gibbs

phase rule. It was shown that the dependence of the composition of the inlet gas mixture on the deposition products is complex and it is possible to establish various means to control the deposition process.

Desphande et al. [12] deposited amorphous boron carbide thin films using hot filament activated CVD at low temperature. Boron trichloride and methane were used with hydrogen as reactant gases. Films were characterized by FTIR, X-Ray photoelectron spectroscopy, XRD, adhesion testing and SEM. High purity, amorphous boron carbide films were obtained using chlorine based precursor BCl_3 .

Conde et al. [13] synthesized boron carbide on fused silica substrates by laser-assisted chemical vapor deposition, using CO_2 laser beam and boron trichloride and methane as precursors. The deposited films presented good adherence, a fine grain morphology and a mean carbon concentration in the range from 9 to 20 atomic percent. The crystal lattice parameters of rhombohedral-hexagonal boron carbide deposits were obtained. Such parameters were plotted against carbon content and a non-linear behaviour was observed, which shows a complex structure of produced boron carbides.

Dilek et al. [14] studied the CVD of B_4C on a tungsten filament from a gas mixture of BCl_3 , CH_4 and H_2 in an impinging jet reactor. The formation of BHCl_2 was verified experimentally and a rate expression for the formation of B_4C was proposed. However, the reaction rate expression was based on the boron trichloride to methane molar ratio rather than the concentrations of these species.

1.2. Objective of the Present Work

Most of the previous studies on CVD of boron carbide consider only the morphology of the deposited products. Usually, the deposition rates have been determined from the thickness of the deposits divided by the deposition time, using cross sectional scanning electron microscopy. Only in one work, a chemical kinetic analysis of the deposition process was carried out, but experiments were carried out using narrow inlet gas composition ranges. Also, there is not any proposed mechanism for the CVD of boron carbide process.

Considering such deficiencies in literature, the objectives of the present study can be listed as follows;

- To construct a CVD reactor in which diffusion effects are minimised
- To obtain kinetic information about the CVD of boron carbide from boron trichloride, hydrogen and methane following the chemical analysis of the product stream
- To get information about the reaction rates and selectivity of the boron carbide deposition reaction
- To investigate the influence of inlet gas composition and the substrate temperature on the kinetics of CVD of boron carbide
- To propose a reaction mechanism for CVD of boron carbide and develop the corresponding rate expressions
- To find out the dependence of physical properties (morphology and hardness) of B_4C deposited on the substrate temperature

CHAPTER 2

EXPERIMENTAL

There is a variety of fundamental physical and chemical principles that can control the deposition rate and quality of a film resulting from a CVD process. The basic processes underlying CVD can be subdivided into mass transport effects and chemical effects, each of which can occur both in the gas and solid phases. In some cases, a particular effect can be separated out as rate limiting, and a CVD process can be said to be ‘mass-transport controlled’ or ‘surface kinetics controlled’.

In this work, the chemical kinetics of the B_4C deposition on the tungsten substrates is being studied. So that, the influence of the mass transport limitations on the reaction rates should be minimised. In order to minimise mass transport effects, an impinging jet reactor is used, which was designed previously by Sezgi et al. [15] to study the CVD of boron (Figure 2.1). In Appendix E.3, it was shown that, the use of impinging jet geometry decreased the mass transfer boundary layer thickness around 30 fold, compared to the parallel flow geometry.

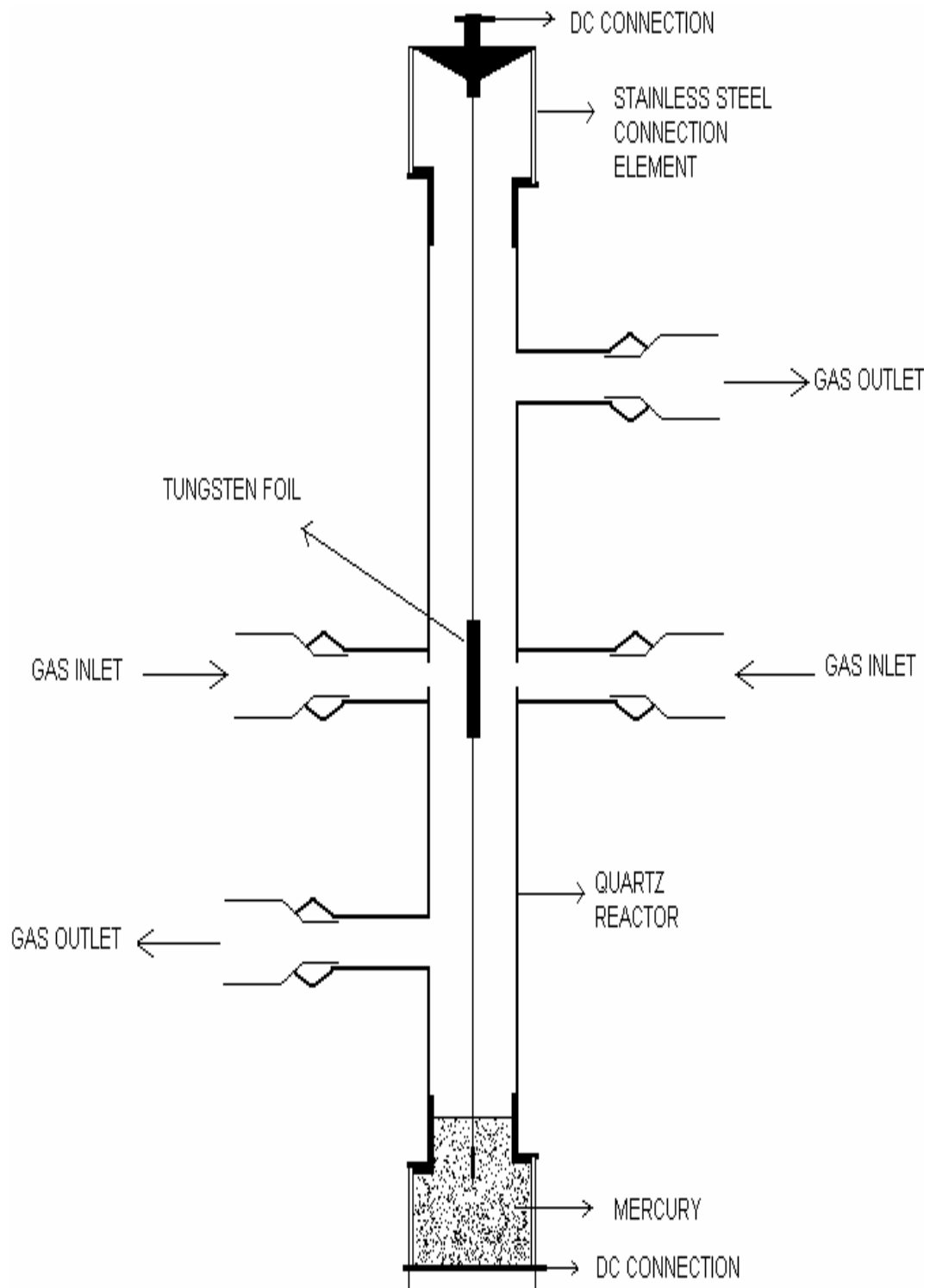


Figure 2.1 Dual Impinging-Jet Chemical Vapor Deposition Reactor

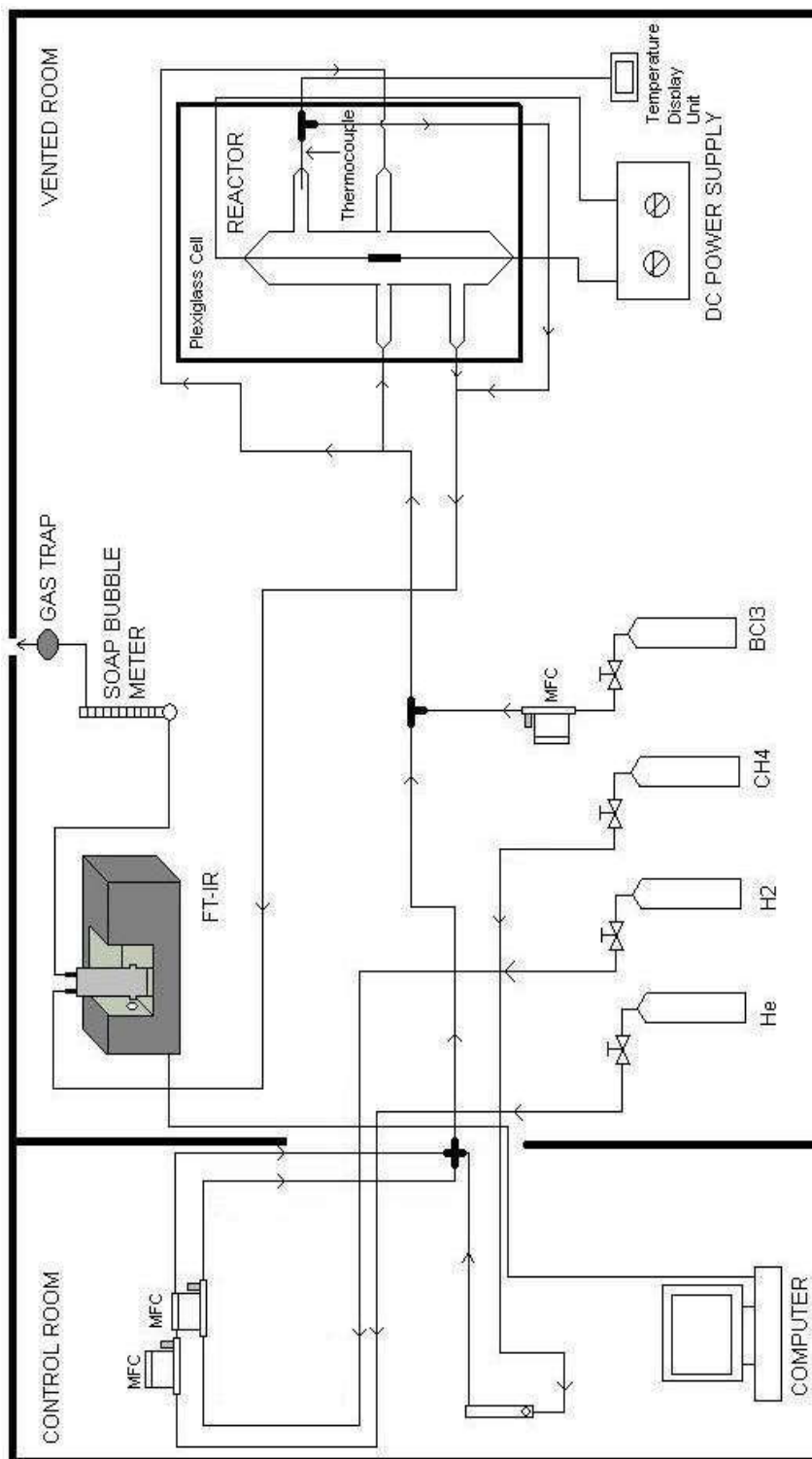


Figure 2.2 Experimental Set-Up

2.1 Experimental Set-up

The schematic drawing of the experimental system is shown in Figure 2.2. The system utilized in this study is similar to the one used by Sezgi et. al. [15]. The dual impinging jet reactor (Figure 2.1) is placed in a closed plexiglass cell considering the fact that boron trichloride is a highly toxic gas. The plexiglass cell is continuously vented during the experiments so that in case of any leakage from the reactor, the dangerous reactant gases could be removed from the medium. Also the part of the experimental system, which contains the pipes, plexiglass cell containing the reactor, and the gas tubes were placed in a vented room for safety reasons. The control equipment, that are mass flow controllers, rotameter and the computer, were placed in the control room, that is separated from the vented room by a small window. So that, in case of any danger in the vented room, the flow of the explosive gases, which are methane and hydrogen, can be stopped immediately. Reactor effluents were sent to a gas trap which is placed on line after FTIR spectrophotometer.

The reactor was made of quartz because of the durability of this material at high temperatures. In this reactor, the inlet gas mixture is fed through two orifices and impinges perpendicularly on to the both sides of the substrate. The orifices and the substrate are placed in the middle of the reactor. The diameter of the reactor is 1 cm whereas the diameter of the orifices are 1 mm. The distance between the orifices and the substrate surface is 0.5 cm.

The reactant gases were boron trichloride, methane and hydrogen. Helium was used in order to purge the system before and after each

run. Flowrates of boron trichloride, hydrogen and helium were controlled using mass flow controllers (Aalborg GFC-171 model), and flowrate of methane was adjusted by a rotameter. Hydrogen and methane gases were mixed in a cross, that is located in the piping system before the impinging jet reactor. Boron trichloride is added to the reactant gas mixture through a tee. The piping system in which the gases flow was made up of ¼ inch brass tubes. The boiling point of BCl₃ is 13.2 °C at 1 atm pressure. In order to avoid condensation of BCl₃, boron trichloride line in the piping system, from the BCl₃ tube exit to the mixing tee, and FTIR gas cell are heated by wrapping heating tapes around them. The FTIR gas cell temperature was kept at 110°C during the experiments. After the mixing, the reactant gases are fed to the reactor through the orifices and thus strike on both sides of the tungsten substrate as a jet. The tungsten substrate was held hanging vertically between two electrodes which were connected to DC power supply (KIKUSUI Electronics PAD 16-30L). The upper electrode was fixed and the lower one was dipped into the mercury pool. The weight of the lower electrode keeps the substrate surface smooth and stretched. The temperature of the substrate surface was measured continuously by using an optical pyrometer. The use of quartz as a reactor material provided the visual access to the substrate material so that the temperature measurements were made possible. The temperature of the substrate varied $\pm 10^{\circ}\text{C}$ throughout the surface during the experiments. For that reason, temperature measurements were carried out at three different points (top, middle and bottom parts of the substrate) and arithmetic averages were accepted as the actual temperature values. Also, in order to measure the reactor outlet temperature, a Cr-Ni thermocouple (K-Type) was connected to the reactor outlet.

The on-line chemical analysis of the reactor effluent was done by using a Perkin Elmer Spectrum One model Fourier Transform Infrared Spectrometer equipped with a Specac Sirocco Series heatable gas cell. The pathlength of the IR beam in the gas cell was variable which allowed the adjustment of best pathlength value for the specific experimental requirements. For the composition ranges utilized in this study a pathlength value of 8 meters was adjusted. In order to obtain quantitative information on the compositions of the reactor inlet and outlet streams, the FTIR spectra of methane, boron trichloride and hydrochloric acid were calibrated, before starting actual experiments. The calibration methods, together with the calibration curves are given in Appendix A.

To test the reliability of the experimental data, reproducibility experiment were carried out, and the standard deviations were calculated accordingly. Details of the experiments and calculation procedure were presented in Appendix F.

2.2 Experimental Procedure

The experimental parameters were the inlet mole fractions of methane and boron trichloride and the temperature of the tungsten substrate. The numerical values of the parameters for the runs conducted in this study are listed in Table 2.1. The first step in the experimental work was the preparation of the tungsten substrate at the desired dimensions. The width, height, and thickness of the tungsten substrates were 2.2 mm, 3 cm, and 0.015 mm, respectively. After that, the substrate must be weighed precisely and placed in the impinging jet reactor. Before each run, the experimental system should be purged with helium gas in order to remove impurities and excess oxygen in

the system. Otherwise, oxygen may react dangerously with hydrogen, which is one of the reactant gases, causing severe explosions.

The desired flowrates of methane, hydrogen, and boron trichloride were adjusted first. The total flowrate of the gas mixture was kept constant around 200 cm³/min in all runs. The composition of the initial gas mixture was inspected continuously by FTIR and hence desired adjustments on the compositions were possible. After the composition adjustment, the tungsten substrate was heated up to the desired temperature resistively by the DC power supply. The heating of the substrate was carried out in a step-by-step manner, with 100°C temperature increments per minute. Also, since the deposition of boron carbide on the substrate surface changes the resistivity, voltage-current adjustments of the DC power supply were necessary to keep the temperature of the substrate constant. Depending on the target temperature in a specific run, the current values varied between 10-25 amperes and the voltage values were varied between 8-15 volts. After the system reaches steady state, and the steady state concentrations of the gases were determined from the FTIR spectra. The temperature of the reactor effluent stream was recorded at the end of each run, and then the whole system was purged with helium gas. Finally, produced boron carbide deposits were removed from the reactor and weighed again precisely.

Table 2.1 Experimental Conditions in the Applied Runs

| Run | Temperature(°C) | y_{CH₄o} | y_{BCl₃o} | y_{H₂o} | Duration (min) |
|------------|------------------------|------------------------------------|-------------------------------------|-----------------------------------|---------------------------|
| MEA | 1150 | 0.01875 | 0.084 | 0.89725 | 62 |
| MEB | 1150 | 0.0387 | 0.084 | 0.8773 | 70 |
| MED | 1150 | 0.0423 | 0.084 | 0.8737 | 73 |
| MEE | 1150 | 0.0309 | 0.084 | 0.8851 | 66 |
| MEF | 1150 | 0.0241 | 0.084 | 0.8919 | 49 |
| BC13B | 1150 | 0.0195 | 0.1181 | 0.8624 | 72 |
| BC13C | 1150 | 0.01989 | 0.0411 | 0.93901 | 63 |
| BC13D | 1150 | 0.01997 | 0.0894 | 0.89063 | 63 |
| BC13E | 1150 | 0.0198 | 0.02287 | 0.95733 | 47 |
| BC13F | 1150 | 0.0195 | 0.0761 | 0.9044 | 54 |
| BC13G | 1150 | 0.02026 | 0.03017 | 0.94957 | 50 |
| TEA | 1000 | 0.02085 | 0.08412 | 0.8977 | 59 |
| TEB | 1100 | 0.02085 | 0.08145 | 0.8977 | 54 |
| TEC | 1200 | 0.02055 | 0.08038 | 0.8980 | 46 |
| TED | 1300 | 0.02031 | 0.08145 | 0.8982 | 53 |
| TEE | 1050 | 0.02055 | 0.08011 | 0.8980 | 50 |
| TEF | 1400 | 0.02070 | 0.08145 | 0.8979 | 27 |

CHAPTER 3

RESULTS AND DISCUSSIONS

3.1. Spectrophotometric Analysis of the Reactor Effluent

The FTIR spectra of the reactor effluent stream were taken continually with 5-minute time intervals during the experiments. From the obtained spectrum, it was possible to reveal the information on both the identity and amount of a constituent within the reactor outlet stream. Typical FTIR spectra of the reactor effluent stream, before and after heating the substrate, taken during a typical experiment are given in Figures 3.1 and 3.2, respectively. The FTIR spectrum given in Figure 3.1 was obtained when the tungsten foil was cold, hence the only detectable peaks belong to the reactor inlet gases, namely, methane and boron trichloride (hydrogen cannot be detected by FTIR since its dipole moment is zero). After heating the substrate to the desired reaction temperature, in addition to the peaks of methane and boron trichloride, characteristic peaks of hydrochloric acid and dichloroborane appear immediately. The FTIR spectrum of the reactor outlet stream after heating the tungsten substrate is given in Figure 3.2, and all of the four constituents can be seen in this figure. The peak groups which are characteristic to any constituent in the effluent

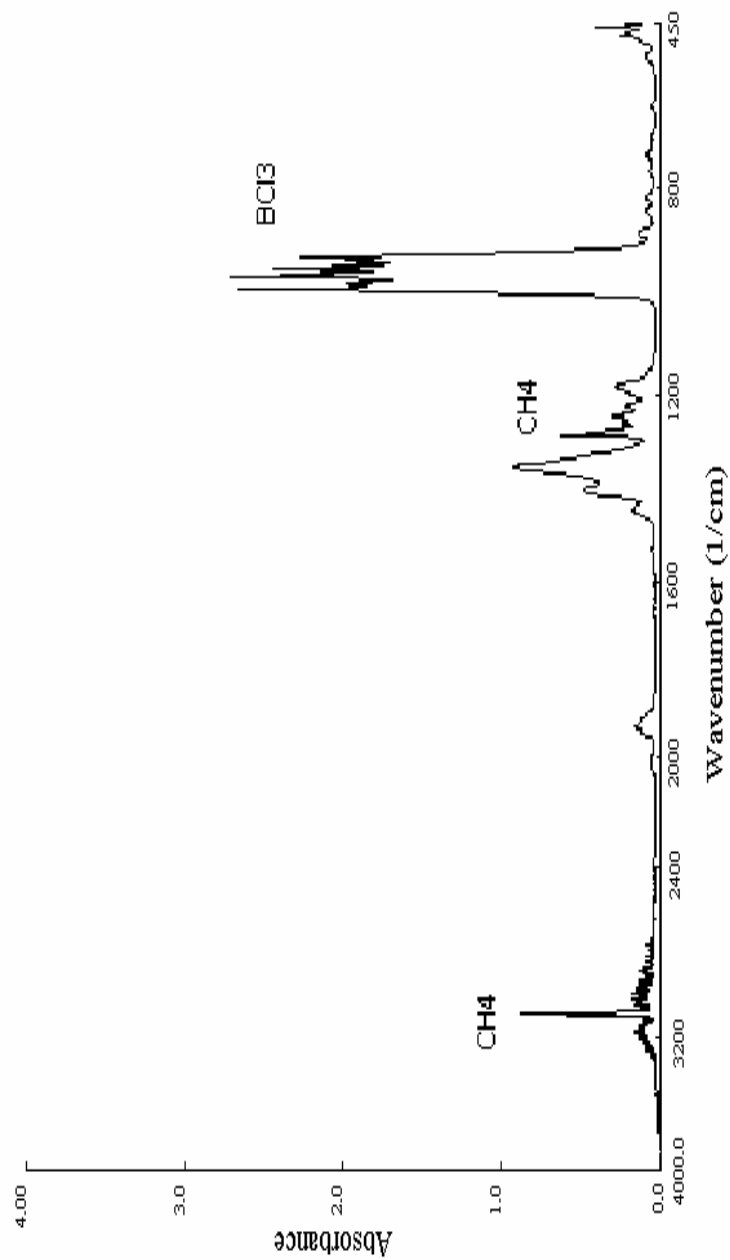


Figure 3.1 Typical FTIR Spectrum of the Reactor Effluent Before Heating the Substrate

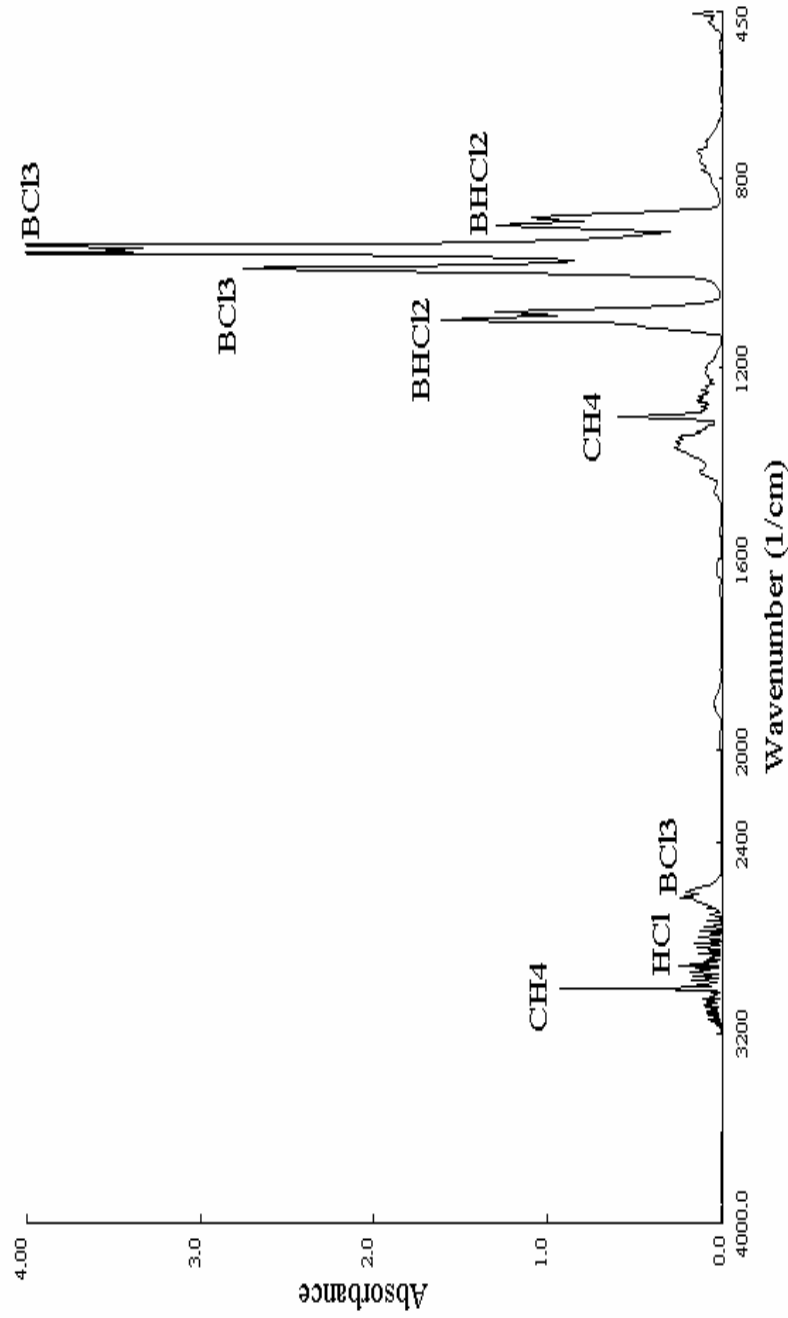


Figure 3.2 Typical FTIR Spectrum of the Reactor Effluent After Heating the Substrate

gas stream appear between certain values of wavenumbers and these values are tabulated in Table 3.1.

Table 3.1 Characteristic wavenumber ranges for the FTIR peaks for the reaction constituents

| Compound | Wavenumber Range (cm ⁻¹) |
|-------------------|--------------------------------------|
| Boron trichloride | 1040-920 |
| Methane | 3207-2843 and 1405-1170 |
| Hydrogen Chloride | 3050-2700 |
| Dichloroborane | 1150-1050, 910-850 and 2625-2700 |

3.2. Analysis of the Reactions Occuring in the Deposition Process

The XPS and XRD analyses of the produced materials have shown that almost all of the solid material that was produced during the deposition process was rhombohedral boron carbide. Also, the existance of the hydrochloric acid and dichloroborane was proven experimentally from the FTIR analysis. Hence, there are altogether 6 chemical species that take part in the overall reaction phenomena, those are methane (CH₄), boron trichloride (BCl₃), hydrogen (H₂), hydrogen chloride (HCl), dichloroborane (BHCl₂) and boron carbide (B₄C). The atomic balances for the species constituting these molecules can be written as follows;

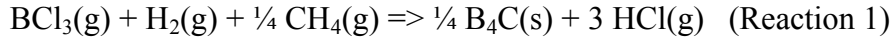
$$\text{B: } R_{\text{BCl}_3} + R_{\text{BHCl}_2} + 4 R_{\text{B}_4\text{C}} = 0 \quad (3.1)$$

$$\text{C: } R_{\text{CH}_4} + R_{\text{B}_4\text{C}} = 0 \quad (3.2)$$

$$\text{H: } 4 R_{\text{CH}_4} + R_{\text{HCl}} + R_{\text{BHCl}_2} + 2 R_{\text{H}_2} = 0 \quad (3.3)$$

$$\text{Cl: } 3 R_{\text{BCl}_3} + R_{\text{HCl}} + 2 R_{\text{BHCl}_2} = 0 \quad (3.4)$$

In the light of foregoing analysis, there must be two overall reactions occurring in the reactor. One of them is the formation reaction of boron carbide over the heated tungsten substrate;



and the other reaction is the formation of dichloroborane as a by-product;



These two reactions, in combination with the four atomic balances given above, are enough to describe the reaction rates of all the six species involved in the reaction phenomena. Taking the reaction rates of methane and boron trichloride as independent variables, the rate expressions for the other species can be derived as follows:

$$R_{\text{H}_2} = + R_{\text{BCl}_3} \quad (3.5)$$

$$R_{\text{B}_4\text{C}} = -R_{\text{CH}_4} \quad (3.6)$$

$$R_{\text{BHCl}_2} = 4 R_{\text{CH}_4} - R_{\text{BCl}_3} \quad (3.7)$$

$$R_{\text{HCl}} = -8 R_{\text{CH}_4} - R_{\text{BCl}_3} \quad (3.8)$$

At this point, in order to construct the stoichiometric table, the conversion terms should be introduced for the main reactions given above (Reaction 1 and Reaction 2).

x_1 : Conversion of boron trichloride to boron carbide in reaction 1

x_2 : Conversion of boron trichloride to dichloroborane in reaction 2

Accordingly, the stoichiometric table, Table 3.2, was constructed with the help of the molar balances, in which the variables are the conversion values, namely x_1 and x_2 .

Table 3.2 Stoichiometric Table

| Species | Feed Rate to Reactor (mol/time) | Change within Reactor (mol/time) | Effluent Rate from Reactor (mol/time) |
|--------------------------|---|---|---|
| BCl ₃ | F _{BCl₃o} | -(F _{BCl₃o} x ₁ +F _{BCl₃o} x ₂) | F _{BCl₃o} -F _{BCl₃o} x ₁ -F _{BCl₃o} x ₂ |
| H ₂ | F _{H₂o} | -(F _{BCl₃o} x ₁ +F _{BCl₃o} x ₂) | F _{H₂o} -F _{BCl₃o} x ₁ -F _{BCl₃o} x ₂ |
| CH ₄ | F _{CH₄o} | -1/4F _{BCl₃o} x ₁ | F _{CH₄o} -1/4F _{BCl₃o} x ₁ |
| HCl | - | +(3F _{BCl₃o} x ₁ +F _{BCl₃o} x ₂) | 3F _{BCl₃o} x ₁ +F _{BCl₃o} x ₂ |
| BHCl ₂ | - | +F _{BCl₃o} x ₂ | F _{BCl₃o} x ₂ |
| Total (=F _T) | F _o (=F _{BCl₃o} + F _{H₂o} + F _{CH₄o}) | +3/4F _{BCl₃o} x ₁ | F _o +3/4F _{BCl₃o} x ₁ |

The mole fraction of a species *i* (*y_i*) in the reactor effluent stream can be written by dividing molar flowrate of this species to the total effluent flowrate from the reactor. Mole fractions for each species are given in equations from 3.9 to 3.13 below.

$$y_{\text{BCl}_3} = \frac{F_{\text{BCl}_3}}{F_T} = \frac{F_{\text{BCl}_3o} (1 - x_1 - x_2)}{F_o + 3/4F_{\text{BCl}_3o} x_1} = \frac{y_{\text{BCl}_3o} (1 - x_1 - x_2)}{1 + 3/4y_{\text{BCl}_3o} x_1} \quad (3.9)$$

$$y_{\text{H}_2} = \frac{F_{\text{H}_2}}{F_T} = \frac{F_{\text{H}_2o} - F_{\text{BCl}_3o} (x_1 + x_2)}{F_o + 3/4F_{\text{BCl}_3o} x_1} = \frac{y_{\text{H}_2o} - y_{\text{BCl}_3o} (x_1 + x_2)}{1 + 3/4y_{\text{BCl}_3o} x_1} \quad (3.10)$$

$$y_{\text{CH}_4} = \frac{F_{\text{CH}_4}}{F_T} = \frac{F_{\text{CH}_4o} - 1/4F_{\text{BCl}_3o} x_1}{F_o + 3/4F_{\text{BCl}_3o} x_1} = \frac{y_{\text{CH}_4o} - 1/4y_{\text{BCl}_3o} x_1}{1 + 3/4y_{\text{BCl}_3o} x_1} \quad (3.11)$$

$$y_{\text{HCl}} = \frac{F_{\text{HCl}}}{F_{\text{T}}} = \frac{F_{\text{HCl}_0} (3x_1 + x_2)}{F_o + 3/4F_{\text{BCl}_3} x_1} = \frac{y_{\text{BCl}_3} (3x_1 + x_2)}{1 + 3/4y_{\text{BCl}_3} x_1} \quad (3.12)$$

$$y_{\text{BHCl}_2} = \frac{F_{\text{BHCl}_2}}{F_{\text{T}}} = \frac{F_{\text{BCl}_3} x_2}{F_o + 3/4F_{\text{BCl}_3} x_1} = \frac{y_{\text{BCl}_3} x_2}{1 + 3/4y_{\text{BCl}_3} x_1} \quad (3.13)$$

Mole fractions of each component in the inlet and outlet streams are given in Appendix D.

In a typical experiment, the change of the mole fractions of the reactor effluent gases with respect to time is given in Figure 3.3. After heating the substrate, the system reached steady state nearly within 30 minutes. This was the common case for all of the experiments conducted.

3.2.1. Reaction Rate Calculations

The reaction rates for each species in the reaction mixture can be found by using the following equations in which the variables are the conversion values x_1 and x_2 for Reaction 1 and Reaction 2, respectively.

$$AR_{\text{BCl}_3} = -F_o y_{\text{BCl}_3} x_1 - F_o y_{\text{BCl}_3} x_2 \quad (3.14)$$

$$AR_{\text{H}_2} = -F_o y_{\text{BCl}_3} x_1 - F_o y_{\text{BCl}_3} x_2 \quad (3.15)$$

$$AR_{\text{HCl}} = 3F_o y_{\text{BCl}_3} x_1 + F_o y_{\text{BCl}_3} x_2 \quad (3.16)$$

$$AR_{\text{CH}_4} = -1/4 F_o y_{\text{BCl}_3} x_1 \quad (3.17)$$

$$AR_{\text{BHCl}_2} = F_o y_{\text{BCl}_3} x_2 \quad (3.18)$$

$$AR_{\text{B}_4\text{C}} = 1/4 F_o y_{\text{BCl}_3} x_1 \quad (3.19)$$

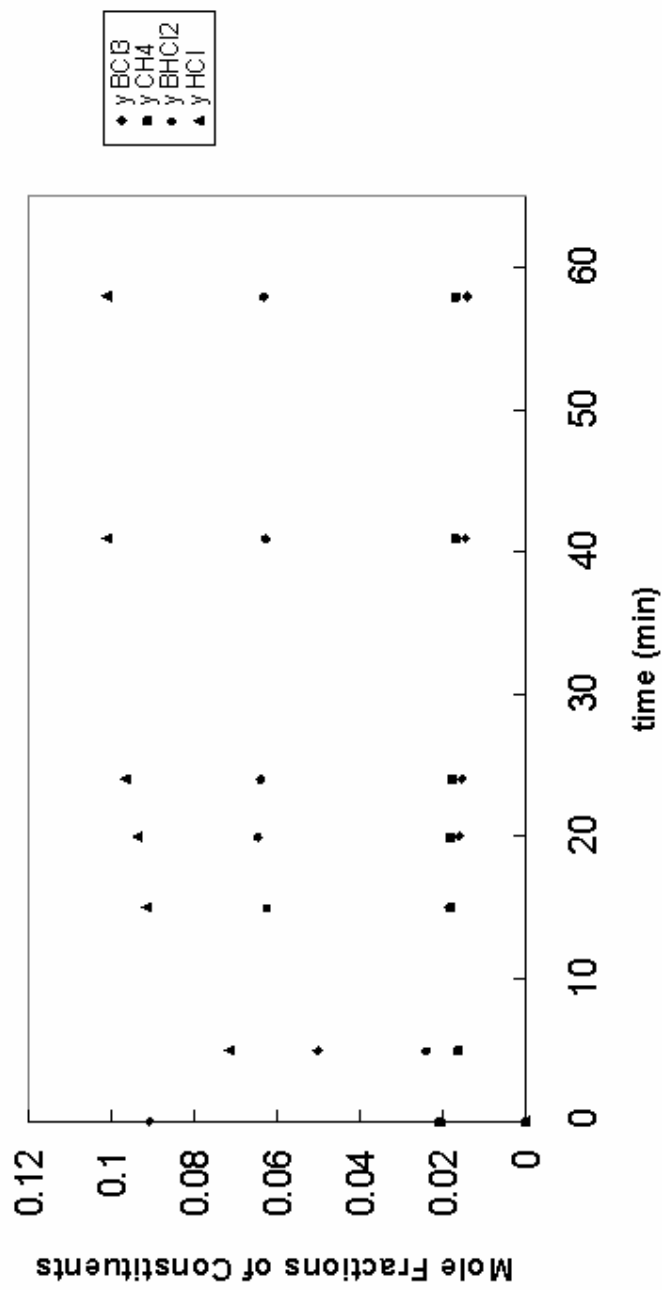


Figure 3.3 Change of mole fractions of reaction constituents with time
 (T=1150°C, y_{BCB,0}=0.089, y_{CH₄,0}=0.02, y_{BCB,0}/y_{CH₄,0}=4.45, y_{H₂,0}=0.891)

where, F_0 is the total molar flowrate of the reactant stream and A is the surface area of the tungsten substrate that is in contact with the reactant gases within the reactor. The rate equations are based on surface area rather than reactor volume. This can be considered as a reasonable procedure for the boron carbide formation reaction because it is already a surface reaction. Although we are not sure at the beginning where dichloroborane reaction occurs (in fact our analyses in Appendix E showed that it occurs in the gas phase) we can still write its formation reaction based on the surface area. The reason behind this approximation is that, the space time of the reactants in the reactor is around 0.35 seconds and the temperature of the effluent stream from the reactor does not exceed 50°C. At such a low temperature, it is not possible to have any reaction to occur in the bulk of the gas in the reactor. So, it can be said that, the homogeneous reactions occurring during the deposition process must be occurring in a very thin thermal boundary layer next to the substrate surface.

In addition to Equation 3.19, the boron carbide formation rate was also determined from the weight change of the filament during the reaction. Comparison of the mass of the boron carbide deposited during a typical run (calculated using equation 3.19, using experimentally observed conversion values) and mass of the boron carbide evaluated from the weight change of the filament agreed well (Figure 3.4). This result demonstrated that the two independent reactions (Reactions 1 and 2) are sufficient to describe the reaction system under consideration.

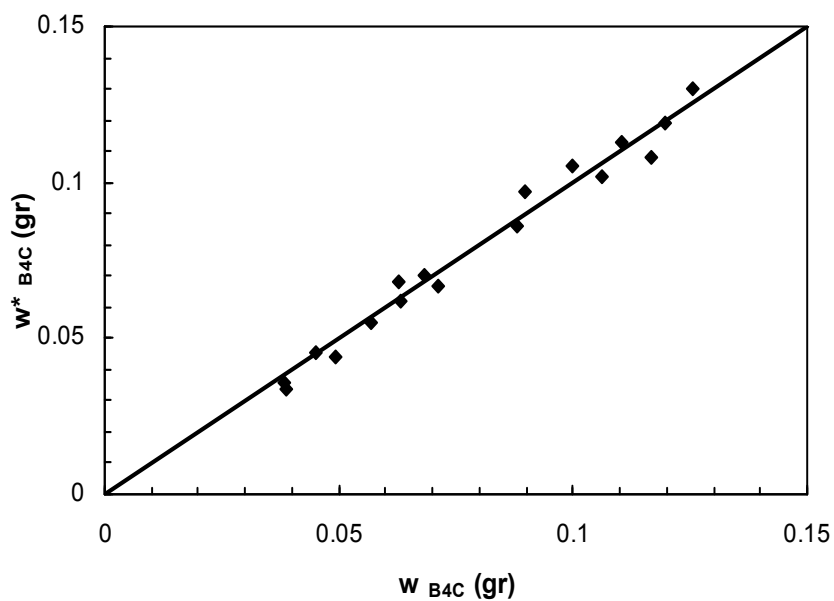


Figure 3.4 Comparison of the calculated B₄C deposit weight (w) with the actual B₄C deposit weight (w*)

3.2.2. Conversion Calculations:

The conversion values in the equations through 3.14-3.19 can be calculated by simultaneous solution of equations 3.9 and 3.11 for x_1 and x_2 .

For Reaction 1 (B₄C formation reaction)

$$x_1 = \frac{y_{\text{CH}_4\text{o}} - y_{\text{CH}_4}}{\left(\frac{3}{4}y_{\text{CH}_4} + \frac{1}{4}\right)y_{\text{BCl}_3\text{o}}} \quad (3.20)$$

For Reaction 2 (BHCl₂ formation reaction)

$$x_2 = \frac{(y_{\text{BCl}_3\text{o}} - y_{\text{BCl}_3})(3y_{\text{CH}_4} + 1) - (y_{\text{CH}_4\text{o}} - y_{\text{CH}_4})(3y_{\text{BCl}_3} + 4)}{y_{\text{BCl}_3\text{o}}(3y_{\text{CH}_4} + 1)} \quad (3.21)$$

3.2.3. Selectivity Calculations:

The selectivities for the reactions 1 and 2 can be found as:

$$S_{\text{B}_4\text{C}} = \frac{R_{\text{B}_4\text{C}}}{-R_{\text{BCl}_3}} = \frac{x_1/4}{x_1 + x_2} \quad (3.22)$$

$$S_{\text{BHCl}_2} = \frac{R_{\text{BHCl}_2}}{-R_{\text{BCl}_3}} = \frac{x_2}{x_1 + x_2} \quad (3.23)$$

where, $S_{\text{B}_4\text{C}}$ is the selectivity of the boron carbide formation rate with respect to the boron trichloride consumption rate, whereas S_{BHCl_2} is the selectivity of the dichloroborane formation rate with respect to the boron trichloride consumption rate.

3.3. Analysis of the Effects of Various Experimental Parameters on the Reaction Kinetics

The effects of the initial boron trichloride mole fraction on the reaction rates were analyzed by changing the boron trichloride molar fraction in the inlet stream between 2.3% and 11.8%. In these experiments, the mole fraction of methane in the reactor inlet stream was kept constant near 2%, and the rest was hydrogen being in excess to sum up the total molar flow rate to 200cm³/min.

Changes in mole fraction of hydrogen in the inlet gas mixture, in the range of 85% and 95% seemed to have no effect on the reaction kinetics. Low hydrogen concentrations in the inlet gas resulted in carbon deposition rather than B₄C formation. The effect of inlet BCl₃ concentration on the reaction rates at a temperature of 1150°C can be

seen in Figure 3.5. The figure indicates that the reaction rate as well as conversion for the boron carbide formation reaction is always lower than that of dichloroborane formation reaction. Dichloroborane formation reaction is believed to occur in the thin boundary layer next to the substrate surface. In appendix E, the calculations for the approximate temperature distribution in the vicinity of the tungsten substrate were presented, and it was observed that there is around 90 mm³ active reaction region around both sides of the filament, in which the temperature is greater than 350°C, above which dichloroborane formation reactions can take place. This may be the reason of higher production rates of dichloroborane than that of boron carbide which occurs only through surface reactions. The rate of boron carbide formation reaction increases with an increase in BCl₃ inlet molar fraction, and has a decreasing trend in the slope at high BCl₃ inlet mole fractions. The rate of the reaction seemed to be surface kinetics controlled. The rate of dichloroborane formation reaction is fast enough to consume the excess amount of BCl₃ at high inlet concentrations of BCl₃. The rate of dichloroborane formation reaction increases with an increase in BCl₃ inlet molar fractions.

In Figure 3.6, the temperature dependence of B₄C and BHCl₂ formation rates are given. As it is seen that, boron carbide formation rate increases continuously with temperature. With temperature rise, the rate of dichloroborane formation reaction also increases, however the change is not significant as compared to the effect of temperature on the formation rate of B₄C. With a change of substrate temperature from 1000 to 1400°C, the rate of B₄C deposition increases almost 4 fold, whereas the rate of BHCl₂ formation increases around 1.05 fold.

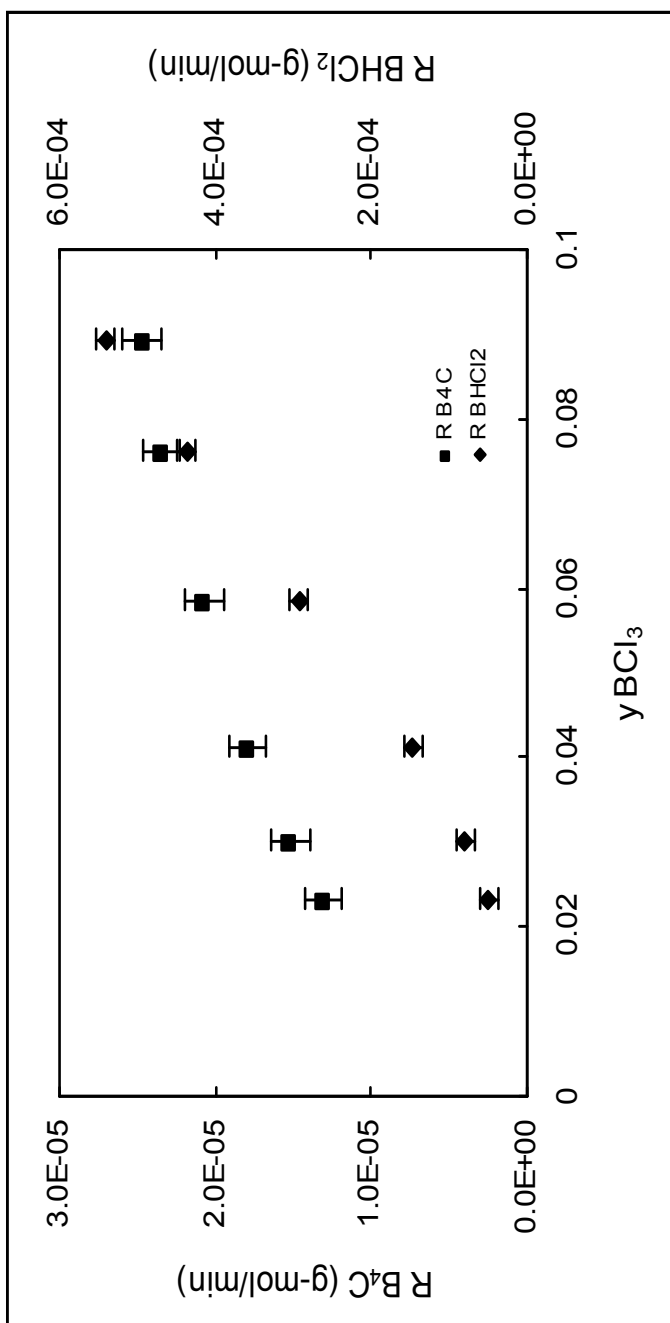


Figure 3.5 Effect of initial BCl_3 mole fraction on the B_4C and BHCl_2 formation rates with the standard deviations indicated by the error bars ($y_{\text{CH}_4} = 0.02$ in hydrogen, $T = 1150^\circ\text{C}$)

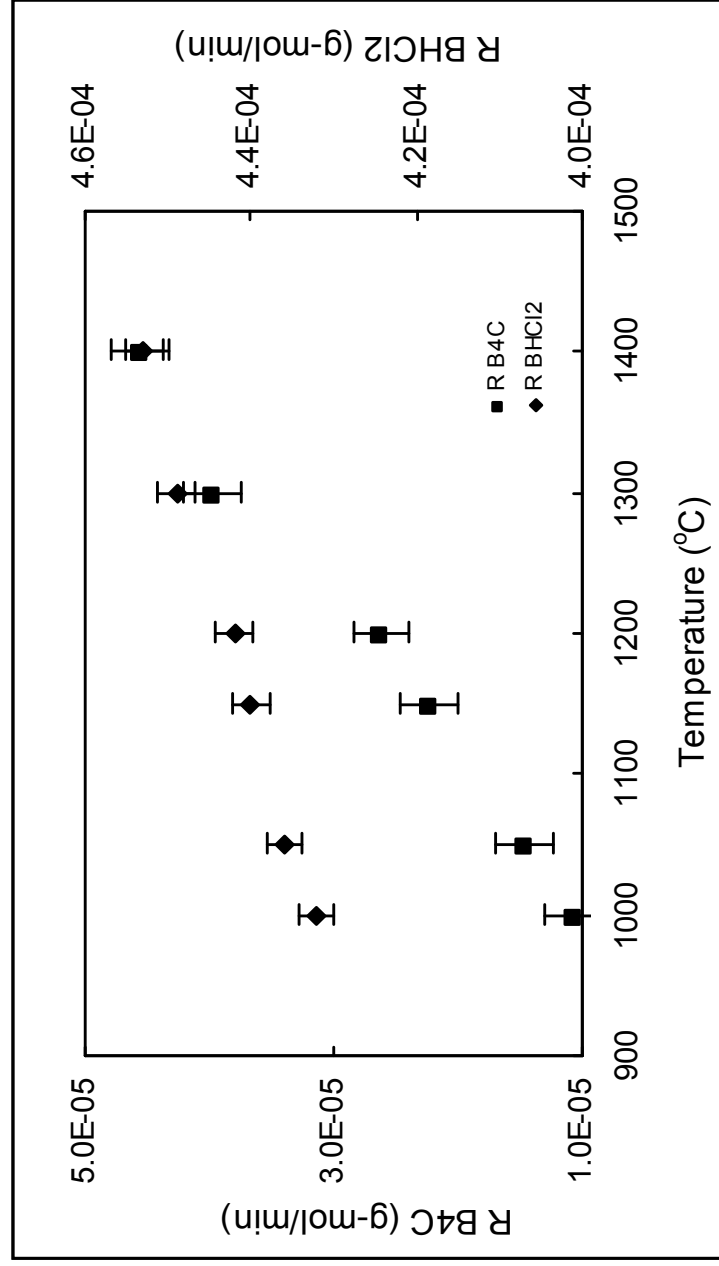


Figure 3.6 Effect of substrate temperature on B₄C and BHCl₂ formation rates with the standard deviations indicated by the error bars ($y_{\text{BCl}_{3_0}}=0.081$, $y_{\text{CH}_4_0}=0.02$, in hydrogen)

This further supports the idea of gas phase formation of dichloroborane in the boundary region next to the substrate surface. It may be expected that a change in surface temperature in this impinging jet system may have smaller effect on the gas-phase kinetics and hence less impact on the reaction rates compared to the solid-phase kinetics in the formation of boron carbide. It is also seen that the reaction rate for boron carbide formation reaction is lower than that of dichloroborane formation reaction for the entire range of temperature studied. The effects of methane concentration in the inlet stream on the reaction rates were analyzed by changing methane mole fraction in the inlet stream in the range of 1.9% and 4.2% and the results are depicted in Figure 3.7. The change of methane mol fraction in the inlet stream has almost no effect on the reaction rate of dichloroborane formation reaction over the composition range of methane that was applied during the runs. However, there is an increasing trend in the rate of boron carbide formation reaction.

By a computerized nonlinear model fitting procedure, the experimental data was analysed to find the model parameters. Hooke and Jeeves [16] iteration method was used for the analysis of the data. After the analysis, the frequency factor, k_0 , and activation energy, E_a , were found to be 0.078 ± 0.008 and 56.1 ± 4.0 kJoule/mol, respectively. The order of reaction with respect to BCl_3 was found as 0.34 ± 0.055 , whereas the order with respect to CH_4 was found as 0.64 ± 0.084 , with a statistical correlation coefficient of 0.95. In Figure 3.8, model predicted B_4C formation rates were compared with the experimentally found B_4C formation rates. Hence the expression for the boron carbide formation rate can be written as,

$$R_{\text{B}_4\text{C}} = k_0 \cdot \exp(-E_a/RT) [\text{BCl}_3]^a [\text{CH}_4]^b \quad (3.24)$$

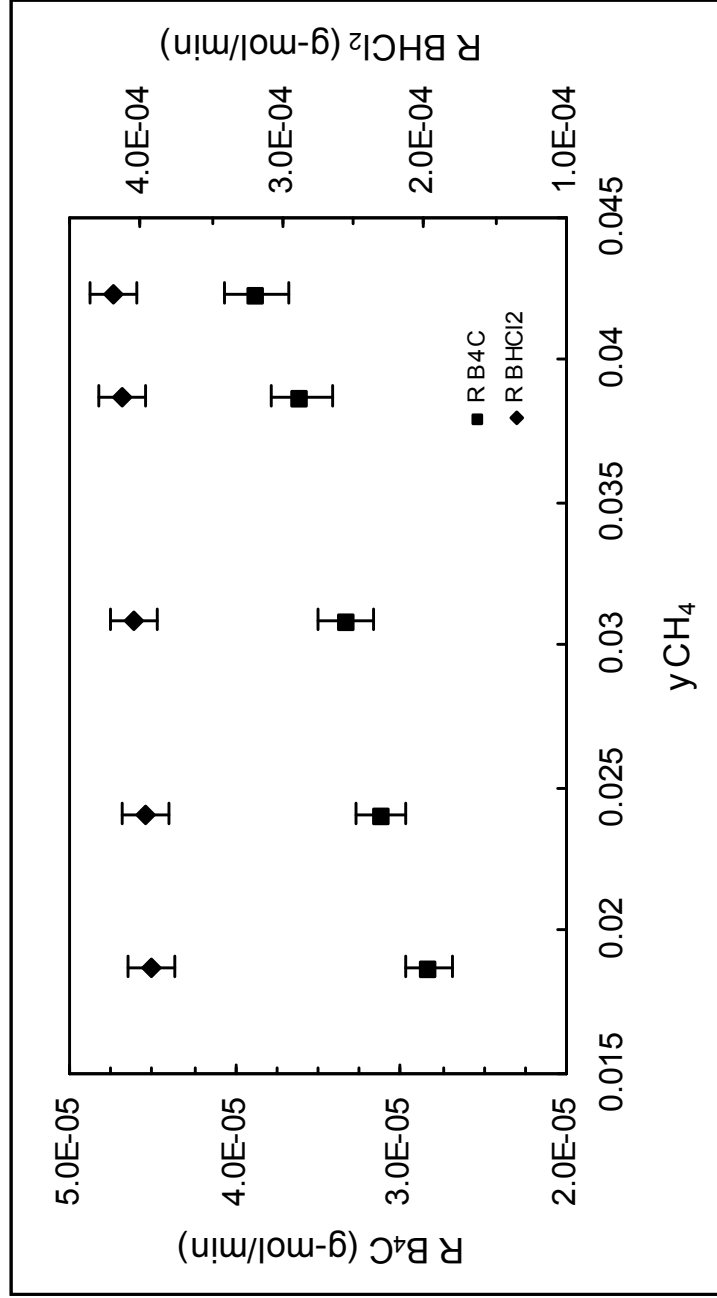


Figure 3.7 Effect of initial CH_4 mole fraction on B_4C and $BHCl_2$ formation rates with the standard deviations indicated by the error bars ($T=1150^\circ C$, $y_{BCl_3_0} = 0.084$ in hydrogen)

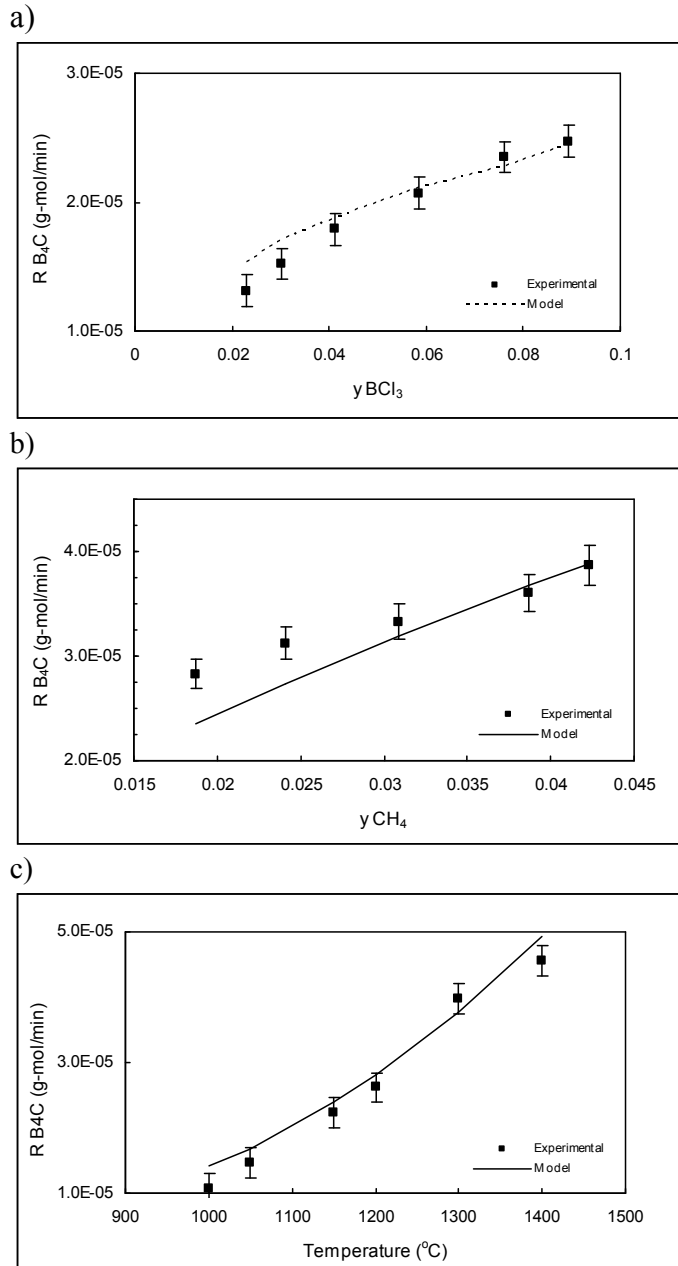


Figure 3.8 Effect of initial BCl_3 ($y_{\text{CH}_4}=0.02$, in hydrogen, $T=1150^\circ\text{C}$)

(a) and CH_4 ($y_{\text{BCl}_3}=0.084$, in hydrogen, $T=1150^\circ\text{C}$) (b) mole

fractions and temperature ($y_{\text{BCl}_3}=0.081$, $y_{\text{CH}_4}=0.02$, in hydrogen) (c)

on B_4C formation rate with the standard deviations indicated by the error bars and model predictions indicated by the dashed lines

where,

$$k_0 = 0.078 \pm 0.008$$

$$E_a = 56.1 \pm 4.0 \text{ kJoule/mol}$$

$$a = 0.34 \pm 0.055$$

$$b = 0.64 \pm 0.084$$

3.3.1. Effects of Experimental Parameters on Selectivities

The selectivities for both reactions were calculated from equations 3.22 and 3.23, and the results are given in Figures 3.9, 3.10 and 3.11. In all of the conducted experiments, the selectivity of dichloroborane was always higher than that of boron carbide and the gap increases rapidly especially at low BCl_3 concentrations (see Figure 3.9). At high values of BCl_3 concentrations, the dependence of selectivities on the boron trichloride composition gradually disappears. Compared to effect of boron trichloride on the selectivities of both reactions, methane has almost no effect on selectivities (Figure 3.10). So it can be said that the selectivities are controlled by boron trichloride composition rather than methane composition in the inlet stream. The temperature increase causes dichloroborane selectivity to decrease. On the other hand, the selectivity of boron carbide formation reaction increases with temperature. It is seen that temperature rise has a positive effect on the boron carbide formation in terms of reaction rate, conversion and selectivity. However, it should be kept in mind that there is a limitation on the temperature to produce boron carbide in desired purity.

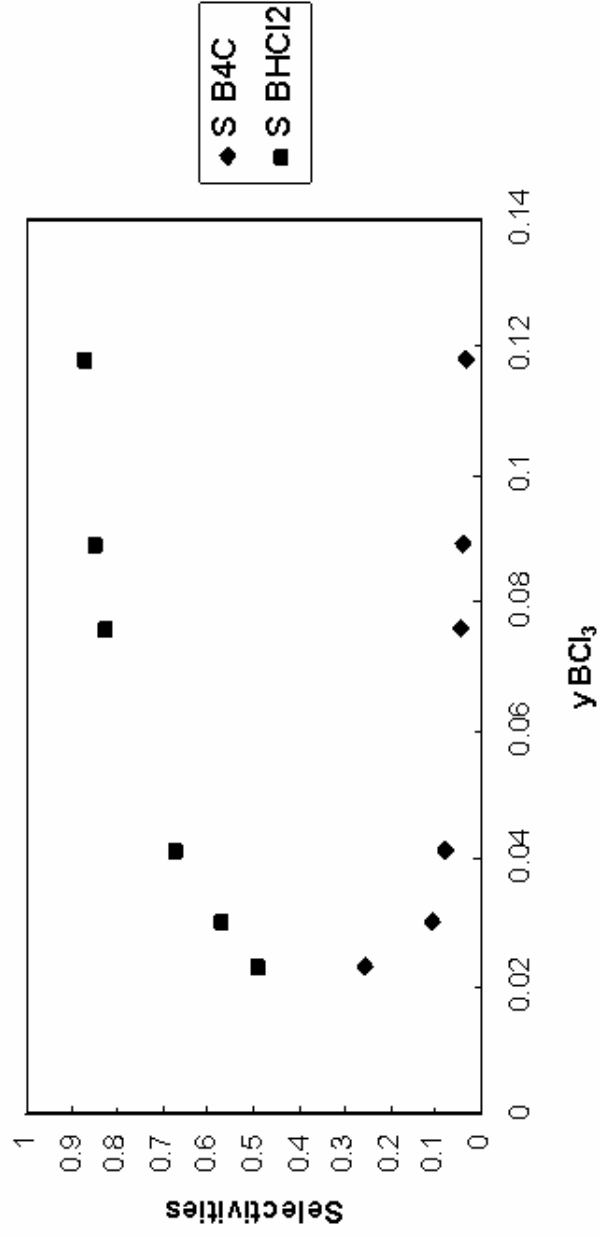


Figure 3.9 Effect of initial BCl_3 mole fraction on B_4C and BHCl_2 selectivities ($y_{\text{CH}_4} = 0.02$ in hydrogen, $T = 1150^\circ\text{C}$)

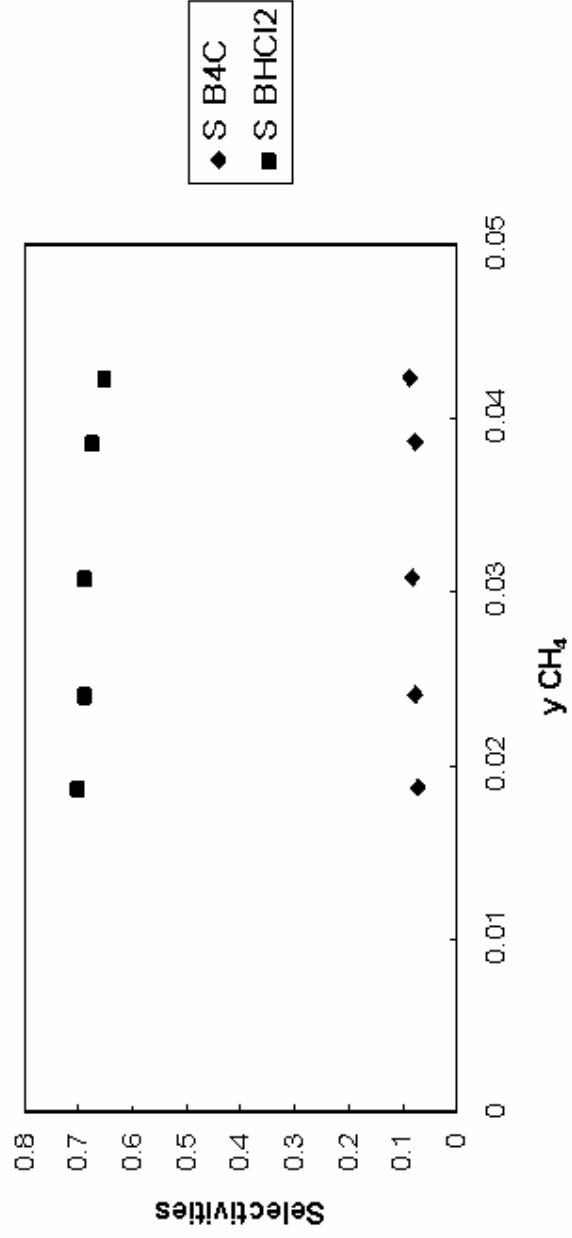


Figure 3.10 Effect of initial CH_4 mole fraction on B_4C and $BHCl_2$ selectivities ($T=1150^\circ C$,

$y_{BCl_{3_0}} = 0.084$ in hydrogen)

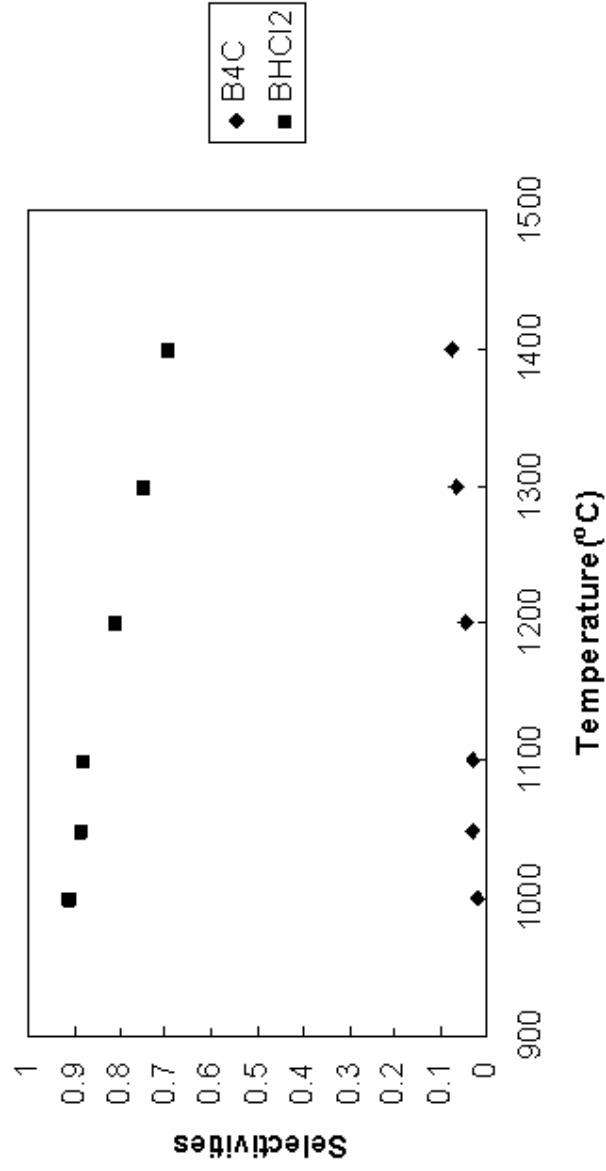


Figure 3.11 Effect of temperature on B₄C and BHCl₂ selectivities ($y_{\text{BCl}_3,0}=0.081$, $y_{\text{CH}_4,0}=0.02$, in hydrogen)

3.3.2. Effects of Experimental Parameters on Boron Carbide Yield

The chemical yield is defined as the mass fraction of the limiting reactant converted to the required product. The percentage yield can be defined as follows,

$$\text{Percentage yield} = \text{actual yield} / \text{theoretical yield} \times 100$$

The theoretical yield was calculated from the reaction stoichiometry, and it is based on the molar amount of BCl_3 , which is assumed to be the rate limiting reactant.

Effects of experimental parameters on boron carbide percentage yields are depicted in Figures 3.12, 3.13, and 3.14. The maximum boron carbide yield observed in this study was 13%. This low yield can be attributed to the high formation rate and selectivity of competing dichloroborane formation reaction compared to the boron carbide formation reaction. Also, it was shown in Appendix G that, boron carbide formation reaction occurs too far from equilibrium, which may be another reason for poor yields observed. Boron carbide percentage yield decreases significantly with increasing boron trichloride inlet molar fraction (Figure 3.12). Methane has little effect on the yield of boron carbide compared to the boron trichloride effect and there is an increasing trend in the yield with increasing methane inlet molar fraction, which can be seen in Figure 3.13. There is a linear increase in boron carbide yield with increasing substrate temperature (Figure 3.14). So it can be said that, maximum yield can be achieved using high substrate temperatures and low boron trichloride inlet molar fractions.

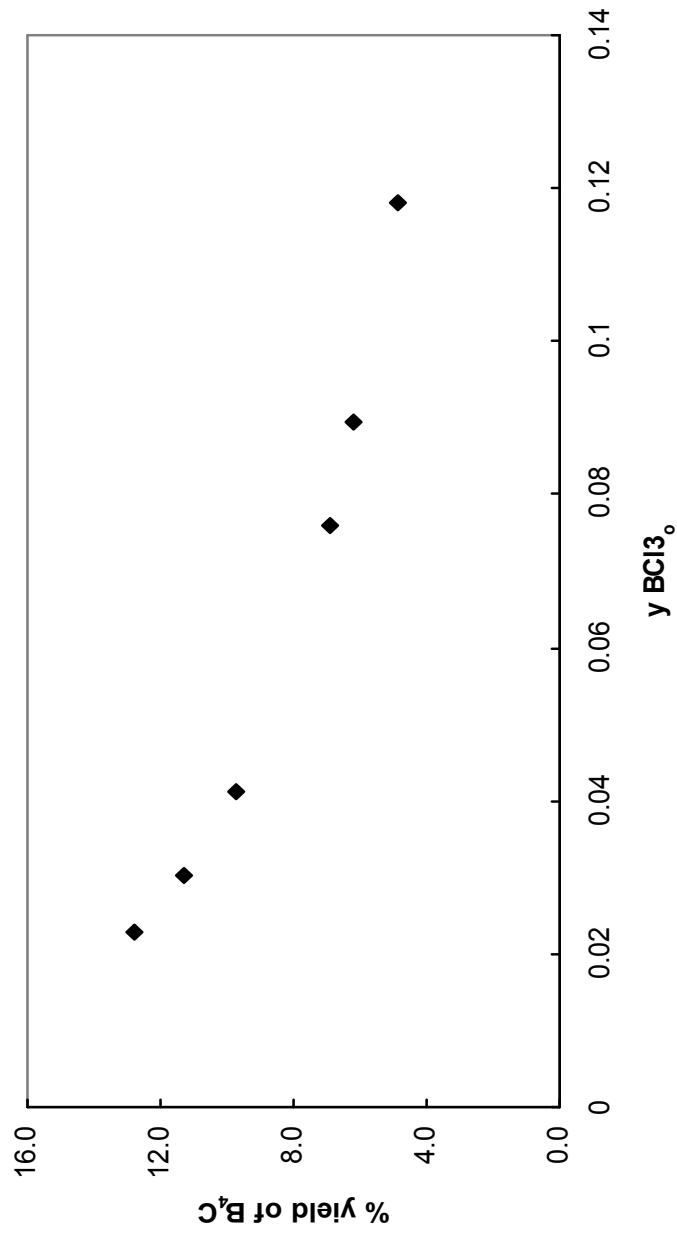


Figure 3.12 Effect of initial BCl_3 mole fraction on B_4C yield ($y_{\text{CH}_4_0}=0.02$ in hydrogen, $T=1150^\circ\text{C}$)

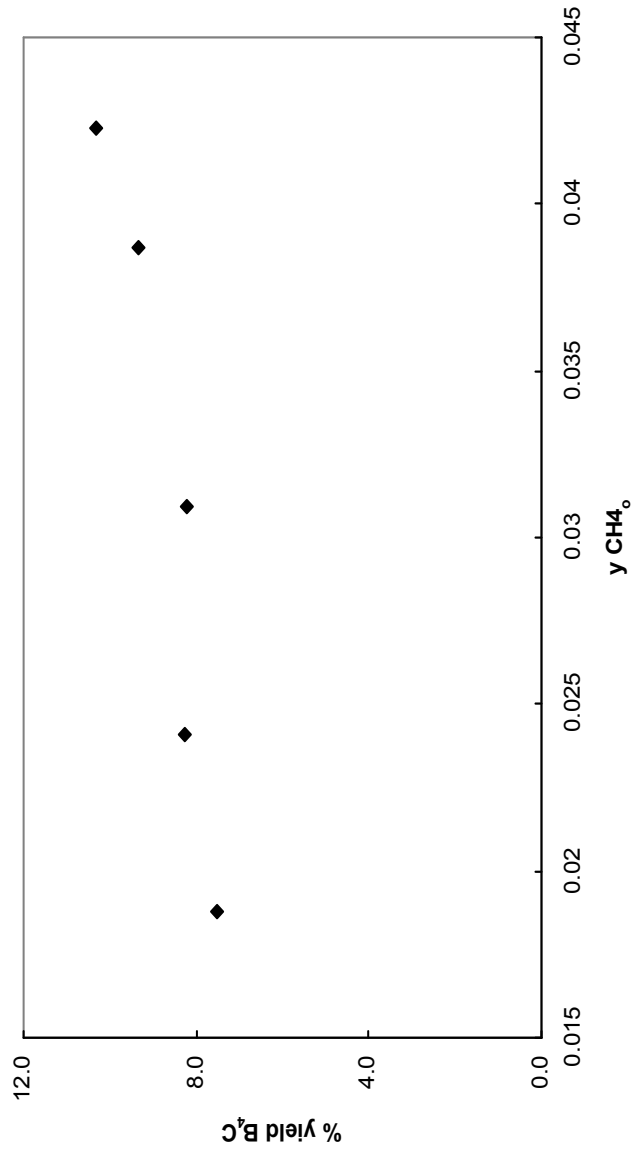


Figure 3.13 Effect of initial CH_4 mole fraction on B_4C yield ($T=1150^\circ C$, $y_{BCl_3_0} = 0.084$ in hydrogen)

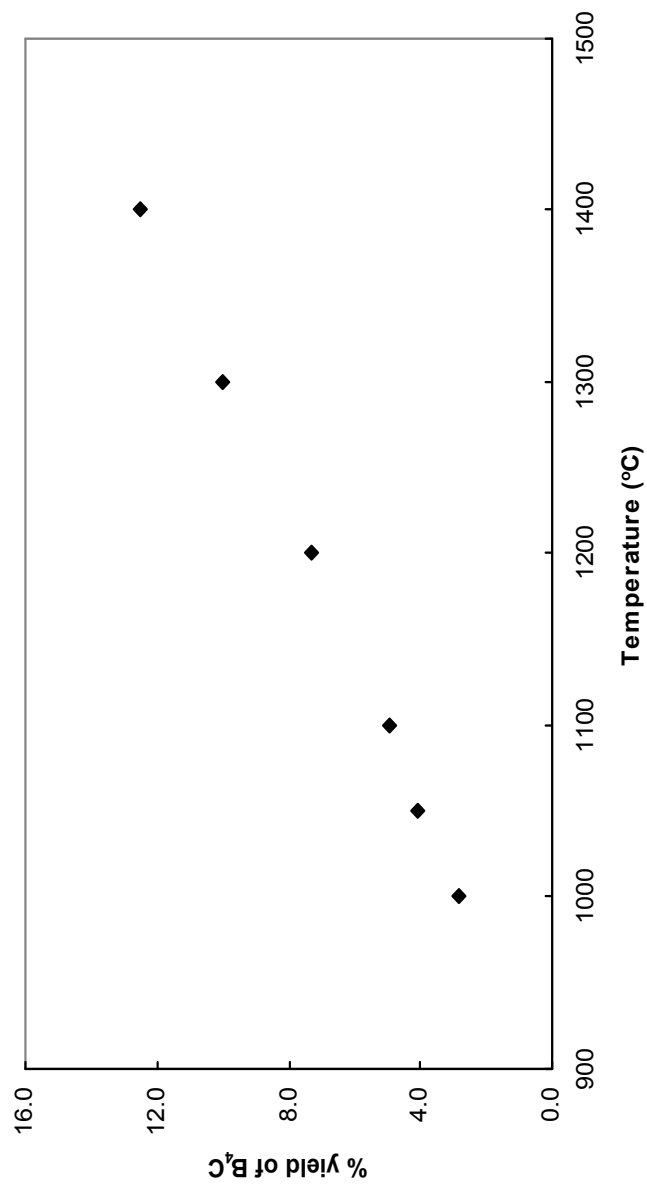


Figure 3.14 Effect of temperature on B₄C yield ($y_{\text{BCl}_3} = 0.081$, $y_{\text{CH}_4} = 0.02$, in hydrogen)

3.4. Mechanism Studies on CVD of Boron Carbide from BCl₃, CH₄ and H₂ Gas Mixture in a Dual Impinging Jet Reactor

In the previous section, an Arrhenius type rate expression was developed for the boron carbide formation rate on tungsten substrate. In this part, a detailed chemical investigation of CVD of boron carbide from a reaction gas mixture of BCl₃, CH₄, and H₂ will be presented to find a plausible reaction mechanism, to predict the formation rate of boron carbide, together with the rate of dichloroborane, which is the only stable intermediate observed in our system.

The mechanism studies are carried out with the rate data for the samples that are produced at 1150°C. At this temperature, the rate of boron carbide formation reaction increases up to a certain value of boron trichloride mole fractions, and then reaches a plateau and remains nearly constant. This result may be the indication of a first order adsorption of BCl₃ on the surface. This observation is also consistent with the study of Sezgi et. al. [17] in which boron deposition was considered to take place in a mechanism involving first order nondissociative adsorption of boron trichloride on the substrate surface.

Other reaction precursors, methane and hydrogen, may or may not adsorb on the surface, and react with adsorbed boron trichloride through Langmuir Hinshelwood or Rideal Eley type of surface reactions, respectively. A large number of reaction models consisting of different types of elementary reaction steps, involving various types of surface reactions, totally gas phase reactions, and some adsorption and desorption reactions were proposed to predict the formation rates

of boron carbide and dichloroborane simultaneously. The rate laws for the formation of boron carbide and dichloroborane were derived from the proposed models and tested with the independent experimental rate data using non-linear regression analysis. After regression process, the proposed models should predict both rates with an acceptable accuracy. Moreover, many of the models contained some common rate parameters appearing in two model rate expressions. So, it is necessary to fit the experimental data to the two model rate expressions simultaneously.

The various combinations of possible elementary reaction steps, together with the selection of the rate determining step among the elementary steps, are the factors that make the difference between the models. Some of the most probable elementary reaction steps considered for this system are shown in Table 3.3.

In the derivation of the models, the only stable adsorbed species were taken as BCl_3 , H_2 and CH_4 . The adsorption terms for the product gases HCl and BHCl_2 were not considered because such species are swept away from the surface during the impingement of the reactant gases to the substrate surface as implied by the FTIR analysis of the exit gases and material balance calculations.

Table 3.3. Some of the probable surface reactions considered for CVD of boron carbide

| | |
|---|-----|
| <u>Adsorption reactions</u> | |
| $\text{BCl}_3 + \text{s} \leftrightarrow \text{BCl}_3\text{s}$ (nondissociative) | a1 |
| $\text{BCl}_3 + 2\text{s} \rightarrow \text{BCl}_2\text{s} + \text{s.Cl}$ (dissociative) | a2 |
| $\text{BCl}_3 + 3\text{s} \rightarrow \text{BCls} + 2\text{Cls}$ (pyrolytic) | a3 |
| $\text{CH}_4 + \text{s} \leftrightarrow \text{CH}_4\text{s}$ (nondissociative) | a4 |
| $\text{CH}_4 + 2\text{s} \leftrightarrow \text{CH}_3\text{s} + \text{s.H}$ (dissociative) | a5 |
| $\text{CH}_4 + \text{s} \rightarrow \text{Cs} + 2\text{H}_2$ (dissociative) | a6 |
| $\text{H}_2 + 2\text{s} \leftrightarrow 2\text{Hs}$ (dissociative) | a7 |
| <u>Surface reactions for boron carbide formation</u> | |
| $\text{BCs} + \text{BCl}_3 + \text{H}_2 + \text{s} \rightarrow \text{B}_2\text{Cs} + 2\text{HCl} + \text{Cls}$ | b1 |
| $\text{B}_2\text{Cs} + \text{BCl}_3 + \text{H}_2 + \text{s} \rightarrow \text{B}_3\text{Cs} + 2\text{HCl} + \text{Cls}$ | b2 |
| $\text{B}_3\text{Cs} + \text{BCl}_3 + \text{H}_2 + \text{s} \rightarrow \text{B}_4\text{Cs} + 2\text{HCl} + \text{Cls}$ | b3 |
| $\text{BCs} + \text{BCls} + \text{H}_2 \rightarrow \text{B}_2\text{Cs} + \text{Hs} + \text{HCl}$ | b4 |
| $\text{B}_2\text{Cs} + \text{BCls} + \text{H}_2 \rightarrow \text{B}_3\text{Cs} + \text{Hs} + \text{HCl}$ | b5 |
| $\text{B}_3\text{Cs} + \text{BCls} + \text{H}_2 \rightarrow \text{B}_4\text{Cs} + \text{Hs} + \text{HCl}$ | b6 |
| $\text{BCls} + \text{Cs} + \text{H}_2 \rightarrow \text{BCs} + \text{Hs} + \text{HCl}$ | b7 |
| $\text{BCs} + \text{BCl}_3\text{s} + \text{H}_2 \rightarrow \text{B}_2\text{Cs} + 2\text{HCl} + \text{Cls}$ | b8 |
| $\text{B}_2\text{Cs} + \text{BCl}_3\text{s} + \text{H}_2 \rightarrow \text{B}_3\text{Cs} + 2\text{HCl} + \text{Cls}$ | b9 |
| $\text{B}_3\text{Cs} + \text{BCl}_3\text{s} + \text{H}_2 \rightarrow \text{B}_4\text{Cs} + 2\text{HCl} + \text{Cls}$ | b10 |
| $\text{BCs} + \text{BCl}_3 + 3/2 \text{H}_2 \rightarrow \text{B}_2\text{Cs} + 3\text{HCl}$ | b11 |
| $\text{B}_2\text{Cs} + \text{BCl}_3 + 3/2 \text{H}_2 \rightarrow \text{B}_3\text{Cs} + 3\text{HCl}$ | b12 |
| $\text{B}_3\text{Cs} + \text{BCl}_3 + 3/2 \text{H}_2 \rightarrow \text{B}_4\text{Cs} + 3\text{HCl}$ | b13 |
| <u>Surface reactions for BCl_3 decomposition</u> | |
| $\text{BCl}_3\text{s} + \text{H}_2 \rightarrow \text{BCls} + 2\text{HCl}$ | c1 |
| $\text{BCl}_3\text{s} + \text{Hs} \rightarrow \text{BCl}_2\text{s} + \text{HCl}$ | c2 |

Table 3.3. Some of the probable surface reactions considered for CVD of boron carbide (cont'd)

| | |
|--|-----|
| $\text{BCl}_3\text{s} + \text{s} \rightarrow \text{BCl}_2\text{s} + \text{Cl}_\text{s}$ | c3 |
| $\text{BCl}_2\text{s} + \text{H}_\text{s} \rightarrow \text{BCl}_\text{s} + \text{HCl}_\text{s}$ | c4 |
| $\text{BCl}_\text{s} + \text{CH}_4 \rightarrow \text{BC}_\text{s} + \text{HCl} + 3/2\text{H}_2$ | c5 |
| $\text{BCl}_3\text{s} + \text{CH}_4 \rightarrow \text{BC}_\text{s} + 3\text{HCl} + 1/2\text{H}_2$ | c6 |
| $\text{BCl}_3\text{s} + \text{CH}_4 \rightarrow \text{BHC}_\text{s} + 3\text{HCl}$ | c7 |
| $\text{BCl}_3 + \text{CH}_3\text{s} \rightarrow \text{BC}_\text{s} + 3\text{HCl}$ | c8 |
| $\text{BCl}_3\text{s} + \text{CH}_3\text{s} \rightarrow \text{BC}_\text{s} + 3\text{HCl} + \text{s}$ | c9 |
| $\text{BCl}_3\text{s} + \text{C}_\text{s} + 2\text{H}_2 \rightarrow \text{BC}_\text{s} + 3\text{HCl} + \text{H}_\text{s}$ | c10 |
| $\text{BCl}_2\text{s} + \text{H}_\text{s} \rightarrow \text{BCl}_\text{s} + \text{HCl} + \text{s}$ | c11 |
| $\text{BCl}_3\text{s} + \text{H}_2 \rightarrow \text{BHCl}_2\text{s} + \text{HCl}$ | c12 |
| <u>BHCl₂ formation</u> | |
| $\text{BCl}_3\text{s} + \text{H}_2 + \text{ns} \rightarrow \text{BHCl}_2\text{s} + \text{HCl}_\text{s} + (\text{n}-1)\text{s}$ | d1 |
| $\text{BCl}_3\text{s} + 2(\text{H}_\text{s}) \rightarrow \text{BHCl}_2\text{s} + \text{HCl}_\text{s} + \text{s}$ | d2 |
| $\text{BCl}_2\text{s} + \text{H}_\text{s} \rightarrow \text{BHCl}_2\text{s} + \text{s}$ | d3 |
| $\text{BCl}_3\text{s} + 2\text{H}_\text{s} \rightarrow \text{BHCl}_2 + \text{HCl} + 3\text{s}$ | d4 |
| $\text{BCl}_3\text{s} + \text{H}_2 \rightarrow \text{BHCl}_2 + \text{HCl} + \text{s}$ | d5 |
| <u>Desorption reactions</u> | |
| $\text{BHCl}_2\text{s} \rightarrow \text{BHCl}_2 + \text{s}$ | e1 |
| $\text{HCl}_\text{s} \rightarrow \text{HCl} + \text{s}$ | e2 |
| $\text{BCl}_2\text{s} \rightarrow \text{BCl}_2 + \text{s}$ | e3 |
| $\text{BCl}_\text{s} \rightarrow \text{BCl} + \text{s}$ | e4 |
| <u>Decomposition of BHCl₂</u> | |
| $\text{BHCl}_2\text{s} + \text{s} \rightarrow \text{BCl}_2\text{s} + \text{H}_\text{s}$ | f1 |
| $\text{BHCl}_2\text{s} + \text{BCl}_3\text{s} \rightarrow 2\text{BCl}_2\text{s} + \text{HCl}$ | f2 |
| $\text{BHCl}_2\text{s} + \text{H}_\text{s} + \text{s} \rightarrow \text{B}_\text{s} + 2\text{HCl}_\text{s}$ | f3 |

BCl_3 adsorption on the substrate surface may be dissociative, partially dissociative or nondissociative (molecular) (Table 3.3, a1-a3). Among the extensive number of the models considered, only the ones in which molecular adsorption of boron trichloride on the surface was included in the mechanisms (a1) gave reasonable fits for the boron carbide formation rate. Hydrogen adsorption was considered to be dissociative (a7) at the substrate temperature studied, however methane adsorption could be either molecular (a4), or dissociative (a5-a6). Free carbon adsorbed to the surface further may react with adsorbed boron trichloride to start the formation of boron carbide phase.

The almost linear increase of the dichloroborane formation rate with initial boron trichloride molar fractions could be mainly due to the gas phase formation reactions. Modelling studies revealed that, the models in which dichloroborane formation reactions was considered to take place only in gas phase, gave very good fits, for the formation rates of both species. On the other hand, models containing surface reaction steps in addition to the gas phase formation reaction for dichloroborane formation (d1-d3), gave poor fits, especially to predict the deposition rate of boron carbide. Moreover, according to the subsequent curve fitting process, the gas phase reaction of dichloroborane formation should be elementary and first order with respect to BCl_3 concentration. Since the hydrogen participates in reaction, one would expect the rate law to have the form $r = P_{\text{BCl}_3} P_{\text{H}_2}$. Because hydrogen is always present in great excess, its concentration remains essentially constant in a given run. Therefore hydrogen was excluded from the rate law and the reaction becomes pseudo first order. In spite of the absence of any decomposition products of BHCl_2

on the solid phase, further dissociation of dichloroborane (f1-f3) was considered in some models and as expected the mechanisms involving such reactions gave poor fits.

Boron carbide formation reactions were considered to take place through successive series reactions, in which boron and carbon atoms are incorporated into the solid structure to form boron carbide finally (b1-b13). In order to eliminate the coverage dependent terms in the final form of the rate equations, steady state approximations were applied for the boron-carbon containing intermediates appearing in the successive series reactions.

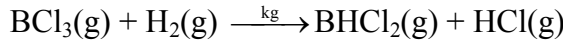
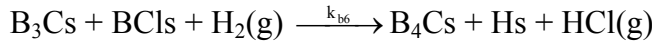
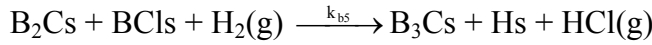
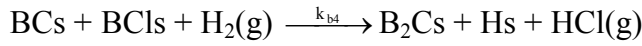
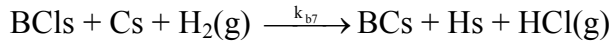
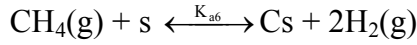
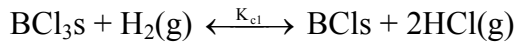
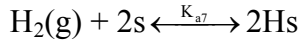
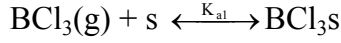
The reactions leading adsorbed boron trichloride to decompose through surface reactions involve the reaction of adsorbed BCl_3 with either gas phase hydrogen and methane (c1, c5-c7), or through reactions involving adsorbed hydrogen (c2), or adsorbed methane (c8).

More than 30 reaction mechanism models were proposed, and among them, following 10 will be considered here.

Model 1

In this model boron trichloride, hydrogen and methane gases were considered to be adsorbed on the substrate surface. Boron trichloride adsorption is thought to be nondissociative, whereas hydrogen and methane adsorptions were taken as dissociative adsorptions. Adsorbed boron trichloride reacts with gaseous hydrogen through a Rideal-Eley type of a reaction mechanism to yield BCl_s, which then reacts with

carbon and hydrogen to produce adsorbed BC. BC reacts with adsorbed BCl and gaseous hydrogen in successive steps to produce boron carbide finally. Dichloroborane is produced through the gas phase reaction between hydrogen and boron trichloride, as well as through the surface reaction of adsorbed boron trichloride and dissociatively adsorbed hydrogen.



The rate limiting step was considered to be the boron carbide formation reaction step. According to the equilibrium calculations, the dependencies of boron carbide and dichloroborane formation reactions on the partial pressures of the reaction gases were calculated as follows;

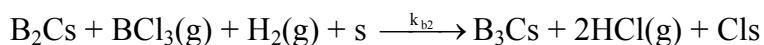
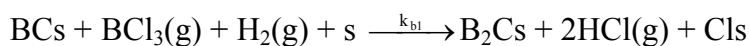
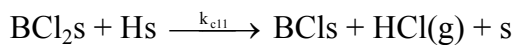
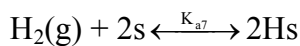
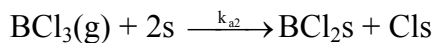
$$R_{\text{B}_4\text{C}} = \frac{k_{b7} K_{a1} K_{c1} K_{a6} P_{\text{BCl}_3} P_{\text{CH}_4}}{P_{\text{HCl}}^2 (1 + K_{a1} P_{\text{BCl}_3} + K_{a6} P_{\text{CH}_4} / P_{\text{H}_2}^2 + (K_{a7} P_{\text{H}_2})^{1/2})^2} \quad (3.25)$$

$$R_{\text{BHCl}_2} = \frac{k_{d4} K_{a1} K_{a7} P_{\text{H}_2} P_{\text{BCl}_3}}{(1 + K_{a1} P_{\text{BCl}_3} + K_{a6} P_{\text{CH}_4} / P_{\text{H}_2}^2 + (K_{a7} P_{\text{H}_2})^{1/2})^3} + k_g P_{\text{BCl}_3} P_{\text{H}_2} \quad (3.26)$$

The model equations were tested with the experimental data, and the results are depicted in Figures 3.15, 3.16, 3.17, 3.18. As it is seen that the model gave poor fit to the experimentally observed data. The model is especially deficient for determining the rate of boron carbide formation reaction. The model parameters together with the correlation coefficients for both reactions are given in Table 3.4.

Model 2

In this model, dissociative adsorption of boron trichloride and hydrogen on the substrate surface is considered. Dissociated intermediate products, BCl_2s and Hs , react on the surface and BCls (adsorbed BCl on the surface) is formed. BCls then undergoes a Rideal-Eley type of a surface reaction with gaseous methane to form BCs . BCs is reacted with gaseous boron trichloride and hydrogen in successive series reactions in the presence of a vacant site, and in each step one boron atom is added to BC , finally forming boron carbide on the substrate surface. Dichloroborane formation is considered to take place in gaseous phase and through surface reactions in this model. In surface reactions, BCl_2s is reacted with adsorbed hydrogen to form adsorbed dichloroborane, which then desorbed to the gaseous phase leaving an empty site behind. The elementary reaction steps proposed for this mechanism are as follows;



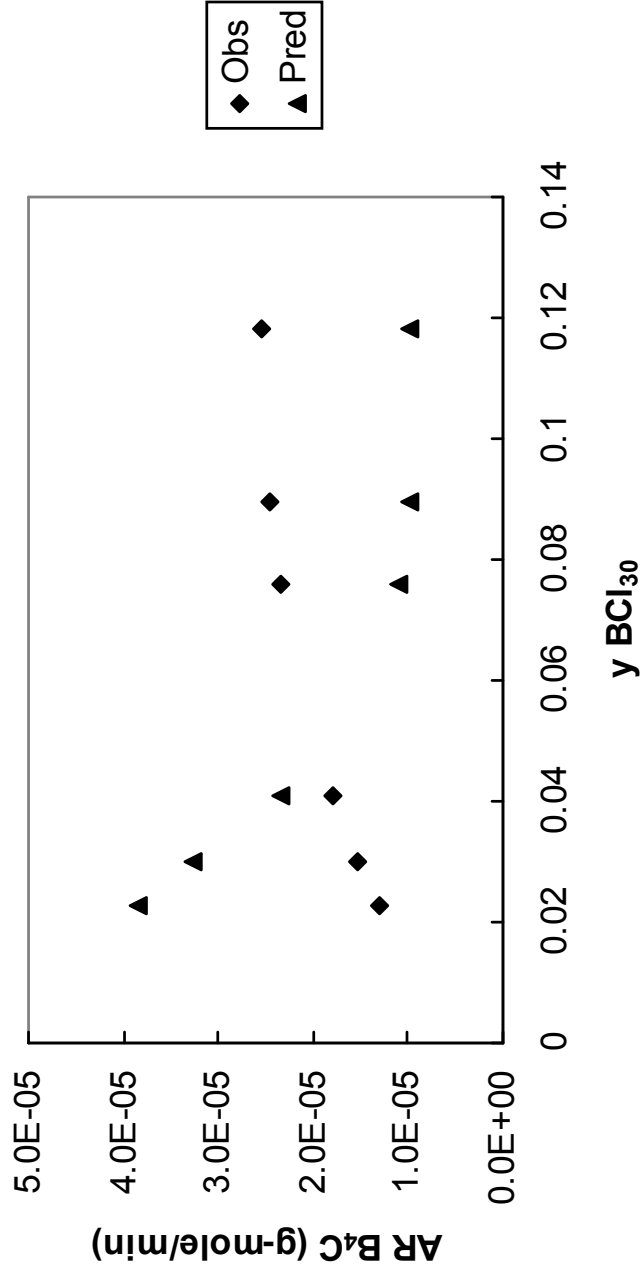


Figure 3.15 Comparison of the effect of BCl₃ inlet mole fractions on the observed and Model 1 predicted formation rates of B₄C (T=1150°C, y CH₄₀=0.02 in hydrogen, y_{BCl₃₀}/y_{CH₄₀}= 1.5- 5.5, simultaneous analysis)

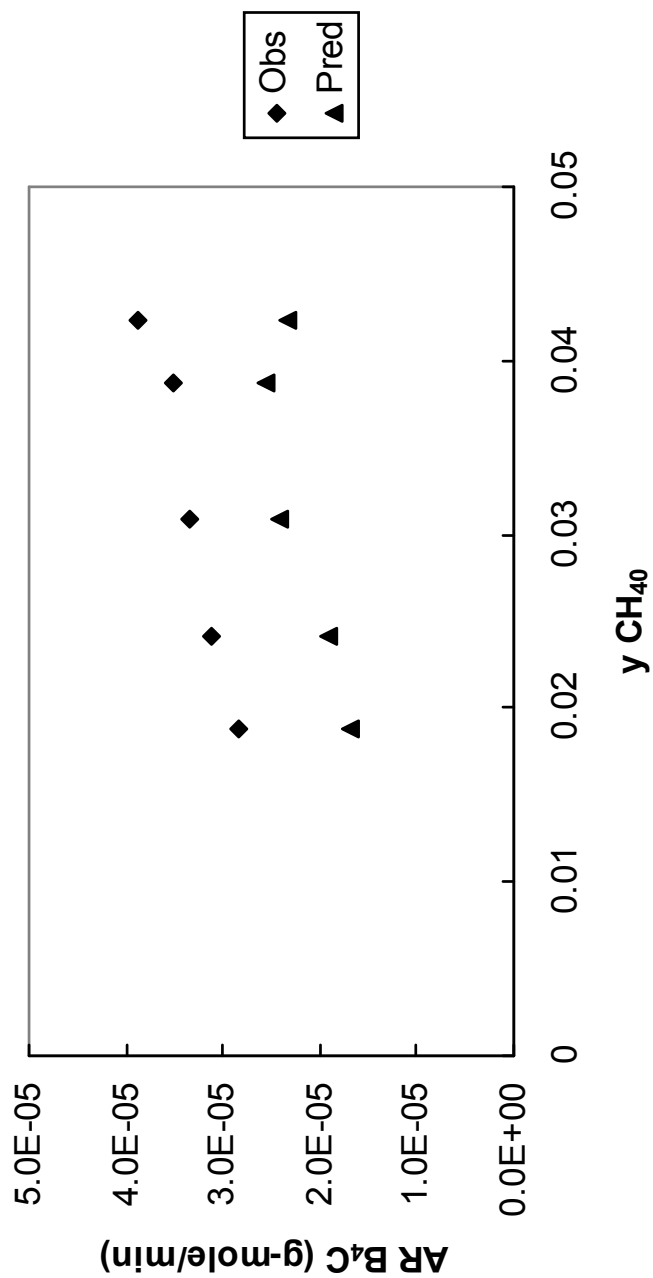


Figure 3.16 Comparison of the effect of CH₄ inlet mole fractions on the observed and Model 1 predicted formation rates of B₄C (T=1150°C, y BCl₃₀=0.084 in hydrogen, y_{BCl30}/y_{CH40}=2-4.5, simultaneous analysis)

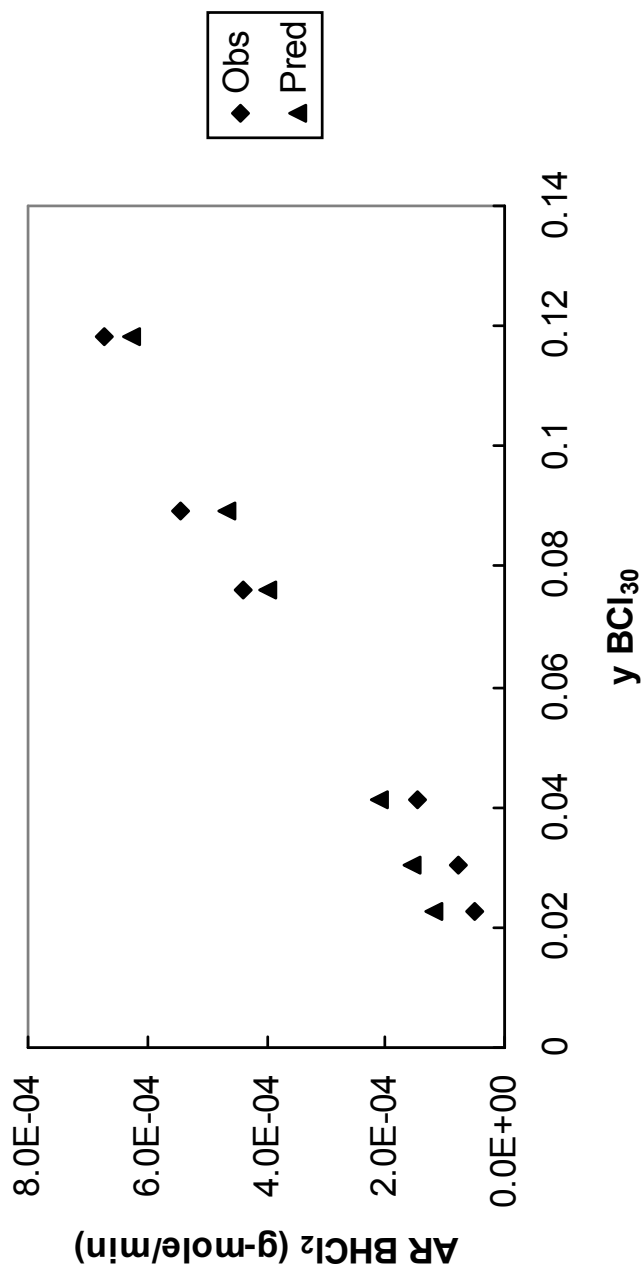


Figure 3.17 Comparison of the effect of BCl₃ inlet mole fractions on the observed and Model 1 predicted formation rates of BHCl₂ (T=1150°C, y CH₄₀=0.02 in hydrogen, y_{BCl₃₀}/y_{CH₄₀}= 1.5- 5.5, simultaneous analysis)

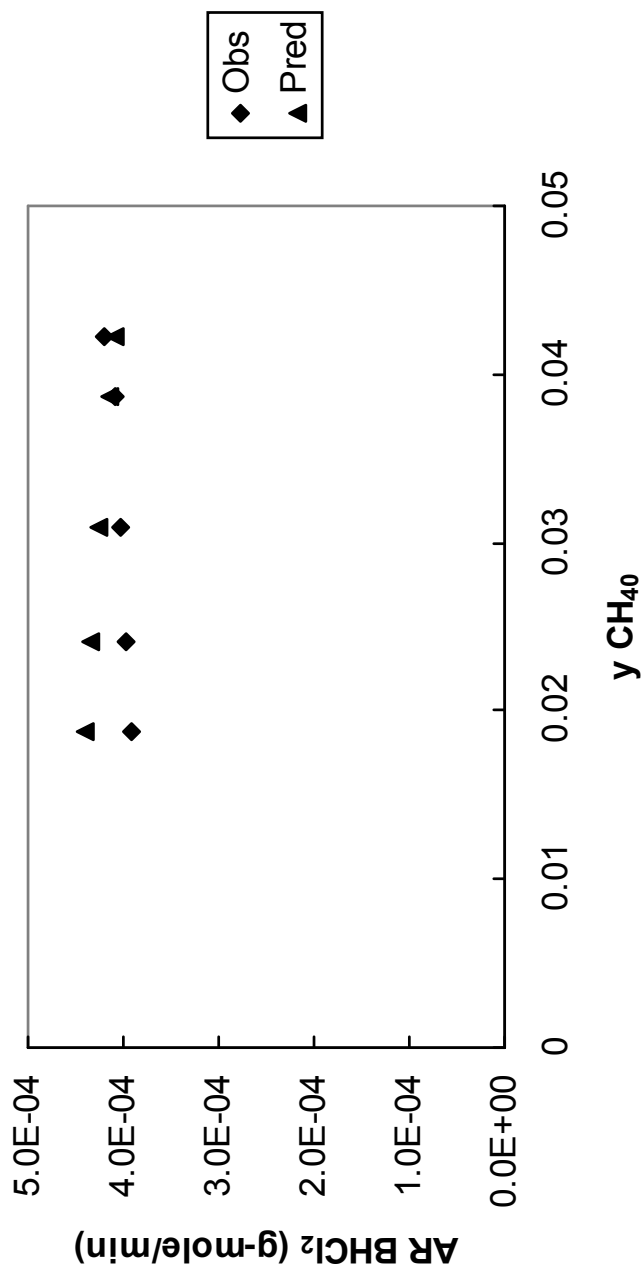
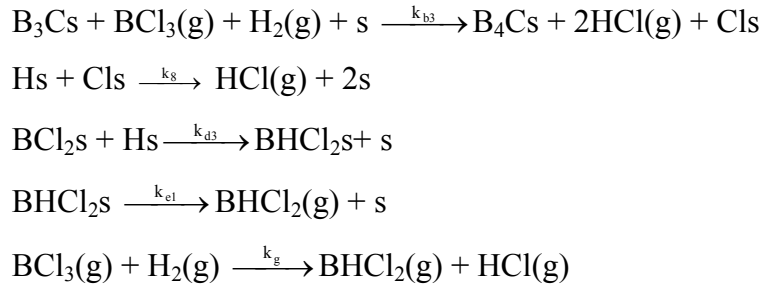


Figure 3.18 Comparison of the effect of CH₄ inlet mole fractions on the observed and Model 1 predicted formation rates of BHC₁₂ (T=1150°C, y BCl₃₀=0.084 in hydrogen, y_{BCl30}/y_{CH40}=2-4.5, simultaneous analysis)



Using these 11 elementary steps, the rate laws for the production rates of boron carbide and dichloroborane were calculated as follows;

$$R_{\text{B}_4\text{C}} = \frac{\frac{k_{a2}k_{c11}}{k_{c11} + k_{d3}} P_{\text{BCl}_3}}{\left(1 + \frac{k_{a2}}{(k_{c11} + k_{d3})K_{a7}^{1/2}} \frac{P_{\text{BCl}_3}}{P_{\text{H}_2}^{1/2}} + (K_{a7}P_{\text{H}_2})^{1/2}\right)^2} \quad (3.27)$$

$$R_{\text{BHCl}_2} = \frac{\frac{k_{d3}}{k_{c11} + k_{d3}} P_{\text{BCl}_3}}{\left(1 + \frac{k_{a2}}{(k_{c11} + k_{d3})K_{a7}^{1/2}} \frac{P_{\text{BCl}_3}}{P_{\text{H}_2}^{1/2}} + (K_{a7}P_{\text{H}_2})^{1/2}\right)^2} + k_g P_{\text{BCl}_3} P_{\text{H}_2} \quad (3.28)$$

The two model equations were tested simultaneously with the experimental data, and the results are given in Figures 3.19, 3.20, 3.21 and 3.22. This model predicts the formation rate of boron carbide better than the previous model, but still far from the desired accuracy, with an R-squared value of 0.22. The model parameters and calculated R-squared values are given in Table 3.4.

Model 3

In this model, boron trichloride is adsorbed on the substrate surface, and adsorbed boron trichloride then reacts with gaseous methane to produce BCs. Then boron is added to BCs in the successive reactions with gaseous boron trichloride and hydrogen. In each successive reactions, HCl gas is produced as a by-product. Boron carbide formation reaction, is considered to be the slowest reaction,

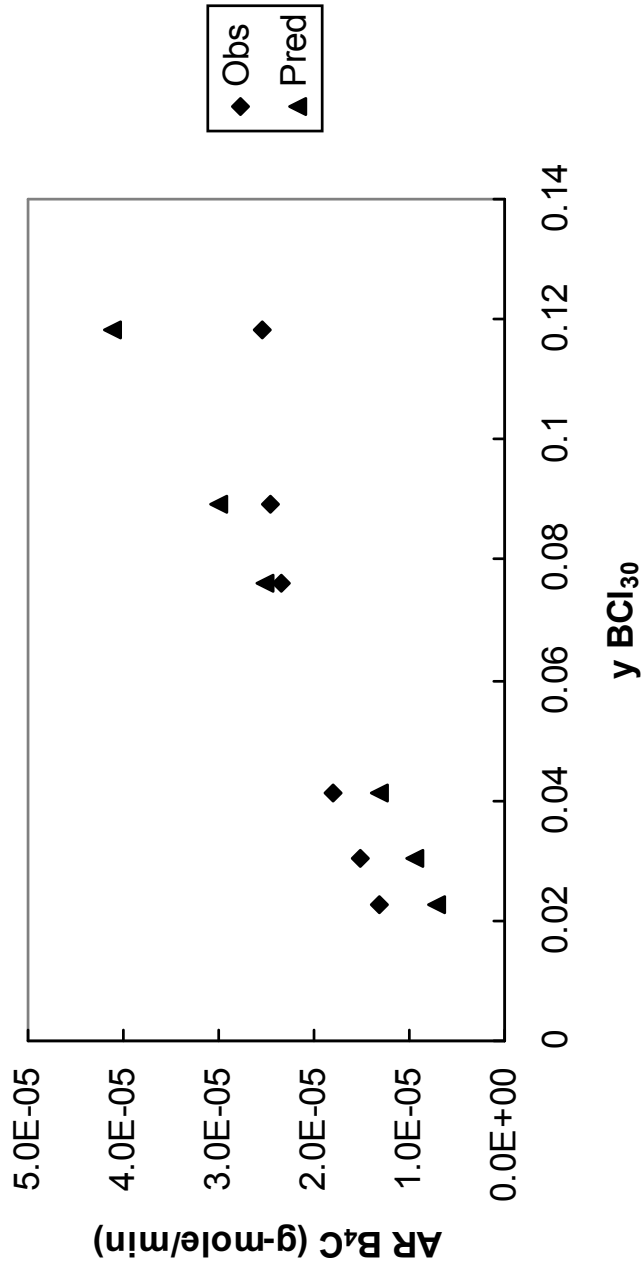


Figure 3.19 Comparison of the effect of BCl₃ inlet mole fractions on the observed and Model 2 predicted formation rates of B₄C (T=1150°C, y CH₄₀=0.02 in hydrogen, y_{BCl₃₀}/y_{CH₄₀}= 1.5- 5.5, simultaneous analysis)

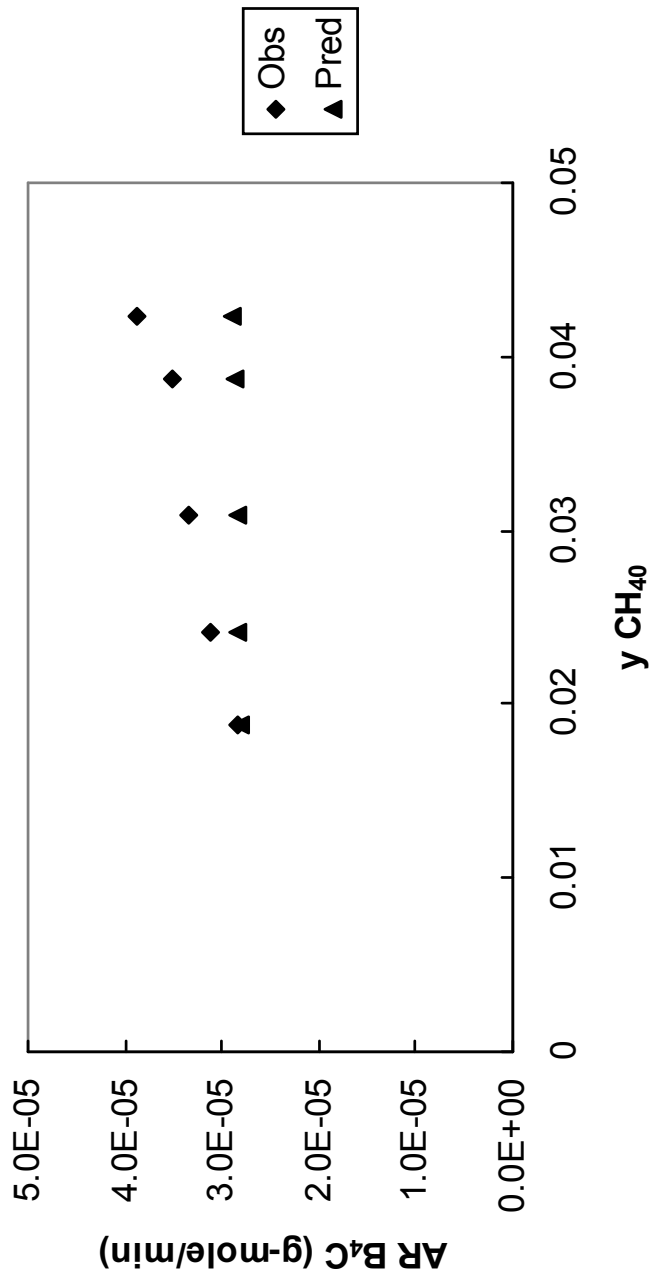


Figure 3.20 Comparison of the effect of CH₄ inlet mole fractions on the observed and Model 2 predicted formation rates of B₄C (T=1150°C, y BCl₃₀=0.084 in hydrogen, y_{BCl₃₀}/y_{CH₄₀}=2-4.5, simultaneous analysis)

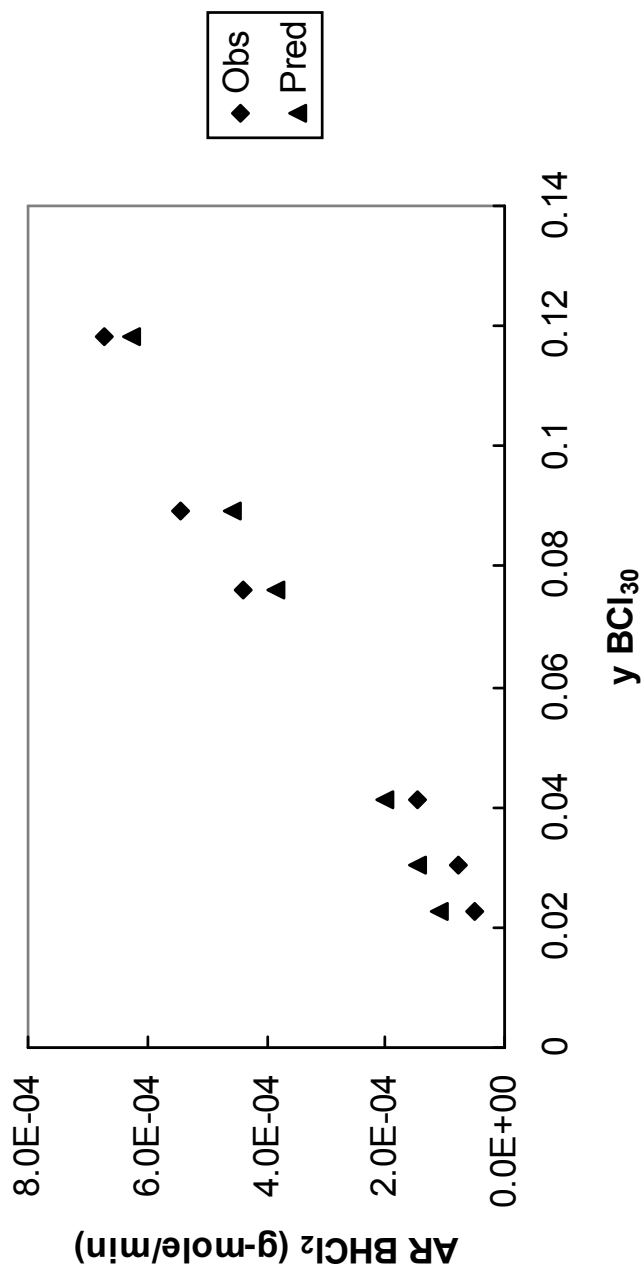


Figure 3.21 Comparison of the effect of BCl₃ inlet mole fractions on the observed and Model 2 predicted formation rates of BHCl₂ (T=1150°C, y CH₄₀=0.02 in hydrogen, y BCl₃₀/y CH₄₀= 1.5- 5.5, simultaneous analysis)

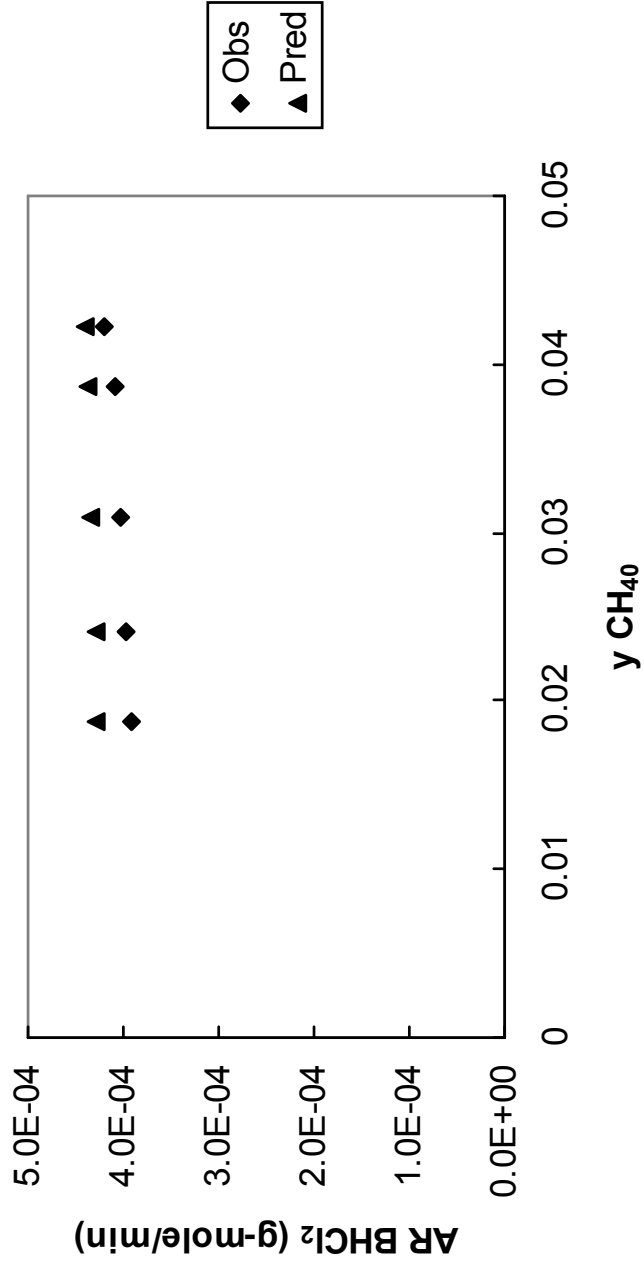
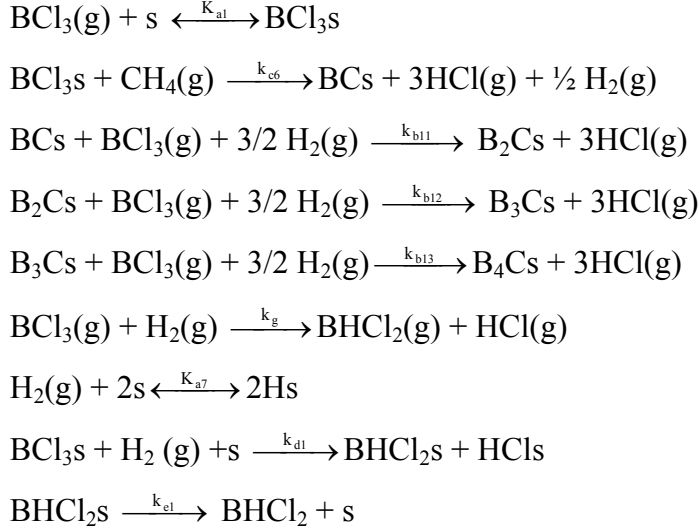


Figure 3.22 Comparison of the effect of CH₄ inlet mole fractions on the observed and Model 2 predicted formation rates of BHC₁₂ (T=1150°C, y BCl₃₀=0.084 in hydrogen, y_{BCl30}/y_{CH40}=2-4.5, simultaneous analysis)

which, means that this reaction is the rate limiting step in this proposed mechanism. The elementary reaction steps are;



The rate expressions derived for this mechanism are;

$$R_{\text{B}_4\text{C}} = \frac{K_{a1}k_{c6}P_{\text{CH}_4}P_{\text{BCl}_3}}{1 + K_{a1}P_{\text{BCl}_3} + (K_{a7}P_{\text{H}_2})^{1/2}} \quad (3.29)$$

$$R_{\text{BHCl}_2} = \frac{k_{d1}K_{a1}P_{\text{H}_2}P_{\text{BCl}_3}}{(1 + K_{a1}P_{\text{BCl}_3} + (K_{a7}P_{\text{H}_2})^{1/2})^2} + k_gP_{\text{BCl}_3}P_{\text{H}_2} \quad (3.30)$$

The results of the nonlinear curve fitting procedure of this model to the observed kinetic data are shown in Figures 3.23 through 26. Although the simultaneous analysis of the experimental data gave reasonable fit to predict the effect of inlet BCl_3 on formation rate of B_4C , the model failed in predicting the effect of inlet CH_4 mole fraction on the B_4C formation rate (see Figure 3.24).

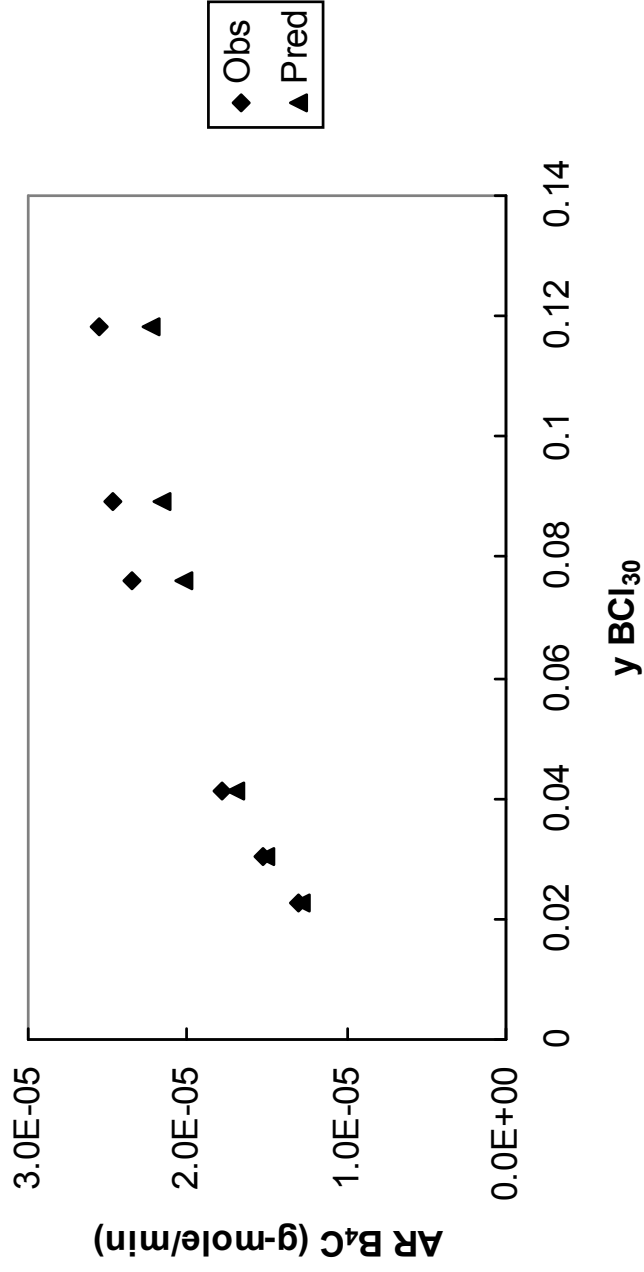


Figure 3.23 Comparison of the effect of BCl₃ inlet mole fractions on the observed and Model 3 predicted formation rates of B₄C (T=1150°C, y CH₄₀=0.02 in hydrogen, y_{BCl₃₀}/y_{CH₄₀}= 1.5- 5.5, simultaneous analysis)

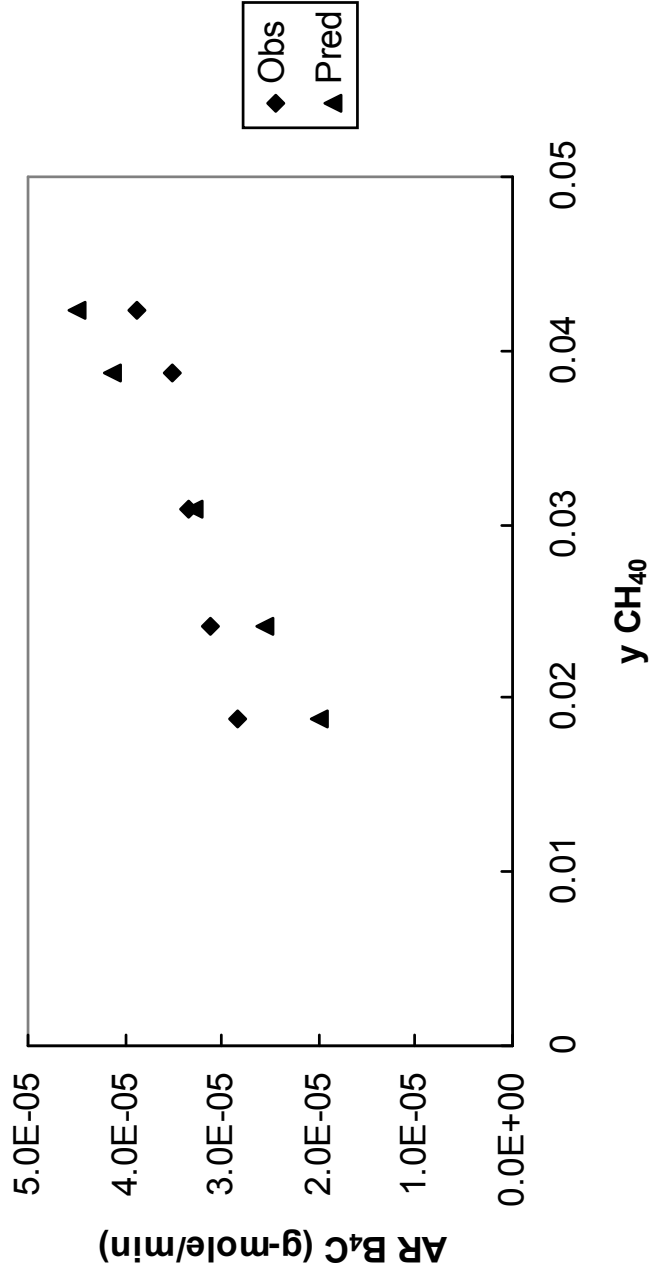


Figure 3.24 Comparison of the effect of CH₄ inlet mole fractions on the observed and Model 3 predicted formation rates of B₄C (T=1150°C, y BCl₃₀=0.084 in hydrogen, y_{BCl₃₀}/y_{CH₄₀}=2-4.5, simultaneous analysis)

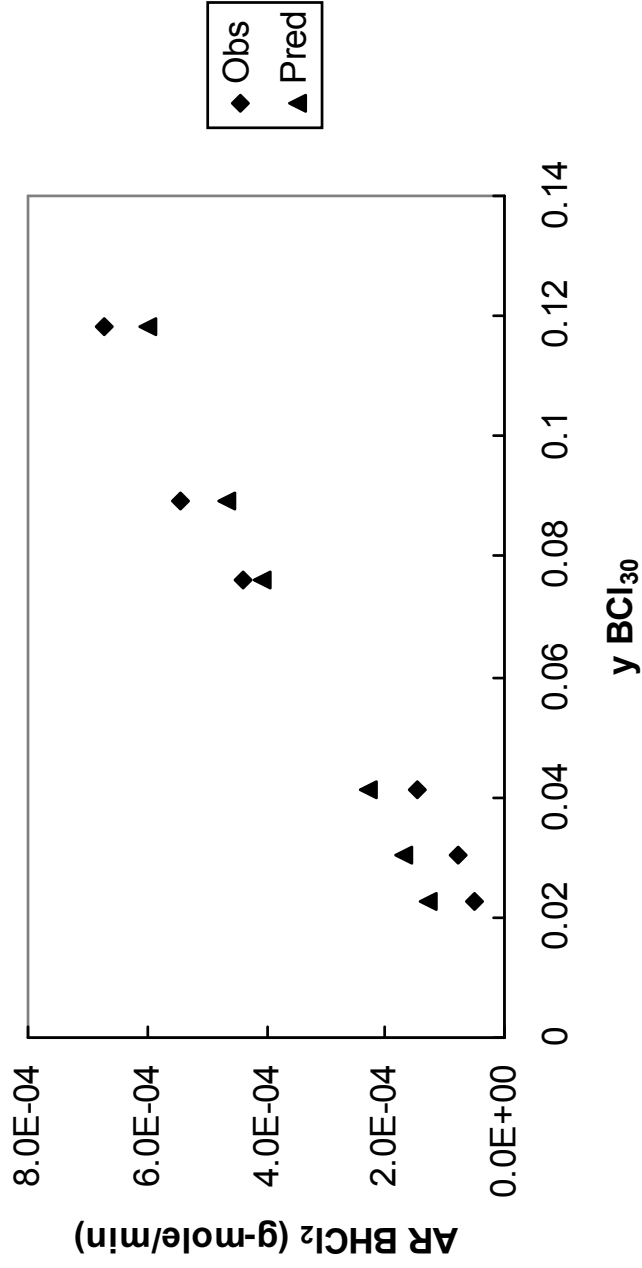


Figure 3.25 Comparison of the effect of BCl₃ inlet mole fractions on the observed and Model 3 predicted formation rates of BHCl₂ (T=1150°C, y CH₄₀=0.02 in hydrogen, y BCl₃₀/y CH₄₀= 1.5- 5.5, simultaneous analysis)

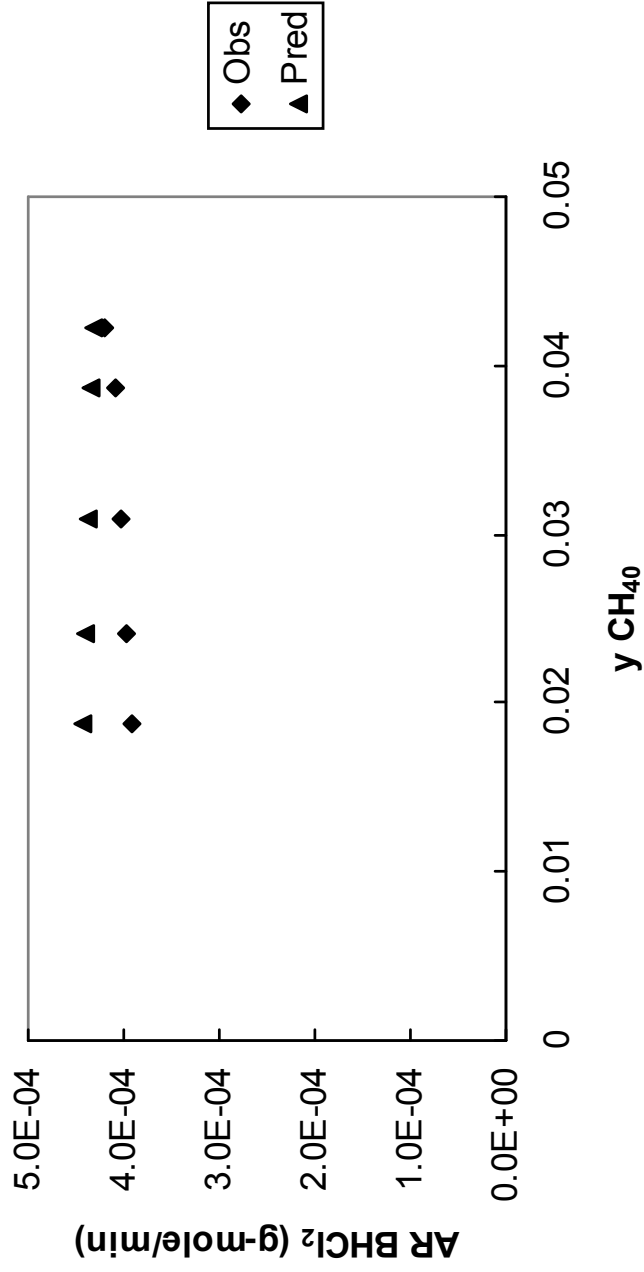
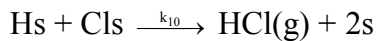
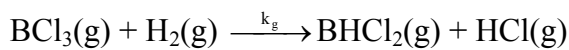
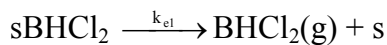
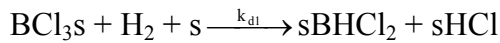
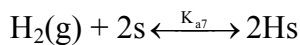
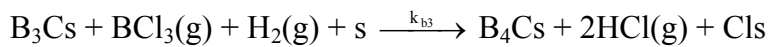
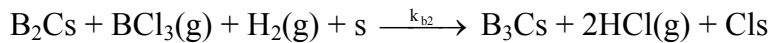
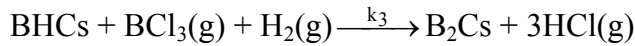
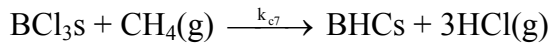
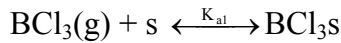


Figure 3.26 Comparison of the effect of CH₄ inlet mole fractions on the observed and Model 3 predicted formation rates of BHCl₂ (T=1150°C, y BCl₃₀=0.084 in hydrogen, y_{BCl30}/y_{CH40}=2-4.5, simultaneous analysis)

Model 4

In this model boron trichloride and hydrogen gases are adsorbed on the solid surface. Then adsorbed boron trichloride reacts with gaseous methane to produce an intermediate in the form of BHCs. Then boron is added to BHCs in the successive reactions with gaseous boron trichloride and hydrogen. In each successive reactions, HCl gas is produced as a by-product. Adsorbed boron trichloride also reacts with hydrogen, in the vicinity of a vacant site to produce adsorbed dichloroborane, which then is desorbed back to the gaseous phase.

The rate of dichloroborane formation reaction is considered to be assisted by this surface reaction series, in addition to the contribution of gas phase formation reaction. The elementary reaction steps are;



The rate expressions derived for Mechanism 4 are ;

$$R_{B_4C} = \frac{k_{c7} K_{a1} P_{CH_4} P_{BCl_3}}{(1 + K_{a1} P_{BCl_3} + (K_{a7} P_{H_2})^{1/2})^2} \quad (3.31)$$

$$R_{BHCl_2} = \frac{k_{d1} K_{a1} P_{H_2} P_{BCl_3}}{(1 + K_{a1} P_{BCl_3} + (K_{a7} P_{H_2})^{1/2})^2} + k_g P_{BCl_3} P_{H_2} \quad (3.32)$$

The rate parameters of this model was found by fitting the experimental data to the rate expressions, simultaneously. The rate parameters are given in Table 3.4. The simultaneous analysis of the rate expressions with the experimental data predicted the BCl_3 effect on the formation rate of B_4C well for low inlet BCl_3 compositions (See Figure 3.27). However at high BCl_3 inlet molar fractions, the model failed. For the effects of inlet CH_4 and BCl_3 molar fraction on the $BHCl_2$ formation rate and for the effect of inlet CH_4 molar fraction on B_4C formation rate, the model does not give satisfactory fit to the experimental data, either, as can be seen in Figures 3.28 through 3.30, and corresponding correlation coefficient values given in Table 3.4.

Model 5

In this model, BCs is formed from the reaction of adsorbed boron trichloride and gaseous methane in a reversible equilibrium reaction, rather than an irreversible reaction. The rate limiting step is assumed to be the step in which, boron carbide is formed on the solid surface. This model assumes that, the adsorption term for hydrogen is negligible, so hydrogen adsorption is not considered in the model. Adsorbed dichloroborane is produced on the surface through the reaction of adsorbed borontrichloride and gaseous hydrogen in an equilibrium stage. Then dichloroborane is desorbed to the gaseous

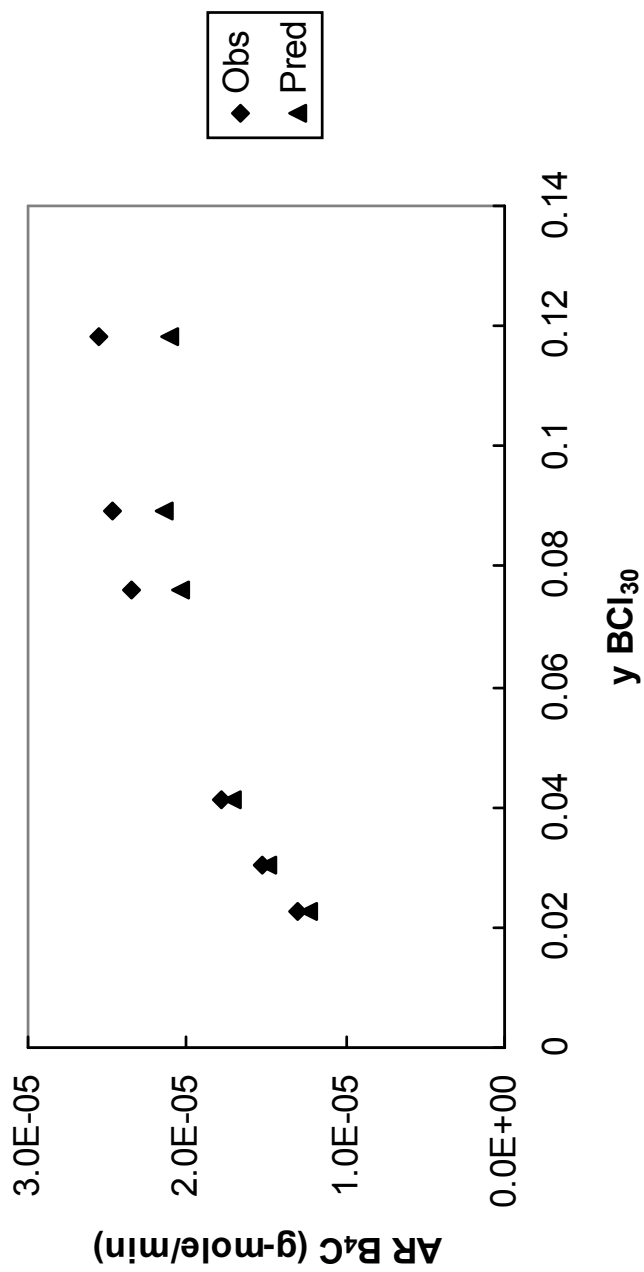


Figure 3.27 Comparison of the effect of BCl₃ inlet mole fractions on the observed and Model 4 predicted formation rates of B₄C (T=1150°C, y CH₄₀=0.02 in hydrogen, y BCl₃₀/y CH₄₀= 1.5- 5.5, simultaneous analysis)

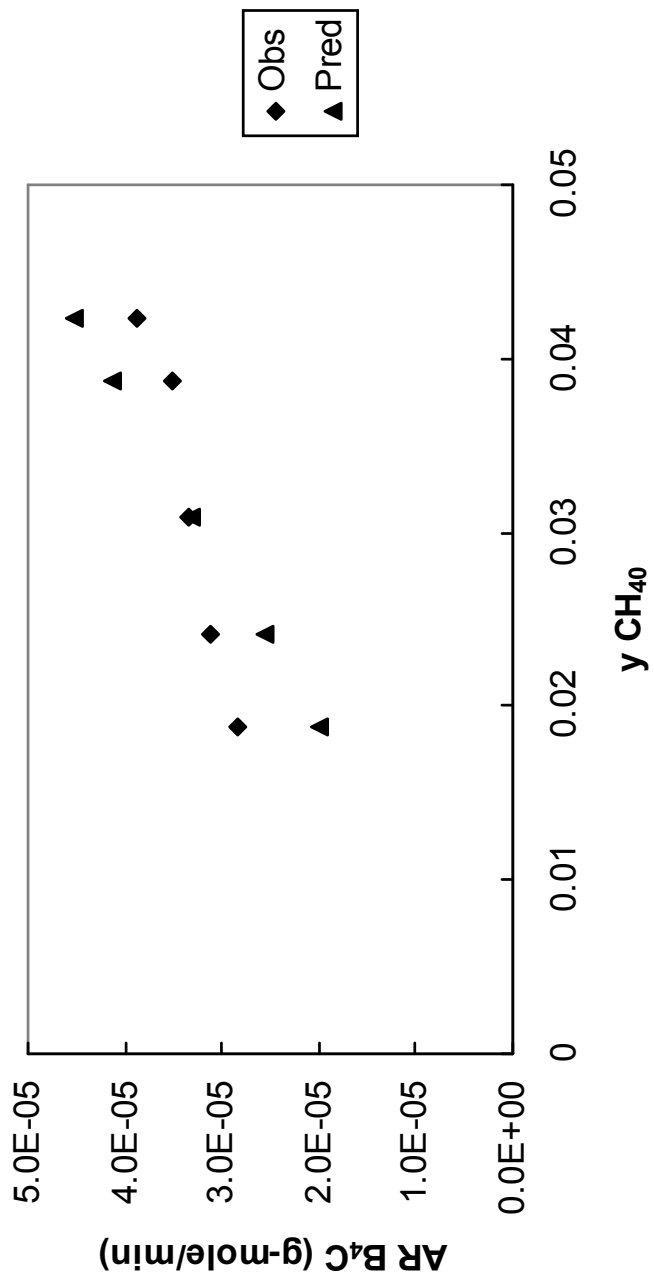


Figure 3.28 Comparison of the effect of CH₄ inlet mole fractions on the observed and Model 4 predicted formation rates of B₄C (T=1150°C, y BCl₃₀=0.084 in hydrogen, y_{BCl₃₀}/y_{CH₄₀}=2-4.5, simultaneous analysis)

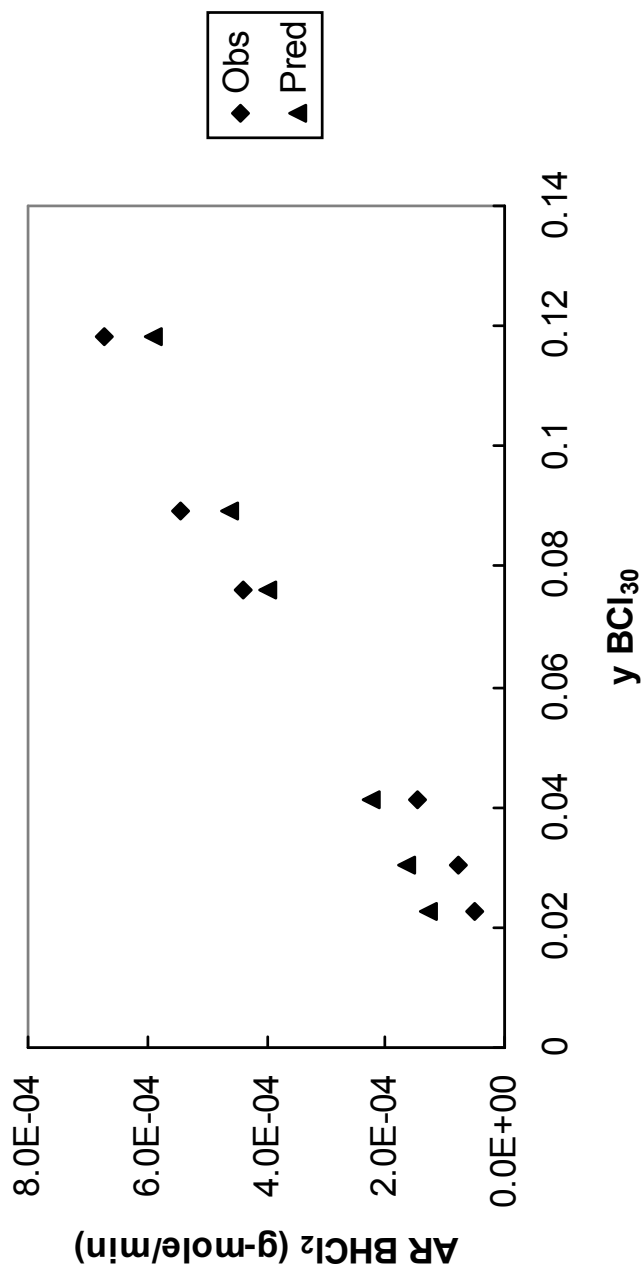


Figure 3.29 Comparison of the effect of BCl₃ inlet mole fractions on the observed and Model 4 predicted formation rates of BHCl₂ (T=1150°C, y CH₄₀=0.02 in hydrogen, y BCl₃₀/y CH₄₀= 1.5- 5.5, simultaneous analysis)

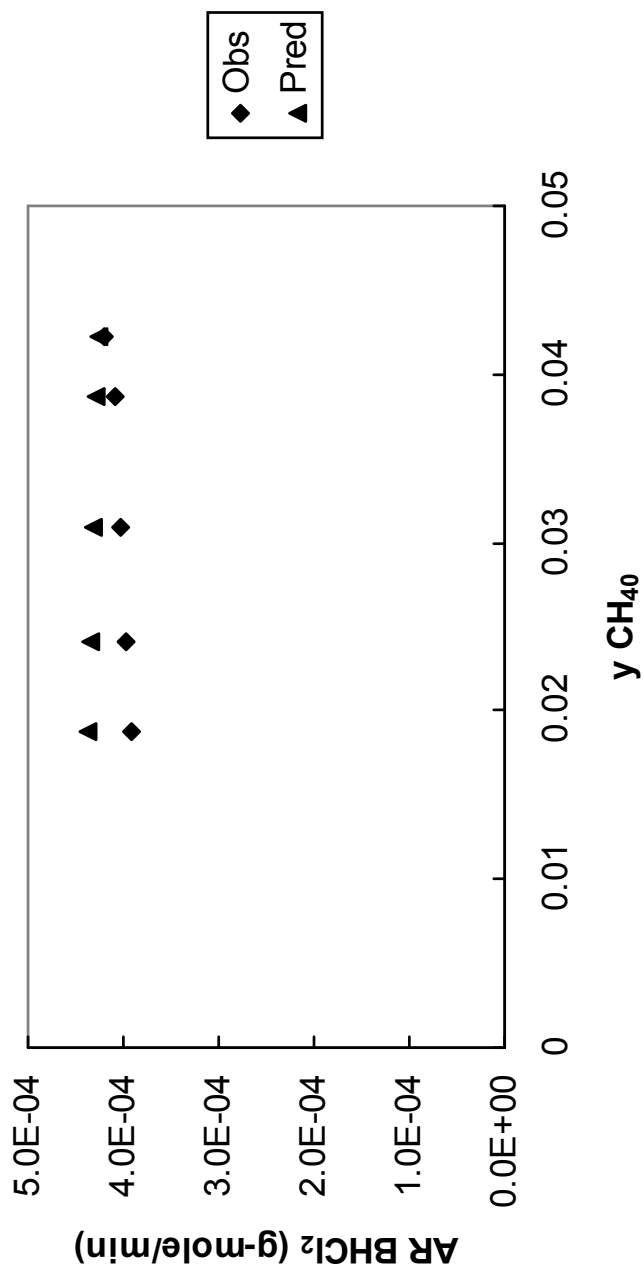
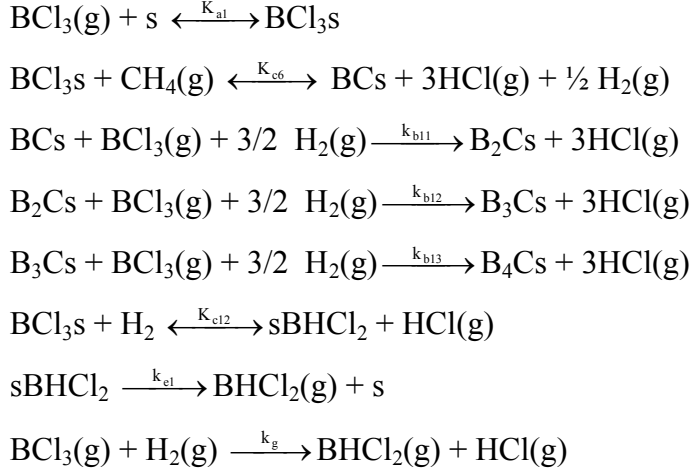


Figure 3.30 Comparison of the effect of CH₄ inlet mole fractions on the observed and Model 4 predicted formation rates of BHC1₂ (T=1150°C, y BCl₃₀=0.084 in hydrogen, y_{BCl30}/y_{CH40}=2-4.5, simultaneous analysis)

phase, together with the gas phase formation of dichloroborane from borontrichloride and hydrogen. The model is as follows;



The corresponding rate expressions derived for this model are;

$$R_{\text{B}_4\text{C}} = \frac{k_{b11} K_{a1} K_{c6} P_{\text{CH}_4} P_{\text{BCl}_3}^2 P_{\text{H}_2}}{P_{\text{HCl}}^3 (1 + K_{a1} P_{\text{BCl}_3})} \quad (3.33)$$

$$R_{\text{BHCl}_2} = \frac{k_{e1} K_{a1} K_{c12} P_{\text{H}_2} P_{\text{BCl}_3}}{P_{\text{HCl}} (1 + K_{a1} P_{\text{BCl}_3})} + k_g P_{\text{BCl}_3} P_{\text{H}_2} \quad (3.34)$$

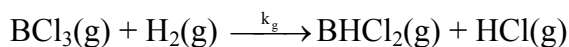
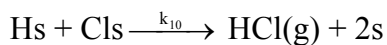
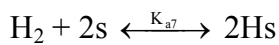
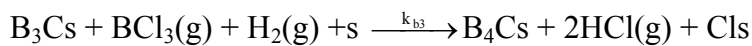
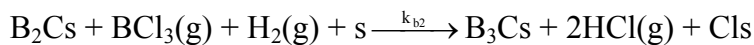
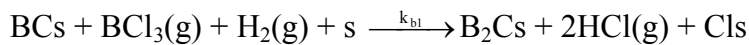
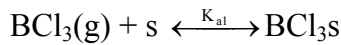
The parameters of these two expressions were found by simultaneous fit of the experimental data to the derived rate equations. The statistical analysis of the results showed a very poor fit to experimental data for the formation of boron carbide. The reason behind this is the existence of the HCl term in the denominator of boron carbide formation reaction, which appears on the rate expression due to the presence of the equilibrium reaction steps for the formation of BCs. This is a similar result with Model 3, in which HCl also appears in the denominator of the expression for the boron carbide formation reaction. The BHCl₂ formation reaction is well

described for this model, on the other hand, with an R-squared value of 0.894. The results are depicted in Figures 3.31, 3.32, 3.33 and 3.34.

Model 6

In model 6, boron trichloride and hydrogen gases are adsorbed on the solid surface and then adsorbed boron trichloride reacts with gaseous methane to yield adsorbed BC. The adsorbed BC, reacts with boron trichloride and hydrogen gases to produce B₂Cs, B₃Cs and finally B₄C in series reactions.

Adsorbed chlorine that is produced in the elementary steps of B₄C formation mechanism, reacts immediately with adsorbed hydrogen to release HCl into the gas phase. Beside the gas phase reaction, dichloroborane is produced also on the surface, in a three site reaction of adsorbed boron trichloride with adsorbed hydrogen. Model 6 reactions are listed as follows;



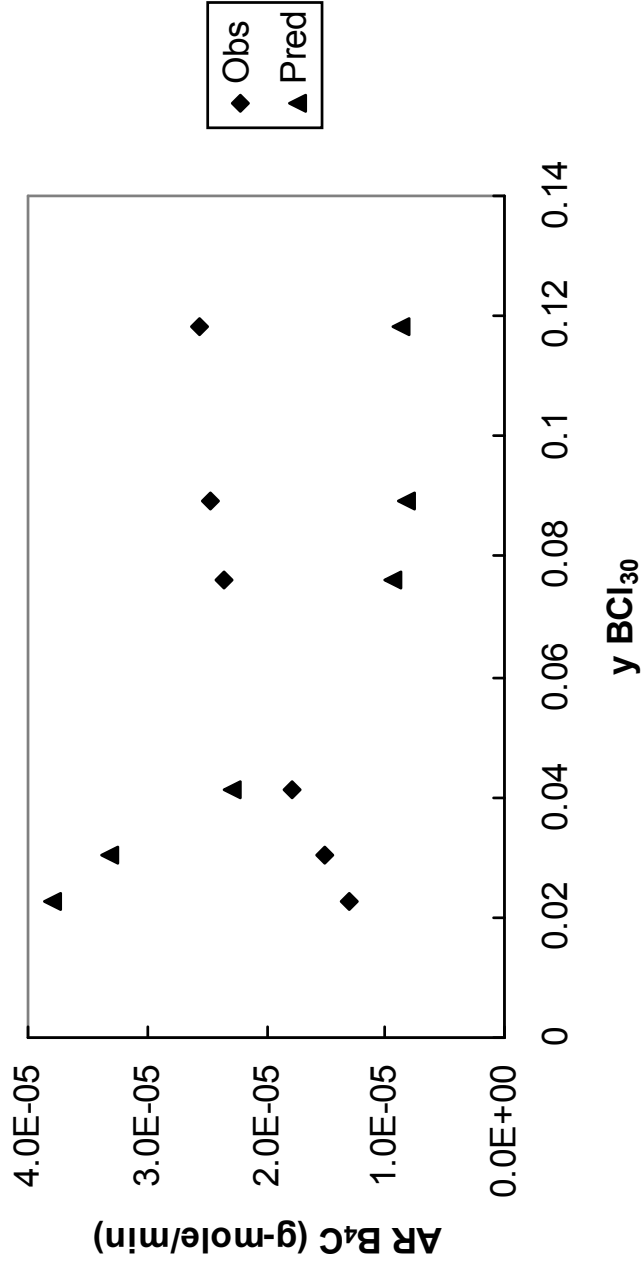


Figure 3.31 Comparison of the effect of BCl₃ inlet mole fractions on the observed and Model 5 predicted formation rates of B₄C (T=1150°C, y CH₄₀=0.02 in hydrogen, y_{BCl30}/y_{CH40}= 1.5- 5.5, simultaneous analysis)

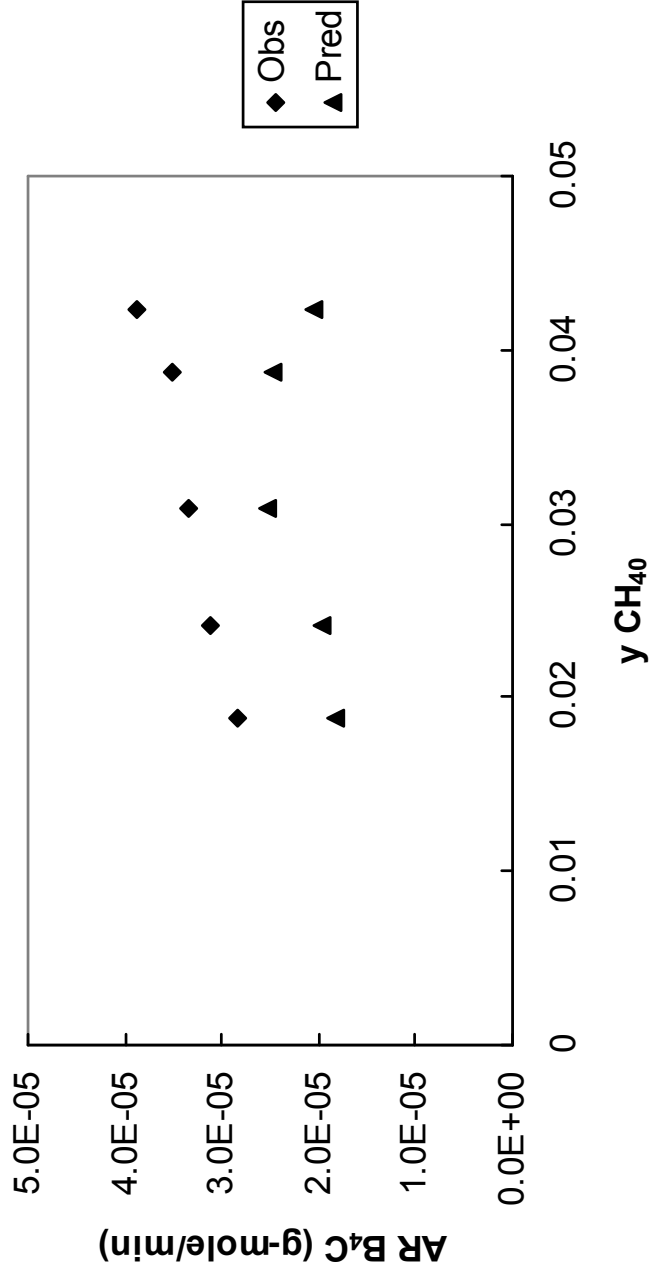


Figure 3.32 Comparison of the effect of CH₄ inlet mole fractions on the observed and Model 5 predicted formation rates of B₄C (T=1150°C, y BCl₃₀=0.084 in hydrogen, y_{BCl₃₀}/y_{CH₄₀}=2-4.5, simultaneous analysis)

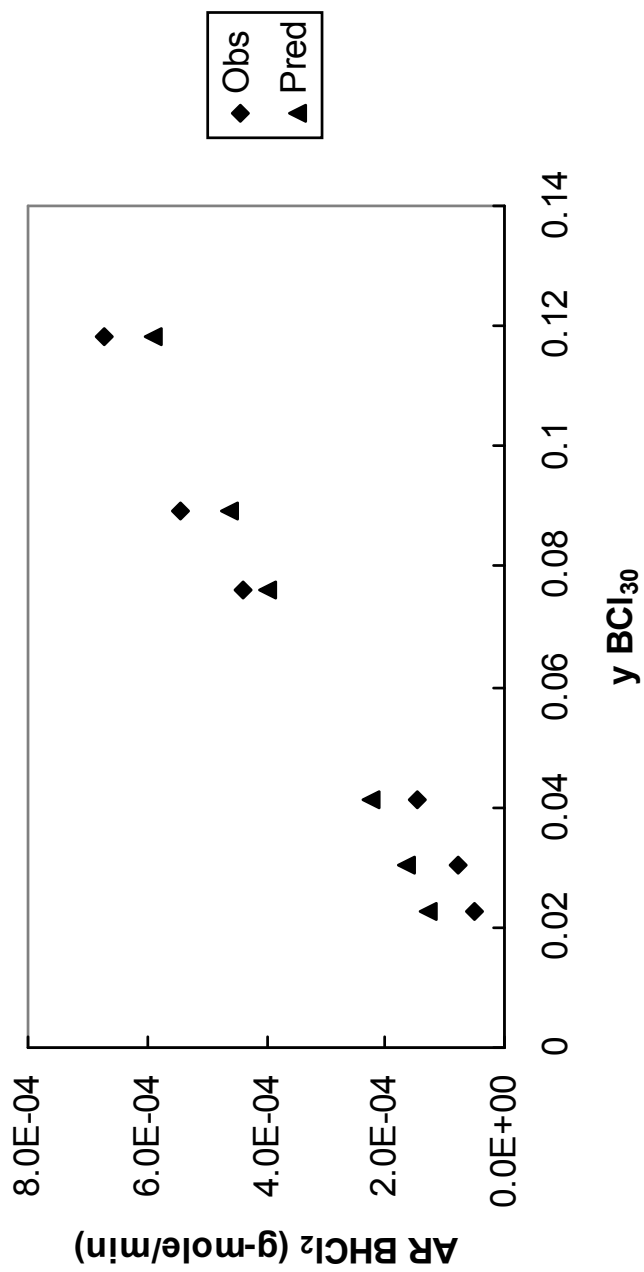


Figure 3.33 Comparison of the effect of BCl₃ inlet mole fractions on the observed and Model 5 predicted formation rates of BHCl₂ (T=1150°C, y CH₄₀=0.02 in hydrogen, y BCl₃₀/y CH₄₀= 1.5- 5.5, simultaneous analysis)

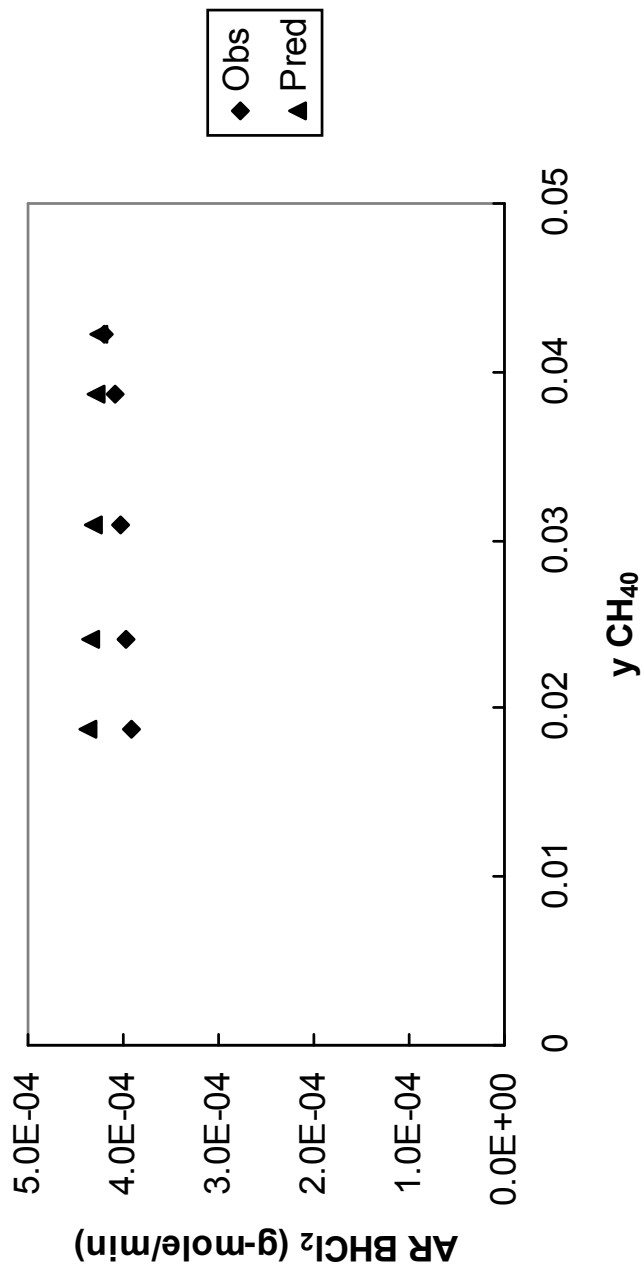


Figure 3.34 Comparison of the effect of CH₄ inlet mole fractions on the observed and Model 5 predicted formation rates of BHC₁₂ (T=1150°C, y BCl₃₀=0.084 in hydrogen, y_{BCl30}/y_{CH40}=2-4.5, simultaneous analysis)

The rate expressions derived from the model are;

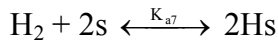
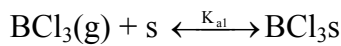
$$R_{B_4C} = \frac{k_{c6} K_{a1} P_{CH_4} P_{BCl_3}}{1 + K_{a1} P_{BCl_3} + (K_{a7} P_{H_2})^{1/2}} \quad (3.35)$$

$$R_{BHCl_2} = \frac{k_{d4} K_{a1} K_{a7} P_{H_2} P_{BCl_3}}{P_{HCl} (1 + K_{a1} P_{BCl_3} + K_{a7} P_{H_2})^{1/2}} + k_g P_{BCl_3} P_{H_2} \quad (3.36)$$

The simultaneous fit of experimental data points to the equations above, resulted in a very poor fit to predict the formation rate of boron carbide. This can be clearly seen in Figures 3.35 and 3.36 for the effects of inlet boron trichloride and methane gases on the boron carbide formation rates, respectively. There is a little improvement in predicting the formation rate of dichloroborane, considering the previous models. The predicted rate parameters for the reactions and corresponding R-squared values are given in Table 3.4.

Model 7

This model differs from the previous models in that it considers the adsorption of methane gas on the solid surface. In previous models, methane was reacted with adsorbed boron trichloride, namely through Rideal Eley type of a reaction. In this model dissociative adsorption of methane was assumed, to produce CH_3s , which then reacted with boron trichloride gas to form BCs. The other parts of the reaction mechanism is similar to that of Model 6. The elementary reaction steps of this model are;



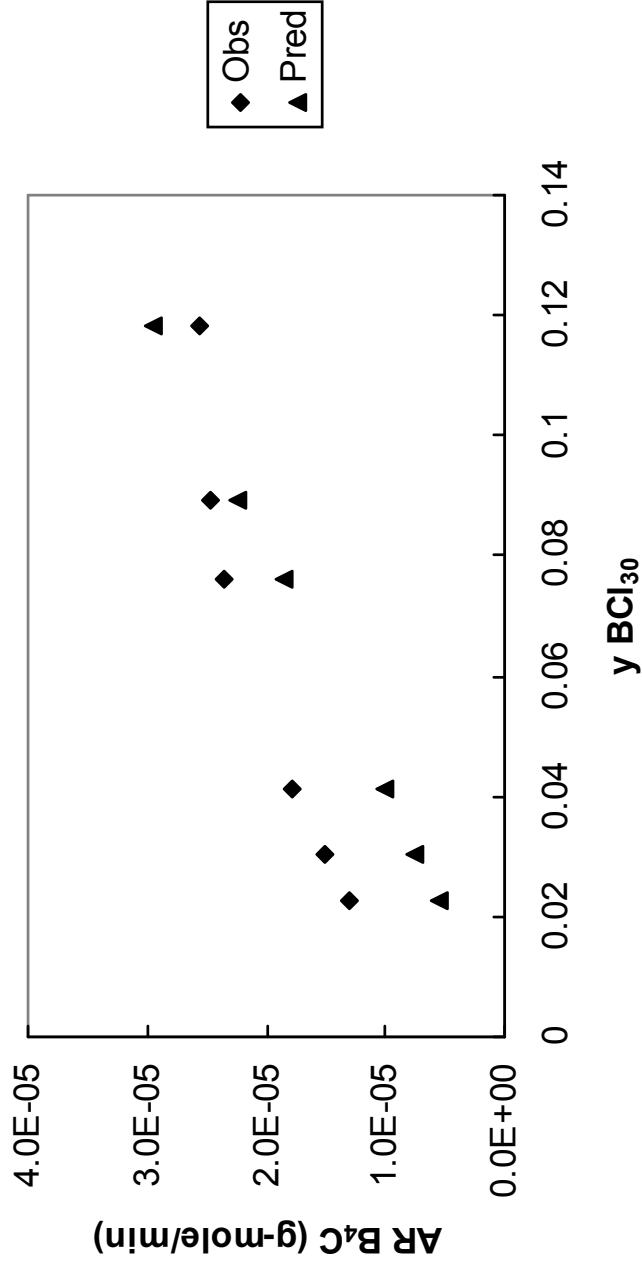


Figure 3.35 Comparison of the effect of BCl₃ inlet mole fractions on the observed and Model 6 predicted formation rates of B₄C (T=1150°C, y CH₄₀=0.02 in hydrogen, y_{BCl₃₀}/y_{CH₄₀}= 1.5- 5.5, simultaneous analysis)

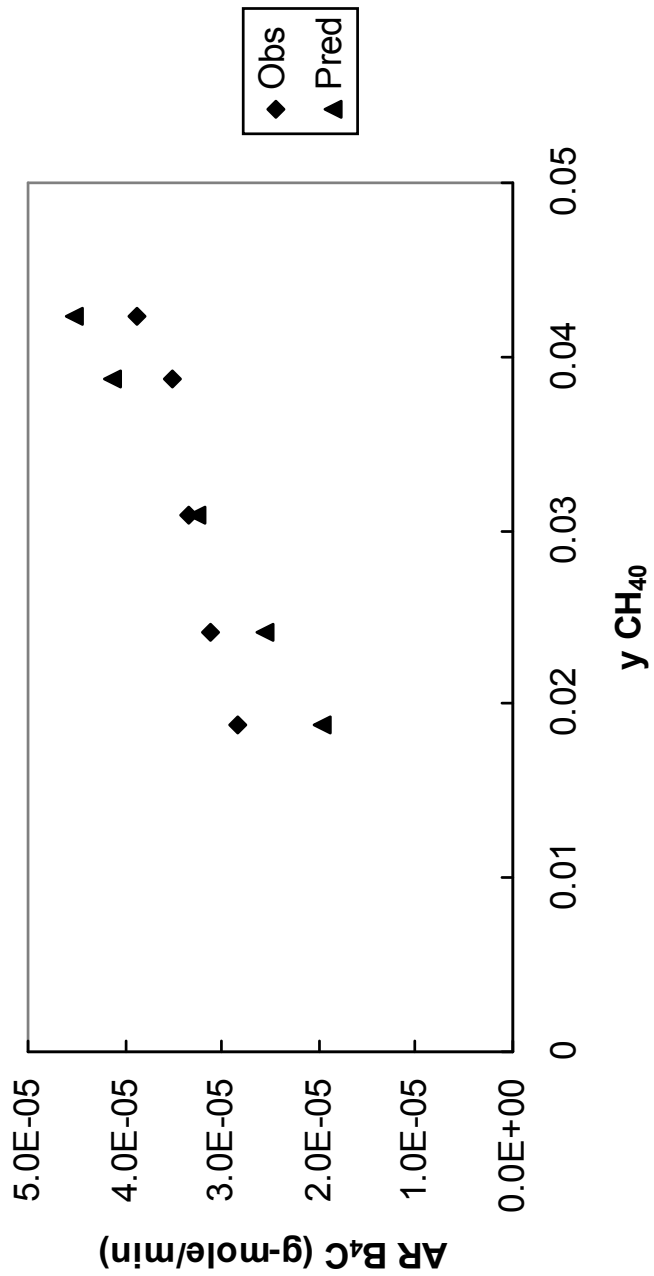


Figure 3.36 Comparison of the effect of CH₄ inlet mole fractions on the observed and Model 6 predicted formation rates of B₄C (T=1150°C, y BCl₃₀=0.084 in hydrogen, y_{BCl₃₀}/y_{CH₄₀}=2-4.5, simultaneous analysis)

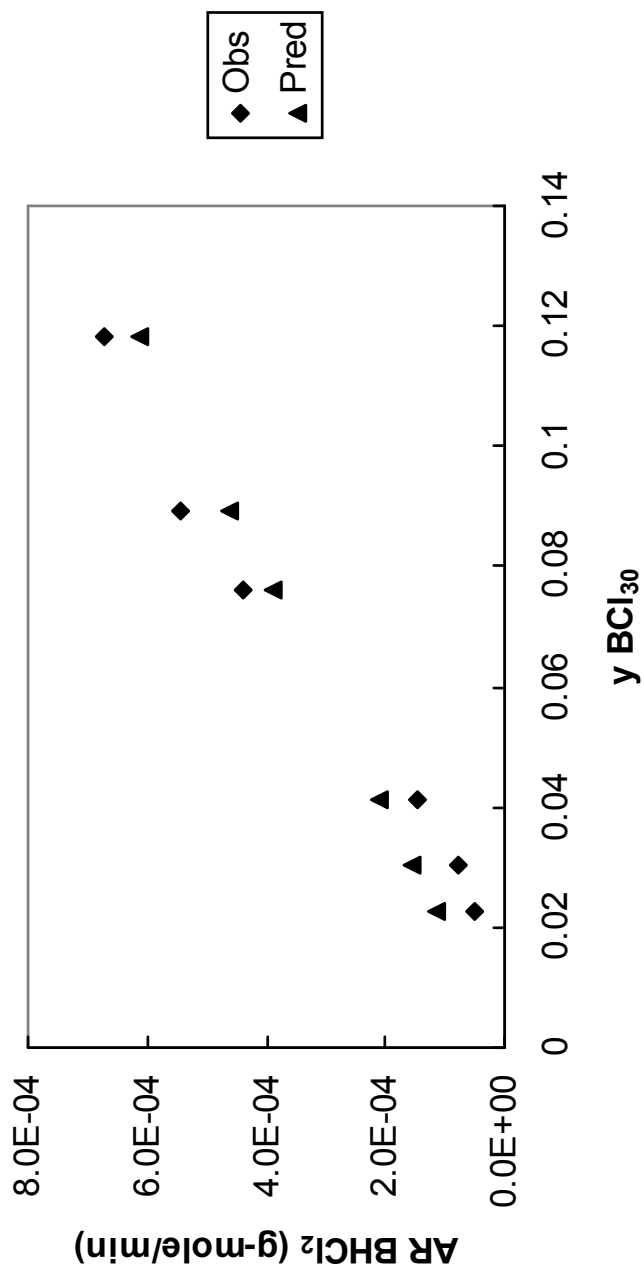


Figure 3.37 Comparison of the effect of BCl₃ inlet mole fractions on the observed and Model 6 predicted formation rates of BHCl₂ (T=1150°C, y CH₄₀=0.02 in hydrogen, y BCl₃₀/y CH₄₀= 1.5- 5.5, simultaneous analysis)

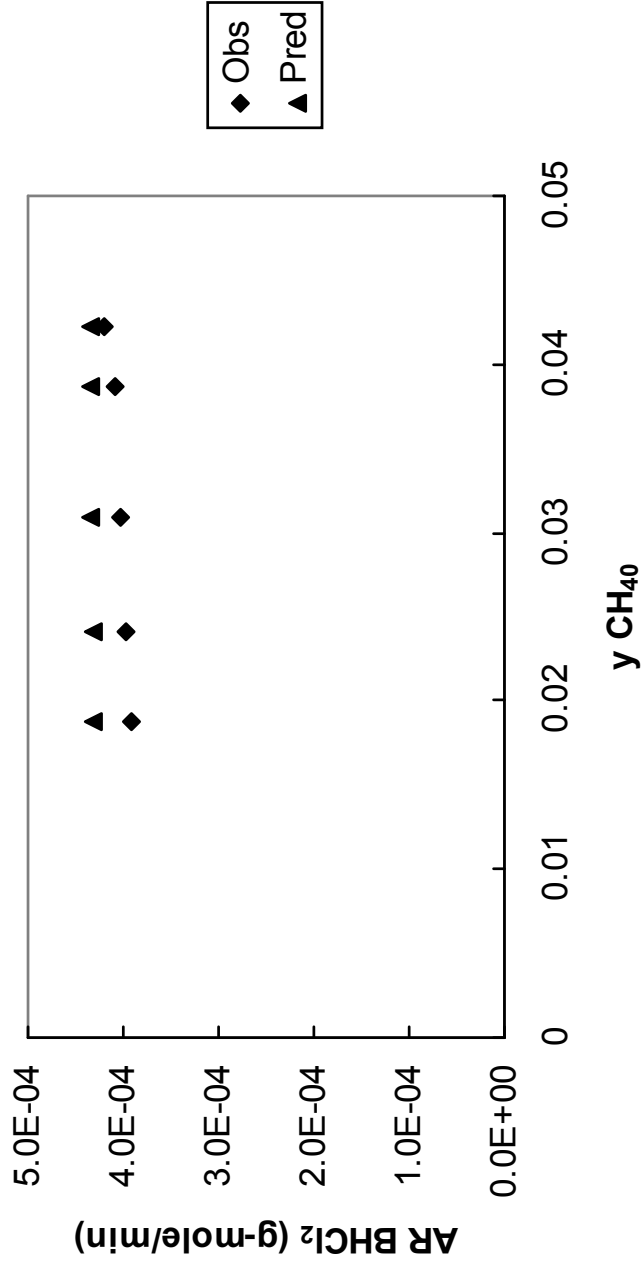
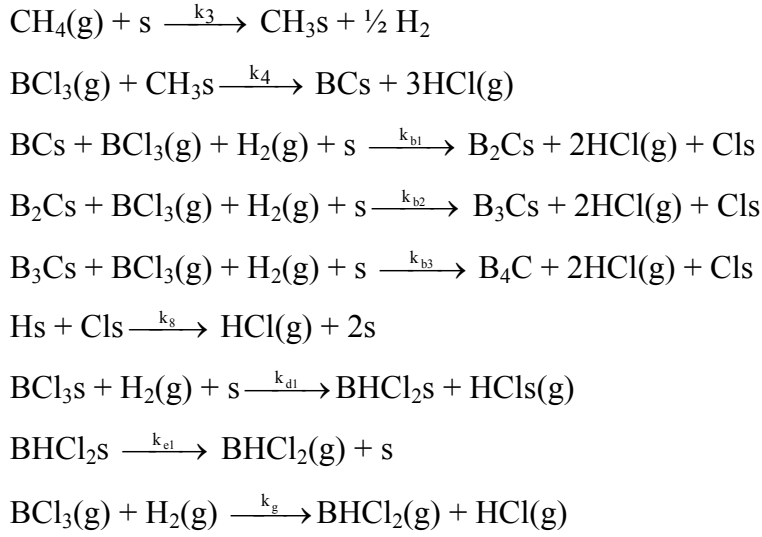


Figure 3.38 Comparison of the effect of CH₄ inlet mole fractions on the observed and Model 6 predicted formation rates of BHC₁₂ (T=1150°C, y BCl₃₀=0.084 in hydrogen, y_{BCl30}/y_{CH40}=2-4.5, simultaneous analysis)



The rate expression derived for this model are as follows;

$$R_{\text{B}_4\text{C}} = \frac{k_3 P_{\text{CH}_4} P_{\text{BCl}_3}}{1 + K_{a1} P_{\text{BCl}_3} + \frac{k_3 P_{\text{CH}_4}}{k_4 P_{\text{BCl}_3}} + (K_{a7} P_{\text{H}_2})^{1/2}} \quad (3.37)$$

$$R_{\text{BHCl}_2} = \frac{k_{d1} K_{a1} P_{\text{H}_2} P_{\text{BCl}_3}}{1 + K_{a1} P_{\text{BCl}_3} + \frac{k_3 P_{\text{CH}_4}}{k_4 P_{\text{BCl}_3}} + (K_{a7} P_{\text{H}_2})^{1/2}} + k_g P_{\text{H}_2} P_{\text{BCl}_3} \quad (3.38)$$

The details of the derivations are given in Appendix C.

The simultaneous analysis of these two rate expressions with the experimental data gave poor agreement (Figures 3.39 and 3.40) especially for the BCl_3 effect on the deposition rate of boron carbide. The model increases the correlation coefficient up to 0.974 (square root of R value) for the prediction of dichloroborane deposition rate (Figures 3.41 and 3.42). The predicted model parameters and R-squared values are given in Table 3.4.

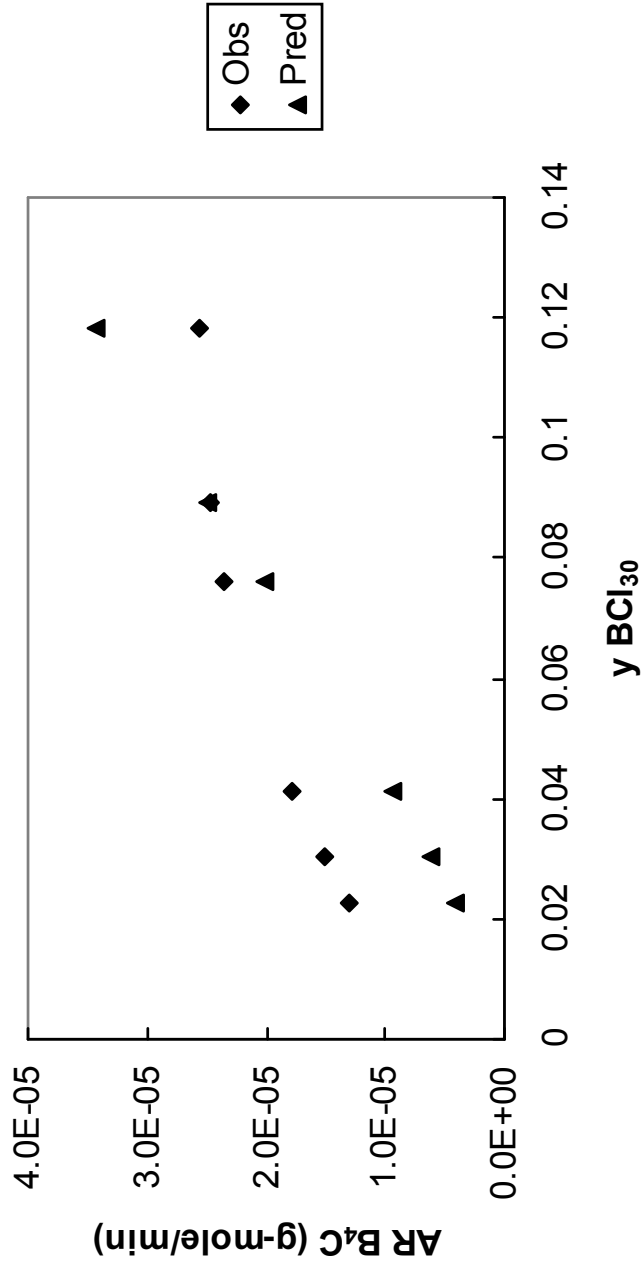


Figure 3.39 Comparison of the effect of BCl_3 inlet mole fractions on the observed and Model 7 predicted formation rates of B_4C ($T=1150^\circ\text{C}$, $y_{\text{CH}_4}=0.02$ in hydrogen, $y_{\text{BCl}_3}/y_{\text{CH}_4}=1.5-5.5$, simultaneous analysis)

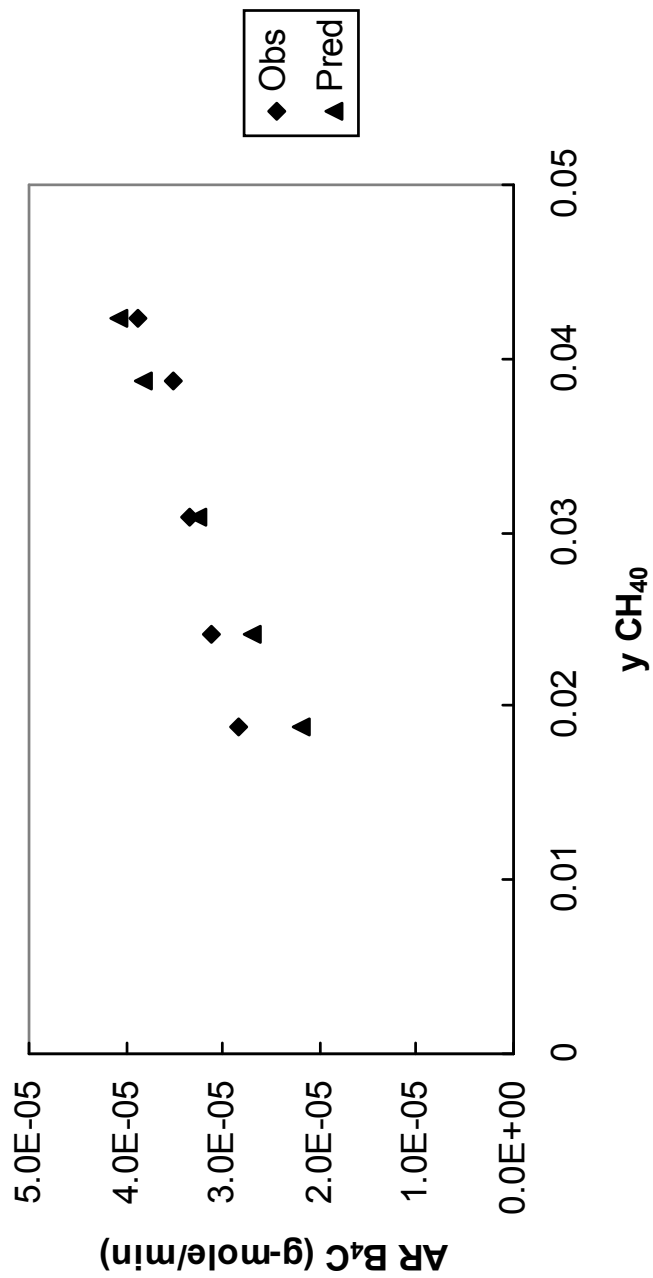


Figure 3.40 Comparison of the effect of CH₄ inlet mole fractions on the observed and Model 7 predicted formation rates of B₄C (T=1150°C, y BCl₃₀=0.084 in hydrogen, y_{BCl₃₀}/y_{CH₄₀}=2-4.5, simultaneous analysis)

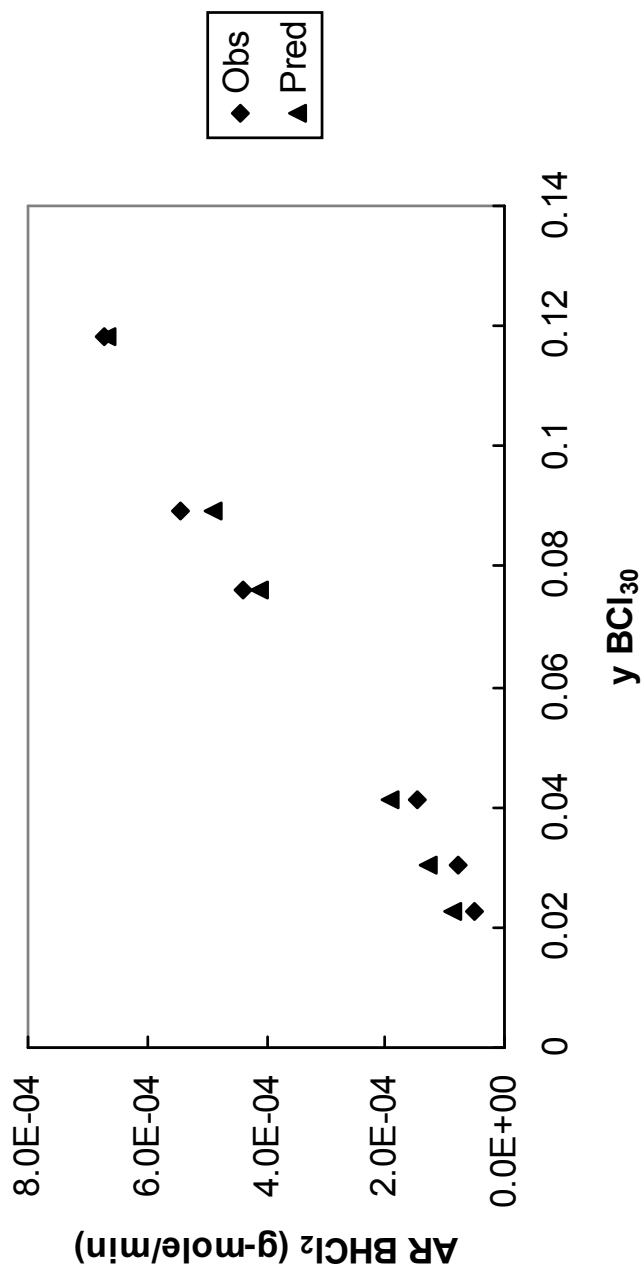


Figure 3.41 Comparison of the effect of BCl₃ inlet mole fractions on the observed and Model 7 predicted formation rates of BHCl₂ (T=1150°C, y CH₄₀=0.02 in hydrogen, y BCl₃₀/y CH₄₀= 1.5- 5.5, simultaneous analysis)

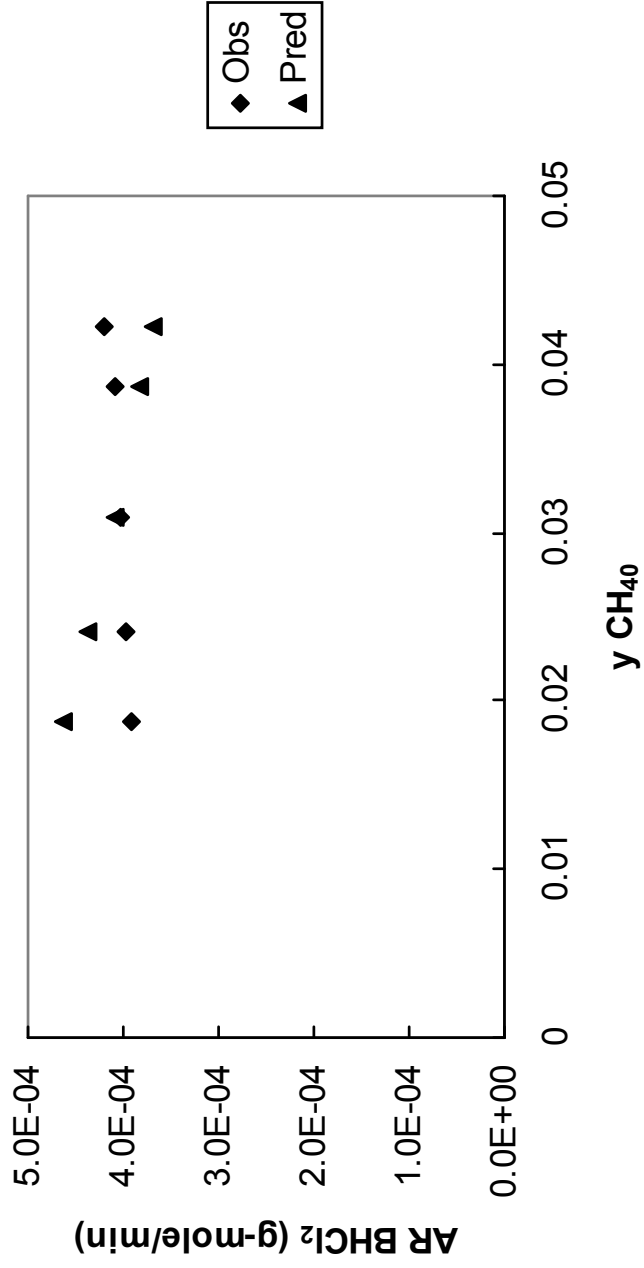
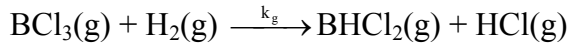
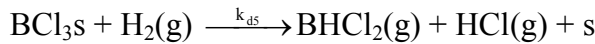
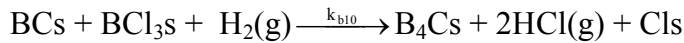
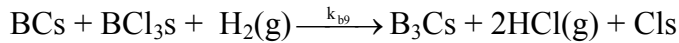
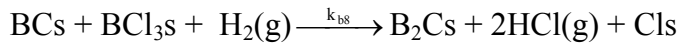
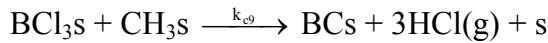
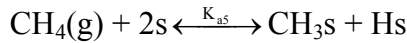
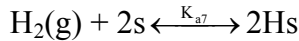
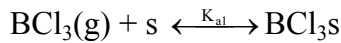


Figure 3.42 Comparison of the effect of CH₄ inlet mole fractions on the observed and Model 7 predicted formation rates of BHC1₂ (T=1150°C, y BCl₃₀=0.084 in hydrogen, y_{BCl30}/y_{CH40}=2-4.5, simultaneous analysis)

Model 8

In this model, in addition to the adsorption of hydrogen and boron trichloride to the solid surface, methane is also adsorbed on the surface dissociatively in an equilibrium reaction. Then BCs is formed through a Langmuir-Hinshelwood type of a reaction kinetics. The formed BCs then reacts with adsorbed boron trichloride and gaseous hydrogen to form boron carbide in successive steps. Dichloroborane, on the other hand, is formed through two reactions. The gas phase formation of dichloroborane involves the reaction between boron trichloride and hydrogen gases. The surface reaction in formation of dichloroborane involves the reaction between adsorbed boron trichloride and gaseous hydrogen. The elementary reaction steps are as follows;



The rate equations that are derived according to Model 8 are;

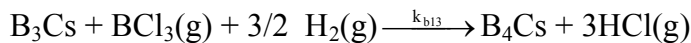
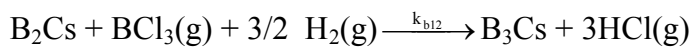
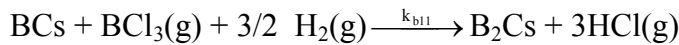
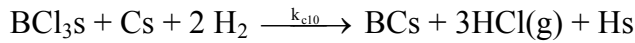
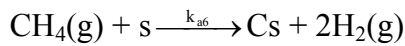
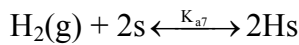
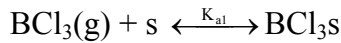
$$R_{\text{B}_4\text{C}} = \frac{\frac{k_{c9}K_{a5}K_{a1}}{K_{a2}^{1/2}} P_{\text{CH}_4} P_{\text{BCl}_3}}{P_{\text{H}_2}^{1/2} (1 + K_{a1}P_{\text{BCl}_3} + \frac{K_{a5}P_{\text{CH}_4}}{K_{a2}^{1/2}P_{\text{H}_2}^{1/2}} + (K_{a2}P_{\text{H}_2})^{1/2})^2} \quad (3.39)$$

$$R_{\text{BHCl}_2} = \frac{k_{d5} K_{a1} P_{\text{H}_2} P_{\text{BCl}_3}}{(1 + K_{a1} P_{\text{BCl}_3} + \frac{K_{a5} P_{\text{CH}_4}}{K_{a2}^{1/2} P_{\text{H}_2}^{1/2}} + (K_{a2} P_{\text{H}_2})^{1/2})} + k_g P_{\text{BCl}_3} P_{\text{H}_2} \quad (3.40)$$

The simultaneous fit of the experimental data to the model predicted rate equations revealed nearly the same fit as in Model 7, for the formation reaction of dichloroborane, with an R-squared value of 0.9255. The results are given in Figures 3.43, 3.44, 3.45 and 3.46. As it is seen clearly from Figure 3.43 that, the model fails to predict the rate of B₄C formation reaction. The estimated parameters and the corresponding R-squared values for Model 8 are given in Table 3.4.

Model 9

In this model, methane gas is adsorbed on the surface dissociatively to produce adsorbed carbon. Adsorbed carbon is reacted with adsorbed boron trichloride to form BCs, which then reacts with gaseous boron trichloride and hydrogen, in successive steps, to obtain boron carbide in solid form. The surface reaction in formation of dichloroborane involves the reaction between adsorbed boron trichloride and adsorbed hydrogen. The elementary reaction steps are;



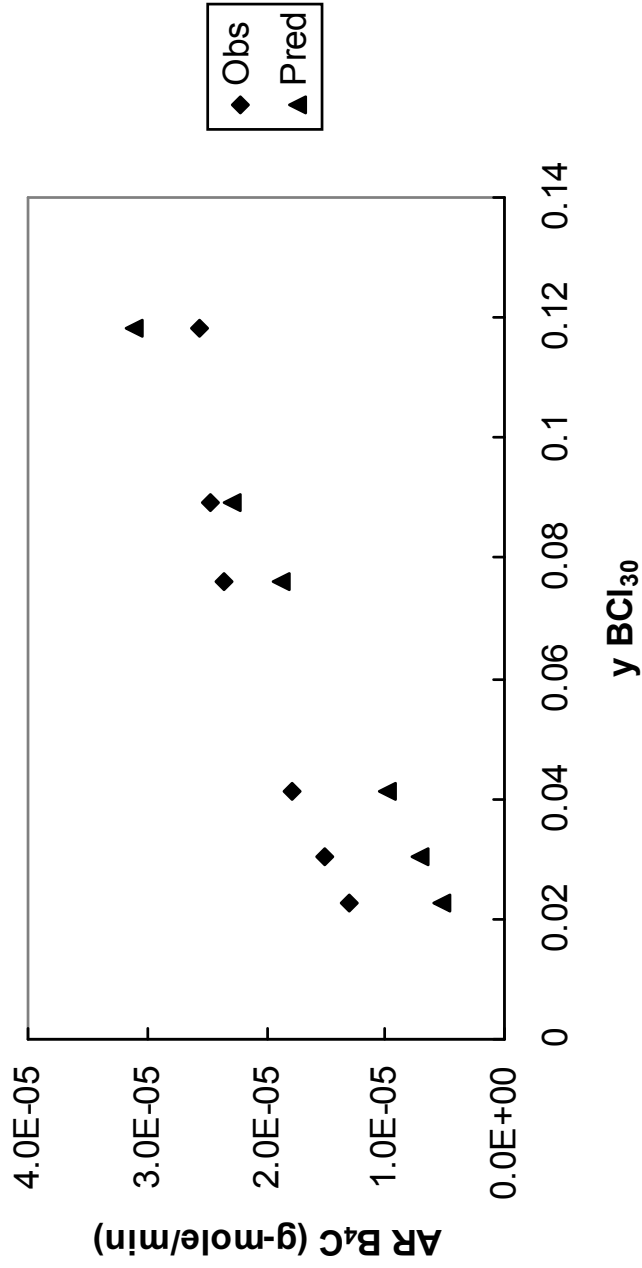


Figure 3.43 Comparison of the effect of BCl_3 inlet mole fractions on the observed and Model 8 predicted formation rates of B_4C ($T=1150^\circ\text{C}$, $y_{\text{CH}_40}=0.02$ in hydrogen, $y_{\text{BCl}_{30}}/y_{\text{CH}_40}=1.5-5.5$, simultaneous analysis)

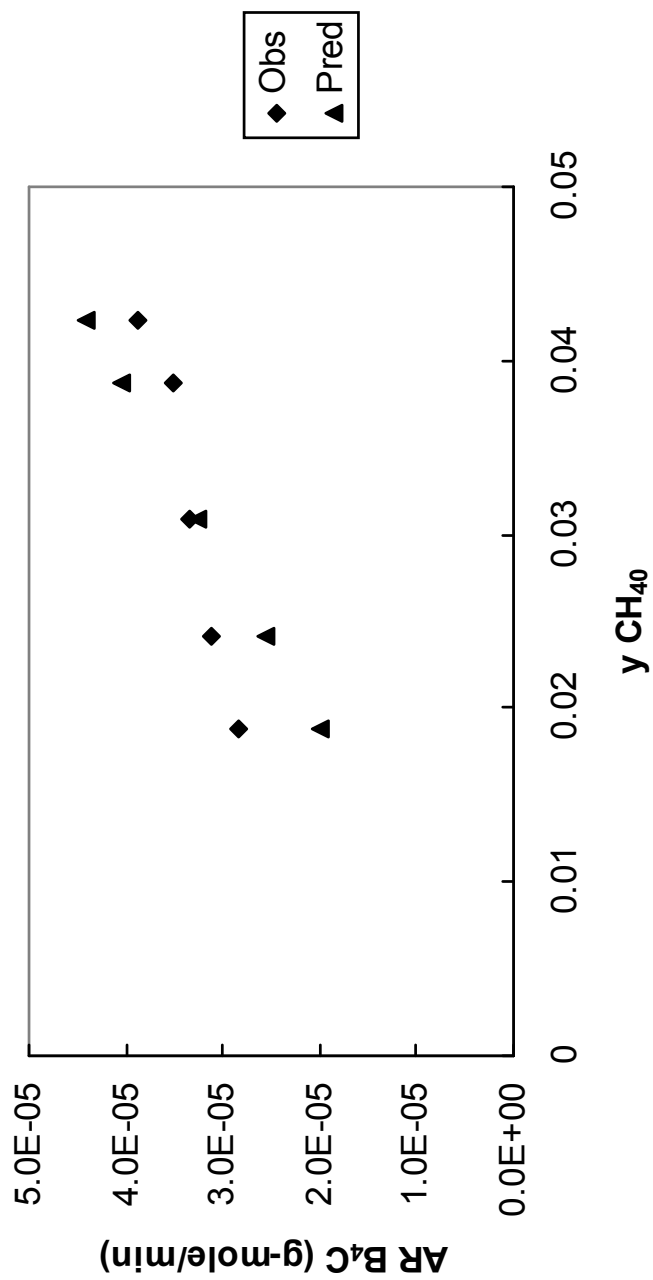


Figure 3.44 Comparison of the effect of CH₄ inlet mole fractions on the observed and Model 8 predicted formation rates of B₄C (T=1150°C, y BCl₃₀=0.084 in hydrogen, y_{BCl₃₀}/y_{CH₄₀}=2-4.5, simultaneous analysis)

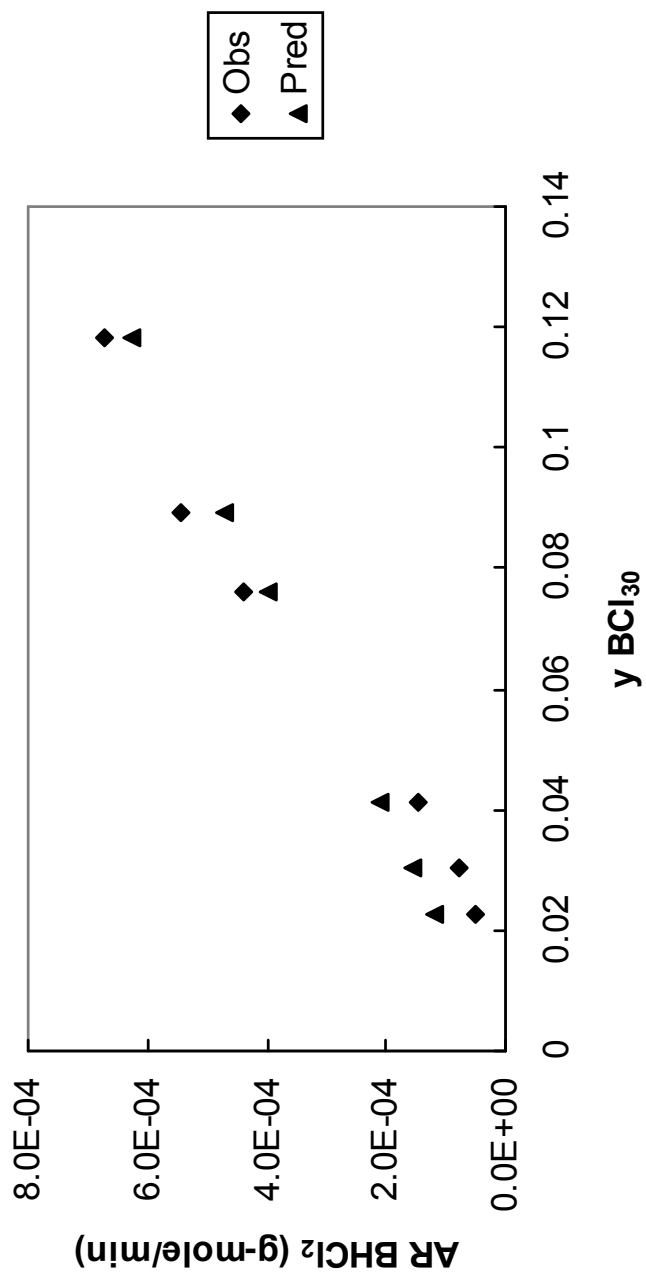


Figure 3.45 Comparison of the effect of BCl₃ inlet mole fractions on the observed and Model 8 predicted formation rates of BHCl₂ (T=1150°C, y CH₄₀=0.02 in hydrogen, y BCl₃₀/y CH₄₀= 1.5- 5.5, simultaneous analysis)

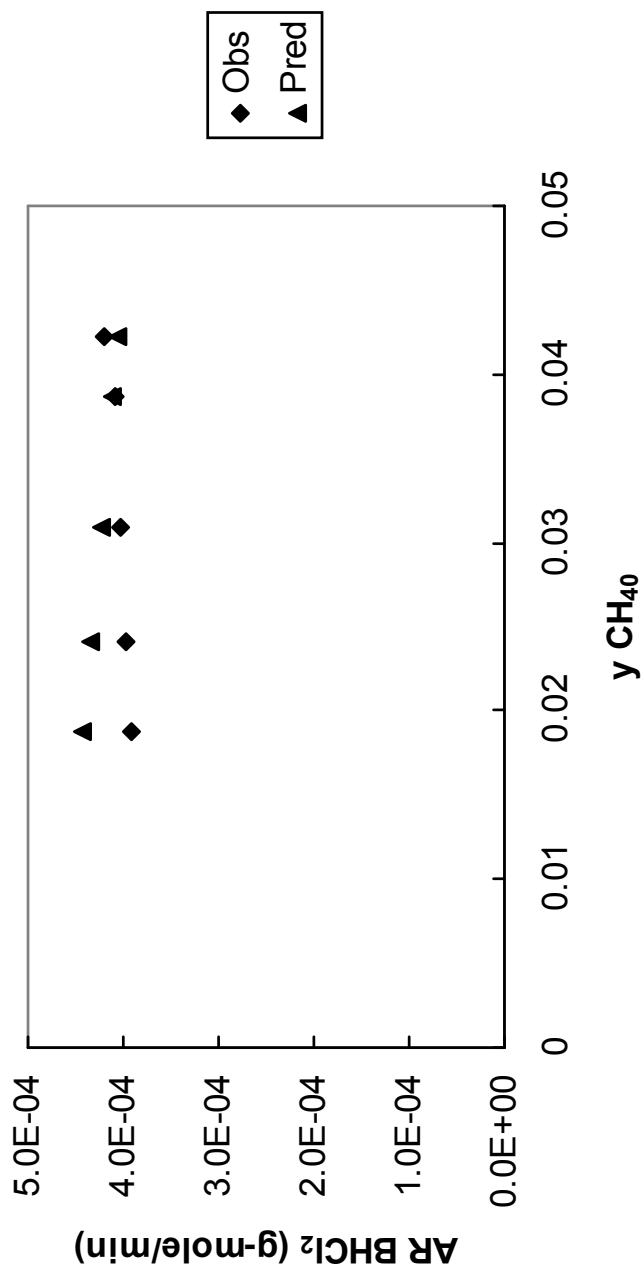
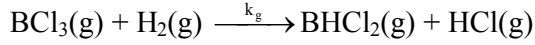


Figure 3.46 Comparison of the effect of CH₄ inlet mole fractions on the observed and Model 8 predicted formation rates of BHC1₂ (T=1150°C, y BCl₃₀=0.084 in hydrogen, y_{BCl30}/y_{CH40}=2-4.5, simultaneous analysis)



The model rate expressions derived for this model are;

$$R_{\text{B}_4\text{C}} = \frac{k_{a6} k_{c10} K_{a1} P_{\text{CH}_4} P_{\text{BCl}_3} P_{\text{H}_2}^{3/2}}{(1 + K_{a1} P_{\text{BCl}_3} + K_{a7}^{1/2} P_{\text{H}_2}^{1/2})^2} \quad (3.41)$$

$$R_{\text{BHCl}_2} = \frac{k_{d4} K_{a1} K_{a7} P_{\text{H}_2} P_{\text{BCl}_3}}{(1 + K_{a1} P_{\text{BCl}_3} + K_{a7}^{1/2} P_{\text{H}_2}^{1/2})^3} + k_g P_{\text{BCl}_3} \quad (3.42)$$

Where,

$$k_{a6} k_{c10} K_{a1} = 60.3$$

$$K_{a1} = 302.0$$

$$(K_{a7})^{1/2} = 38.58$$

$$k_{d4} K_{a1} K_{a7} = 3.6 * 10^{-3}$$

$$k_g = 5.2 * 10^{-3}$$

The simultaneous fit of the experimental data to the derived rate expressions give poor fit for the formation of boron carbide on the surface (Figures 3.47 and 3.48). For dichloroborane formation, model predictions are well, for both boron trichloride and methane effects, with an R-squared value of 0.924 (Figures 3.49 and 3.50).

Model 10

In model 10, boron trichloride is adsorbed on the surface nondissociatively, whereas hydrogen and methane are adsorbed dissociatively. BC is formed on the solid surface through the reaction of adsorbed boron trichloride with adsorbed methane in the form of CH_3s . Produced BC is reacted in successive series reactions including

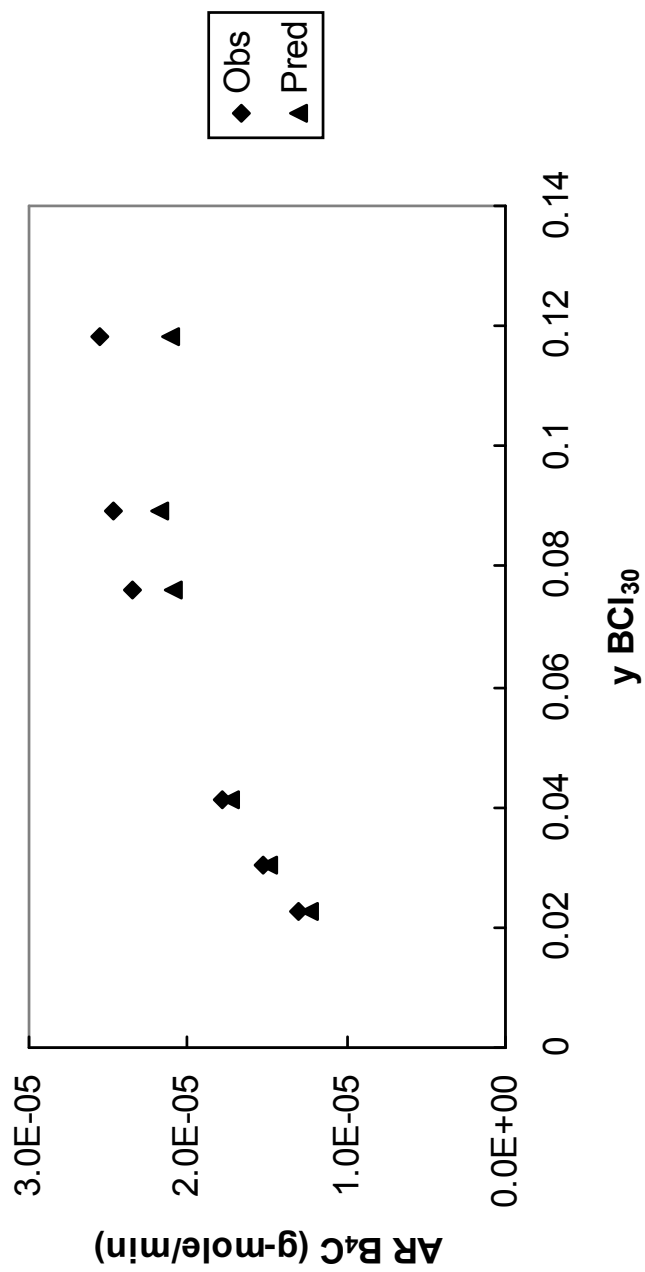


Figure 3.47 Comparison of the effect of BCl₃ inlet mole fractions on the observed and Model 9 predicted formation rates of B₄C (T=1150°C, y CH₄₀=0.02 in hydrogen, y_{BCl30}/y_{CH40}= 1.5- 5.5, simultaneous analysis)

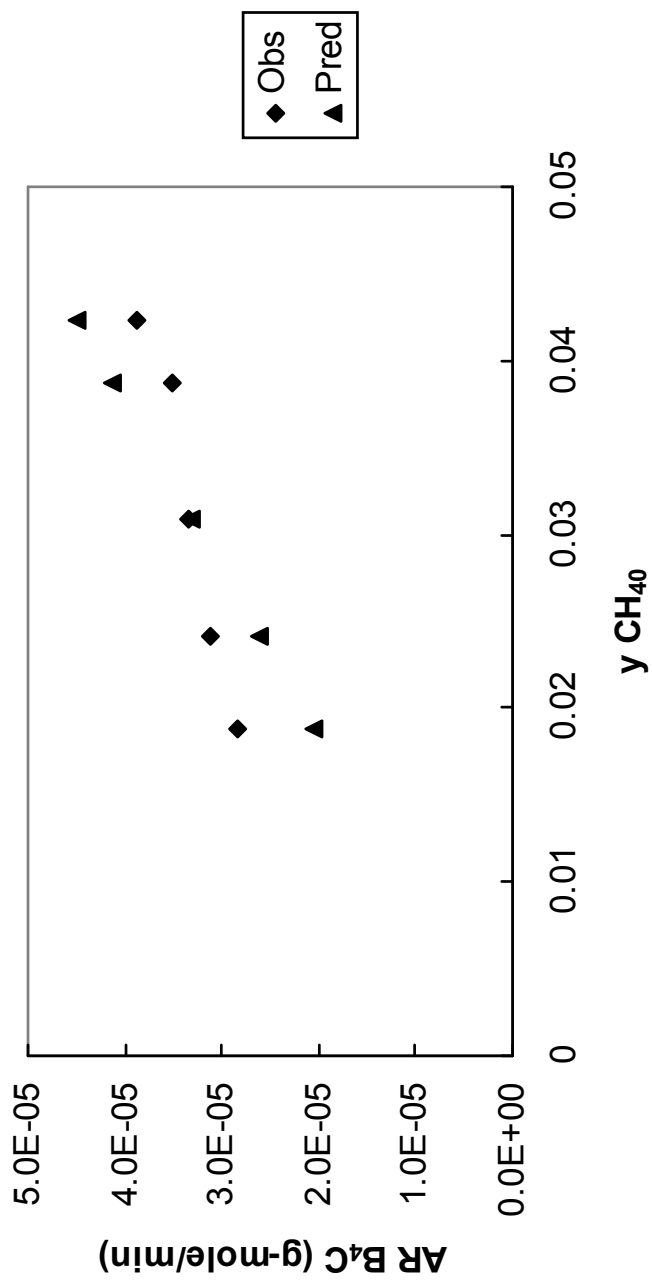


Figure 3.48 Comparison of the effect of CH₄ inlet mole fractions on the observed and Model 9 predicted formation rates of B₄C (T=1150°C, y BCl₃₀=0.084 in hydrogen, y BCl₃₀/y CH₄₀=2-4.5, simultaneous analysis)

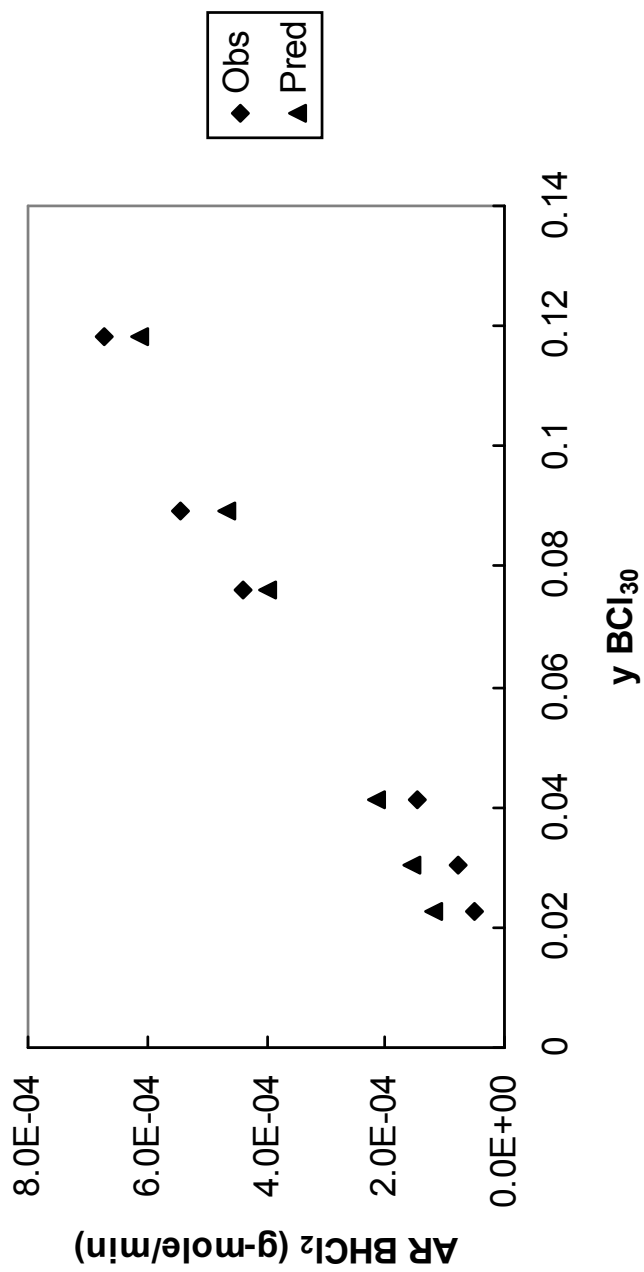


Figure 3.49 Comparison of the effect of BCl₃ inlet mole fractions on the observed and Model 9 predicted formation rates of BHCl₂ (T=1150°C, y CH₄₀=0.02 in hydrogen, y BCl₃₀/y CH₄₀= 1.5- 5.5, simultaneous analysis)

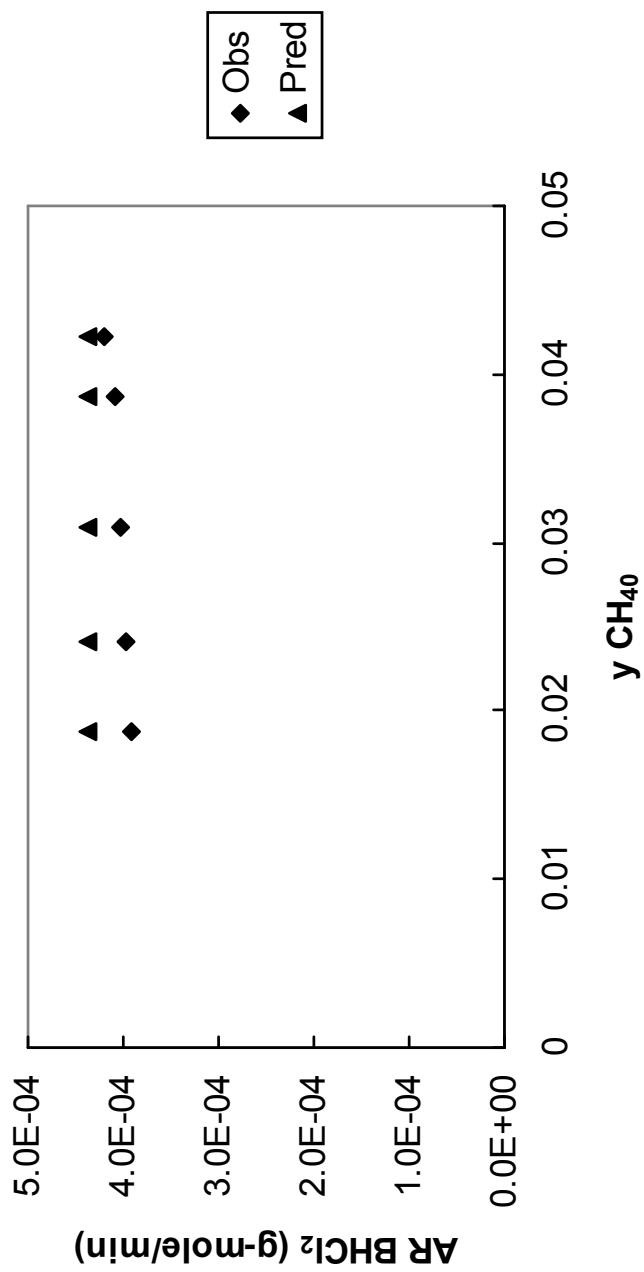
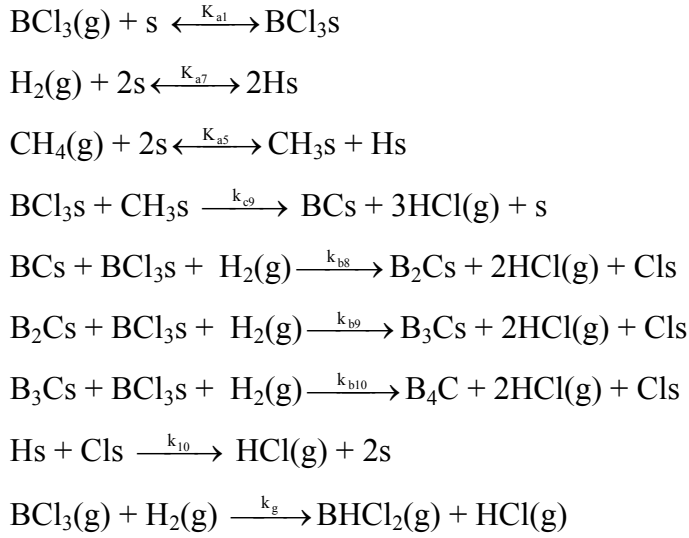


Figure 3.50 Comparison of the effect of CH₄ inlet mole fractions on the observed and Model 9 predicted formation rates of BHC₁₂ (T=1150°C, y BCl₃₀=0.084 in hydrogen, y BCl₃₀/y CH₄₀=2-4.5, simultaneous analysis)

adsorbed boron trichloride and gaseous hydrogen. In the proposed mechanism, dichloroborane is produced only through the gas phase reaction between boron trichloride and hydrogen. The model equations are as follows;



The rate equations that are derived according to Model 10 are;

$$R_{\text{B}_4\text{C}} = \frac{\frac{k_{c9}K_{a5}K_{a1}}{K_{a7}^{1/2}} P_{\text{CH}_4} P_{\text{BCl}_3}}{P_{\text{H}_2}^{1/2} \left(1 + K_{a1}P_{\text{BCl}_3} + \frac{K_{a5}P_{\text{CH}_4}}{K_{a7}^{1/2}P_{\text{H}_2}^{1/2}}\right)^2} \quad (3.43)$$

$$R_{\text{BHCl}_2} = k_g P_{\text{BCl}_3} \quad (3.44)$$

The simultaneous fit of the experimental data to the model expression gave good fits for the boron carbide and dichloroborane formation reactions. The results are given in Figures 3.51 through 3.54. Estimated model parameters together with the statistical R-squared values are summarised in Table 3.4.

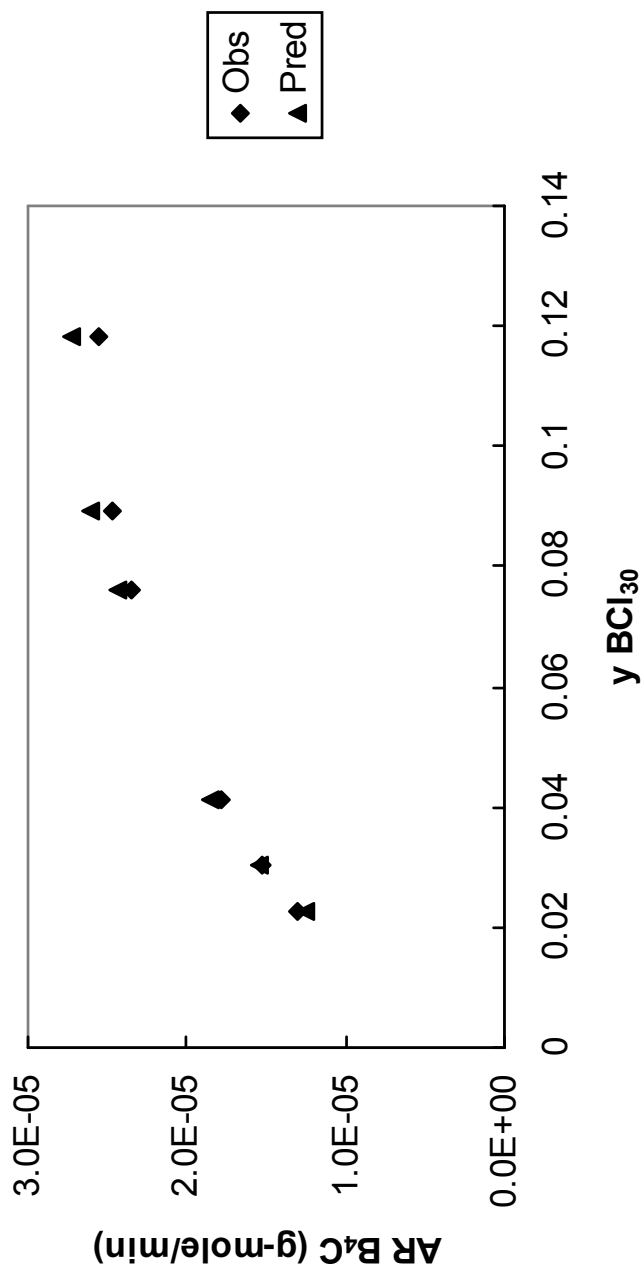


Figure 3.51 Comparison of the effect of BCl₃ inlet mole fractions on the observed and Model 10 predicted formation rates of B₄C (T=1150°C, y CH₄₀=0.02 in hydrogen, y_{BCl₃₀}/y_{CH₄₀}= 1.5- 5.5, simultaneous analysis)

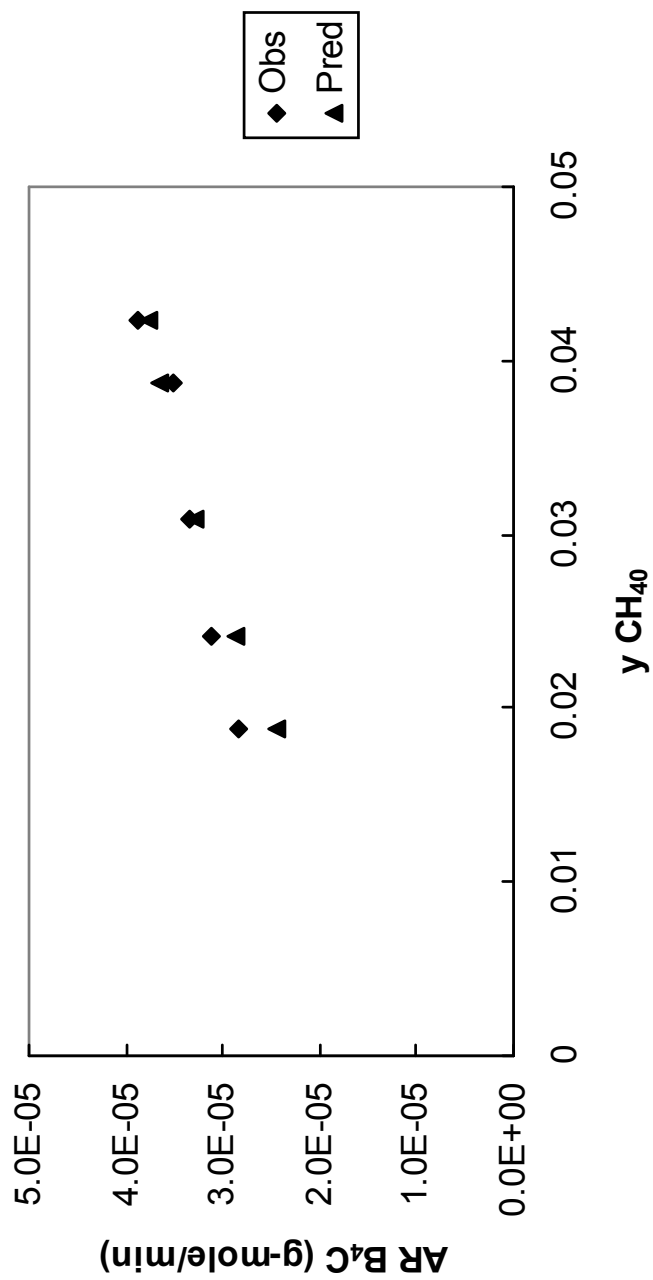


Figure 3.52 Comparison of the effect of CH₄ inlet mole fractions on the observed and Model 10 predicted formation rates of B₄C (T=1150°C, y BCl₃₀=0.084 in hydrogen, y BCl₃₀/y CH₄₀=2-4.5, simultaneous analysis)

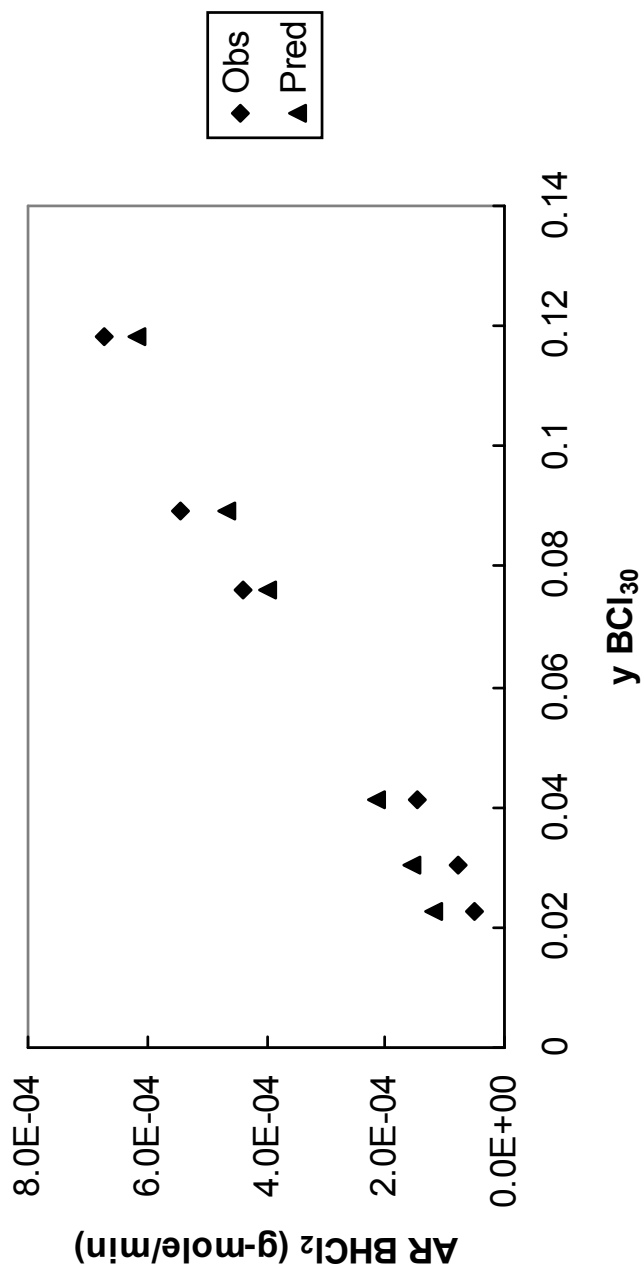


Figure 3.53 Comparison of the effect of BCl₃ inlet mole fractions on the observed and Model 10 predicted formation rates of BHCl₂ (T=1150°C, y CH₄₀=0.02 in hydrogen, y BCl₃₀/y CH₄₀= 1.5- 5.5, simultaneous analysis)

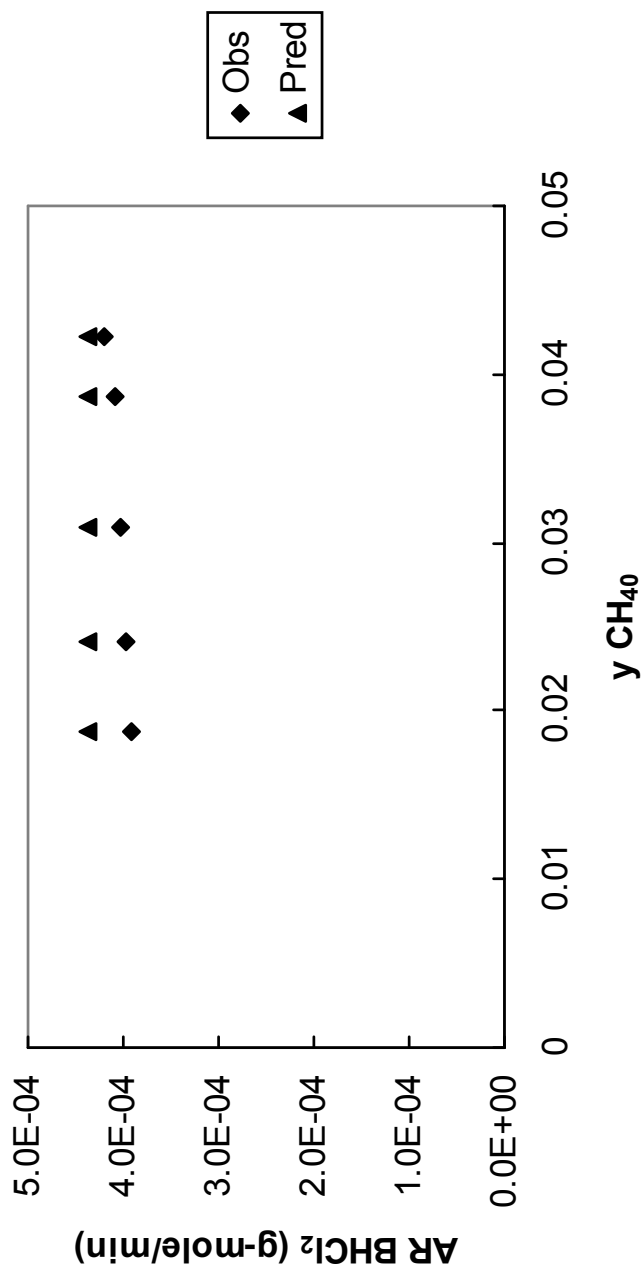


Figure 3.54 Comparison of the effect of CH₄ inlet mole fractions on the observed and Model 10 predicted formation rates of BHC1₂ (T=1150°C, y BCl₃₀=0.084 in hydrogen, y_{BCl30}/y_{CH40}=2-4.5, simultaneous analysis)

The rate parameters for model 10 are,

$$\frac{k_{c9}K_{a5}K_{a1}}{K_{a7}^{1/2}} = 0.0682, K_{a1} = 9.36, \frac{K_{a5}}{K_{a7}^{1/2}} = 18.47, \text{ and } k_g = 0.00521$$

It is evident from Figures 3.51, 3.52, 3.53, and 3.54 that, the experimental data was best described by Model 10. This model predicts the deposition rate of B_4C and $BHCl_2$ well for the entire range of parameters studied. The model does not consider the probable surface reactions in the formation of $BHCl_2$, and hence formation rate is independent of methane partial pressure. This is also conformed by the experimental observation in which dichloroborane formation rate is almost unchanged with the variation of methane mole fraction.

Table 3.4 Model Parameters and Correlation Coefficients

| Model | Rate expressions derived from proposed reaction mechanisms | Parameters | $R^2_{B_4C}$ | $R^2_{BHC_2}$ |
|-------|---|--|--------------|---------------|
| 1 | $R_{B_4C} = \frac{k_{b7}K_{a1}K_{c1}K_{a6}P_{BCl_3}P_{CH_4}}{P_{HCl}^2(1 + K_{a1}P_{BCl_3} + K_{a6}P_{CH_4}/P_{H_2}^2 + (K_{a7}P_{H_2})^{1/2})^2}$ $R_{BHC_2} = \frac{k_{d4}K_{a1}K_{a7}P_{H_2}P_{BCl_3}}{(1 + K_{a1}P_{BCl_3} + K_{a6}P_{CH_4}/P_{H_2}^2 + (K_{a7}P_{H_2})^{1/2})^3} + k_gP_{BCl_3}P_{H_2}$ | $k_{b7}K_{a1}K_{c1}K_{a6}$ =0.0874 $K_{a1}=3.6*10^{-6}$ $K_{a6}=35.2$ $K_{a7}=1708.0$ $k_{d4}K_{a1}K_{a7} = 401.5$ $k_g = 9.6*10^{-10}$ | ---- | 0.923 |
| 2 | $R_{B_4C} = \frac{\frac{k_{a2}k_{c11}}{k_{c11} + k_{d3}}P_{BCl_3}}{(1 + \frac{k_{a2}}{(k_{c11} + k_{d3})K_{a7}^{1/2}}\frac{P_{BCl_3}}{P_{H_2}^{1/2}} + (K_{a7}P_{H_2})^{1/2})^2}$ $R_{BHC_2} = \frac{\frac{k_{d3}}{k_{c11} + k_{d3}}P_{BCl_3}}{(1 + \frac{k_{a2}}{(k_{c11} + k_{d3})K_{a7}^{1/2}}\frac{P_{BCl_3}}{P_{H_2}^{1/2}} + (K_{a7}P_{H_2})^{1/2})^2} + k_gP_{BCl_3}P_{H_2}$ | $\frac{k_{a2}k_{c11}}{k_{c11} + k_{d3}} = 31.1$ $\frac{k_{a2}}{(k_{c11} + k_{d3})K_{a7}^{1/2}} = 4.69*10^{-8}$ $K_{a7} = 472.82$ $\frac{k_{d3}}{k_{c11} + k_{d3}} = 472.8$ $k_g = 2.73*10^{-14}$ | 0.221 | 0.925 |

Table 3.4 Model Parameters and Correlation Coefficients (cont'd)

| Model | Rate expressions derived from proposed reaction mechanisms | Parameters | $R^2_{B_4C}$ | $R^2_{BHCl_2}$ |
|-------|--|---|--------------|----------------|
| 3 | $R_{B_4C} = \frac{K_{a1}k_{c6}P_{CH_4}P_{BCl_3}}{1 + K_{a1}P_{BCl_3} + (K_{a7}P_{H_2})^{1/2}}$ $R_{BHCl_2} = \frac{k_{d1}K_{a1}P_{H_2}P_{BCl_3}}{(1 + K_{a1}P_{BCl_3} + (K_{a7}P_{H_2})^{1/2})^2} + k_gP_{BCl_3}P_{H_2}$ | $K_{a1}k_{c6} = 0.053$ $K_{a1} = 37.87$ $K_{a7} = 1.8 \cdot 10^{-11}$ $k_{d1}K_{a1} = 5.88 \cdot 10^{-3}$ $k_g = 1.09 \cdot 10^{-4}$ | 0.693 | 0.893 |
| 4 | $R_{B_4C} = \frac{k_{c7}K_{a1}P_{CH_4}P_{BCl_3}}{(1 + K_{a1}P_{BCl_3} + (K_{a7}P_{H_2})^{1/2})^2}$ $R_{BHCl_2} = \frac{k_{d1}K_{a1}P_{H_2}P_{BCl_3}}{(1 + K_{a1}P_{BCl_3} + (K_{a7}P_{H_2})^{1/2})^2} + k_gP_{BCl_3}P_{H_2}$ | $k_{c7}K_{a1} = 0.1387$ $K_{a1} = 17.576$ $K_{a7} = 0.7721$ $k_{d1}K_{a1} = 3.42 \cdot 10^{-7}$ $k_g = 0.0058$ | 0.670 | 0.894 |
| 5 | $R_{B_4C} = \frac{k_{b11}K_{a1}K_{c6}P_{CH_4}P_{BCl_3}^2P_{H_2}}{P_{HCl}^3(1 + K_{a1}P_{BCl_3})}$ $R_{BHCl_2} = \frac{k_{e1}K_{a1}K_{c12}P_{H_2}P_{BCl_3}}{P_{HCl}(1 + K_{a1}P_{BCl_3})} + k_gP_{BCl_3}P_{H_2}$ | $k_{b11}K_{a1}K_{c6} = 5.3 \cdot 10^{-5}$ $K_{a1} = 5.8 \cdot 10^{-3}$ $k_{e1}K_{a1}K_{c12} = 1.63 \cdot 10^{-12}$ $k_g = 2.1 \cdot 10^{-7}$ | ---- | 0.894 |

Table 3.4 Model Parameters and Correlation Coefficients (cont'd)

| Model | Rate expressions derived from proposed reaction mechanisms | Parameters | $R^2_{B_4C}$ | $R^2_{BHCl_2}$ |
|-------|--|---|--------------|----------------|
| 6 | $R_{B_4C} = \frac{k_{c6} K_{a1} P_{CH_4} P_{BCl_3}}{1 + K_{a1} P_{BCl_3} + (K_{a7} P_{H_2})^{1/2}}$ $R_{BHCl_2} = \frac{k_{d4} K_{a1} K_{a7} P_{H_2} P_{BCl_3}}{P_{HCl} (1 + K_{a1} P_{BCl_3} + K_{a7} P_{H_2})^{1/2}}^3 + k_g P_{BCl_3} P_{H_2}$ | $k_{c6} K_{a1} = 2.85$ $K_{a1} = 2.0 \cdot 10^{-5}$ $K_{a7} = 57343$ $k_{d4} K_{a1} K_{a7} = 53413$ $k_g = 1.21 \cdot 10^{-3}$ | 0.399 | 0.915 |
| 7 | $R_{B_4C} = \frac{k_3 P_{CH_4} P_{BCl_3}}{1 + K_{a1} P_{BCl_3} + \frac{k_3 P_{CH_4}}{k_4 P_{BCl_3}} + (K_{a7} P_{H_2})^{1/2}}$ $R_{BHCl_2} = \frac{k_{d1} K_{a1} P_{H_2} P_{BCl_3}}{1 + K_{a1} P_{BCl_3} + \frac{k_3 P_{CH_4}}{k_4 P_{BCl_3}} + (K_{a7} P_{H_2})^{1/2}} + k_g P_{H_2} P_{BCl_3}$ | $k_3 = 2.656$ $K_{a1} = 5.84 \cdot 10^{-6}$ $\frac{k_3}{k_4} = 154.9$ $K_{a7} = 26670$ $k_{d1} K_{a1} = 1.167$ $k_g = 2.035 \cdot 10^{-10}$ | 0.414 | 0.926 |
| 8 | $R_{B_4C} = \frac{\frac{k_{c9} K_{a5} K_{a1}}{K_{a2}^{1/2}} P_{CH_4} P_{BCl_3}}{P_{H_2}^{1/2} (1 + K_{a1} P_{BCl_3} + \frac{K_{a5} P_{CH_4}}{K_{a2}^{1/2} P_{H_2}^{1/2}} + (K_{a2} P_{H_2})^{1/2})^2}$ $R_{BHCl_2} = \frac{k_{d5} K_{a1} P_{H_2} P_{BCl_3}}{(1 + K_{a1} P_{BCl_3} + \frac{K_{a5} P_{CH_4}}{K_{a2}^{1/2} P_{H_2}^{1/2}} + (K_{a2} P_{H_2})^{1/2})} + k_g P_{BCl_3} P_{H_2}$ | $\frac{k_{c9} K_{a5} K_{a1}}{K_{a2}^{1/2}} = 617.2$ $K_{a1} = 1.02 \cdot 10^{-5}$ $\frac{K_{a5}}{K_{a2}^{1/2}} = 303.8$ $K_{a2} = 53564$ $k_{d5} K_{a1} = 68111$ $k_g = 3.92 \cdot 10^{-10}$ | 0.402 | 0.926 |

Table 3.4 Model Parameters and Correlation Coefficients (cont'd)

| Model | Rate expressions derived from proposed reaction mechanisms | Parameters | $R^2_{B_4C}$ | $R^2_{BHCl_2}$ |
|-------|---|--|--------------|----------------|
| 9 | $R_{B_4C} = \frac{k_{a6} k_{c10} K_{a1} P_{CH_4} P_{BCl_3} P_{H_2}^{3/2}}{(1 + K_{a1} P_{BCl_3} + K_{a7}^{1/2} P_{H_2}^{1/2})^2}$ $R_{BHCl_2} = \frac{k_{d4} K_{a1} K_{a7} P_{H_2} P_{BCl_3}}{(1 + K_{a1} P_{BCl_3} + K_{a7}^{1/2} P_{H_2}^{1/2})^3} + k_g P_{BCl_3}$ | $k_{a6} k_{c10} K_{a1} = 60.3$ $K_{a1} = 302.0$ $K_{a7} = 1488.4$ $k_{d4} K_{a1} K_{a7} = 3.6 \cdot 10^{-3}$ $k_g = 5.2 \cdot 10^{-3}$ | 0.754 | 0.955 |
| 10 | $R_{B_4C} = \frac{\frac{k_{c9} K_{a5} K_{a1}}{K_{a7}^{1/2}} P_{CH_4} P_{BCl_3}}{P_{H_2}^{1/2} (1 + K_{a1} P_{BCl_3} + \frac{K_{a5} P_{CH_4}}{K_{a7}^{1/2} P_{H_2}^{1/2}})^2}$ $R_{BHCl_2} = k_g P_{BCl_3}$ | $\frac{k_{c9} K_{a5} K_{a1}}{K_{a7}^{1/2}} = 0.0682$ $K_{a1} = 9.36$ $\frac{K_{a5}}{K_{a7}^{1/2}} = 18.47$ $k_g = 0.00521$ | 0.977 | 0.948 |

In section 3.3, the formation rate of boron carbide was expressed in terms of an Arrhenius type of a rate equation. In Figure 3.55, model predicted values of B_4C formation rates (mechanism model 10) were compared with the rate values predicted from the Arrhenius equation. The correlation coefficient for B_4C formation rate was improved from 0.950 to 0.977, with the proposed model (Model 10), so that the model predicted values are closer to the experimentally observed values. Arrhenius type of rate expression is based totally on the curve fitting of the experimental values to a single equation. However, the modelling studies involve the theoretical correlations between the reaction rates and elementary steps constituting the overall reaction mechanism. So it is much more reliable, and efficient to describe the formation rate for entire range of parameter variables.

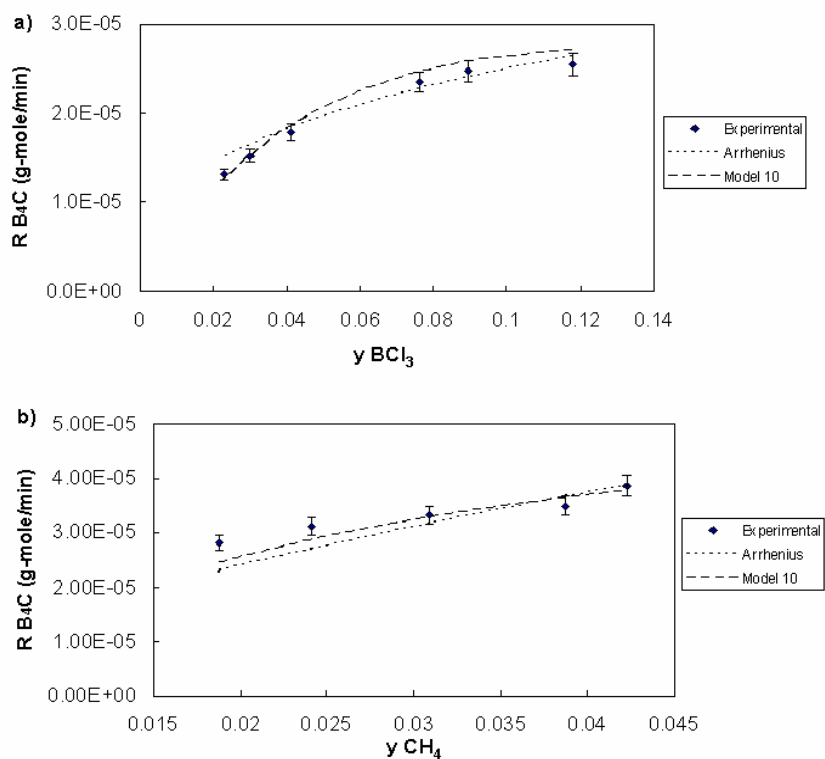


Figure 3.55 Comparison of reaction rates predicted by reaction mechanism model 10 and Arrhenius equation with the experimental data

3.5. Morphological Investigations of the Deposits

3.5.1. X-Ray Photoelectron Spectroscopy Results

The chemical compositions of the deposited films were determined by XPS (Specs instruments) analyses which have been carried out with a monochromatic MgK α (hw=1253.6eV) radiation. Survey scan showed that the main ingredients of the films are boron and carbon, together

with a trace amount of oxygen (Figure 3.56). Despite the high purity of gases employed and careful purging of the system before the experiments, the oxygen intake of the films was seen clearly from the obtained spectrum. The oxidation of boron carbide particles may be attributed to the impingement of energetic oxygen particles onto the substrate surface [1]. It is well known that molecular oxygen is not very reactive in oxidation of boron carbides. However, the formation of active oxygen ions in the boundary layer next to the substrate surface may be the reason of the oxidation. On the other hand, reaction with boron and carbon after adsorption of trace oxygen on the B_4C surface should not be ruled out as a possibility. After the survey scan, the samples were bombarded with 3 keV Ar^+ ions for 10 minutes, in order to investigate composition change between the surface and the film bulk. In Figure 3.57, B_{1s} , C_{1s} and O_{1s} spectra obtained with the XPS scan before and after the sputtering process are presented. Spectrum deconvolutions of each species were carried out for the sputtered samples, which show the existence of different chemical states. The deconvolution for the B_{1s} spectrum (Fig.3.51.a) shows the existence of the two possible boron chemical states with binding energies centered at 188.3 and 192.4, which correspond to B-C and B-O bonds, respectively [18].

The shift of B_{1s} spectrum to higher binding energy values after sputtering is attributed to the existence of the oxy-boron species in the inner shells. C_{1s} spectrum has a dominating peak at a binding energy value of 282.9, which corresponds to carbide phase. The spectrum has a shoulder on the left, which is due to the oxy-boron carbide species at binding energy values of 286.4 (C=O) and 283.8 (C-O) [19]. The

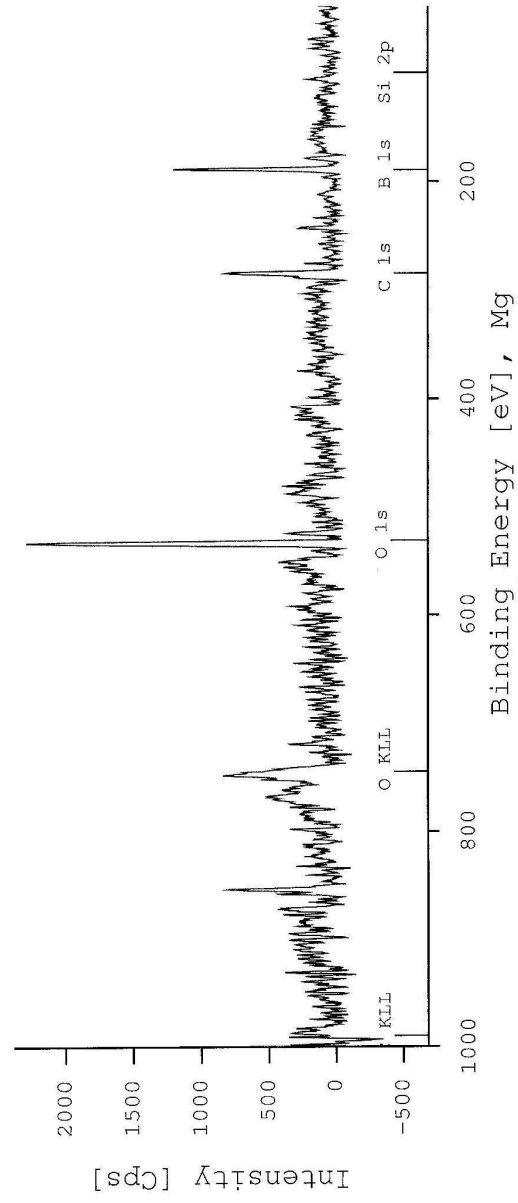


Figure 3.56 XPS survey scan for boron carbide produced at 1150°C with initial boron trichloride to methane molar ratio of 4.0 in hydrogen

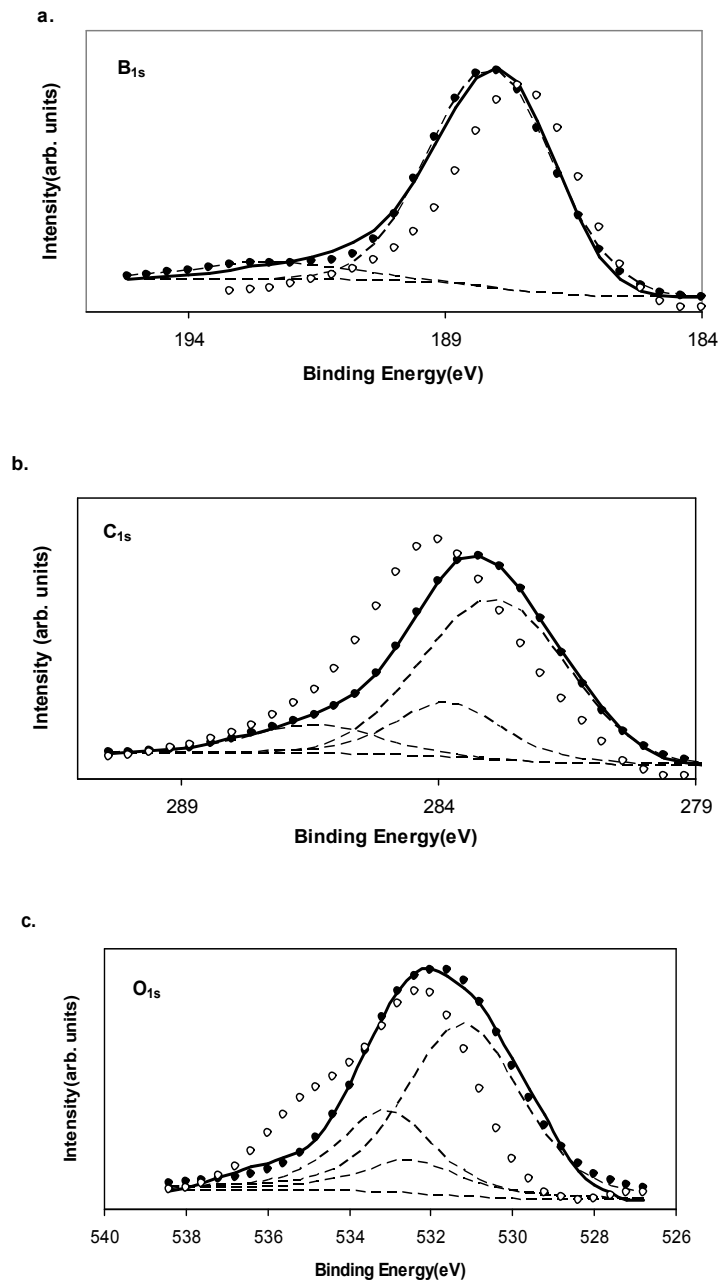


Figure 3.57 XPS spectra of the produced solid phase before (circles) and after (dots) the sputtering process and spectrum deconvolutions (deconvoluted components (dashed lines), fitted results (solid lines)) ($T=1150^{\circ}\text{C}$, $y_{\text{BCl}_3}/y_{\text{CH}_4}=4.0$ in hydrogen)

sputtering shifted the C_{1s} spectrum to the lower binding energy values, indicating that the oxides are more likely to occur on the sample surface. The deconvolution results for the O_{1s} spectrum showed the existence of oxy-boron, and oxy-carbide species. The oxygen content of the samples decreased from 7.2 at.% to 4 at.% after ion sputtering process which supports the idea of the surface contamination. The films contained around 17.2 at.% carbon, which is in the homogeneity range of stable, single phase boron carbides.

3.5.2. X-Ray Diffraction Results

X-ray diffraction patterns of the samples produced at different temperatures were obtained by a Philips PW 1840 model diffractometer with a $CuK\alpha$ ($\lambda=1.54$ Å) radiation. The diffractograms of the films produced at 1100, 1200 and 1300°C are shown in Figure 3.58. The most intense diffraction peaks were observed from the (021) and (104) reflections, which are both characteristics of rhombohedral boron carbide. However, there is a change in the 2θ angular position of both reflections with temperature variation. At 1300 °C, (021) and (104) reflections are observed at 2θ angular positions of 37.8 and 34.95, respectively, which both correspond to technical grade rhombohedral $B_{12}C_3$ stoichiometry (JCPDS 35-0798) [20]. With a decrease in temperature, the angular positions shift to lower 2θ angles at both reflections, implying a structure change. The reflections observed at 1200°C are more like the ones obtained at 1300°C, with an angular deviation of only 0.3° of 2θ . The shifts are especially significant at 1100°C, at which rhombohedral boron carbide reflections represent a $B_{13}C_2$ structure (JCPDS 33-0225) [20]. Therefore less carbon atom can be introduced into the B-C structure with a decrease in the substrate temperature. D spacing and

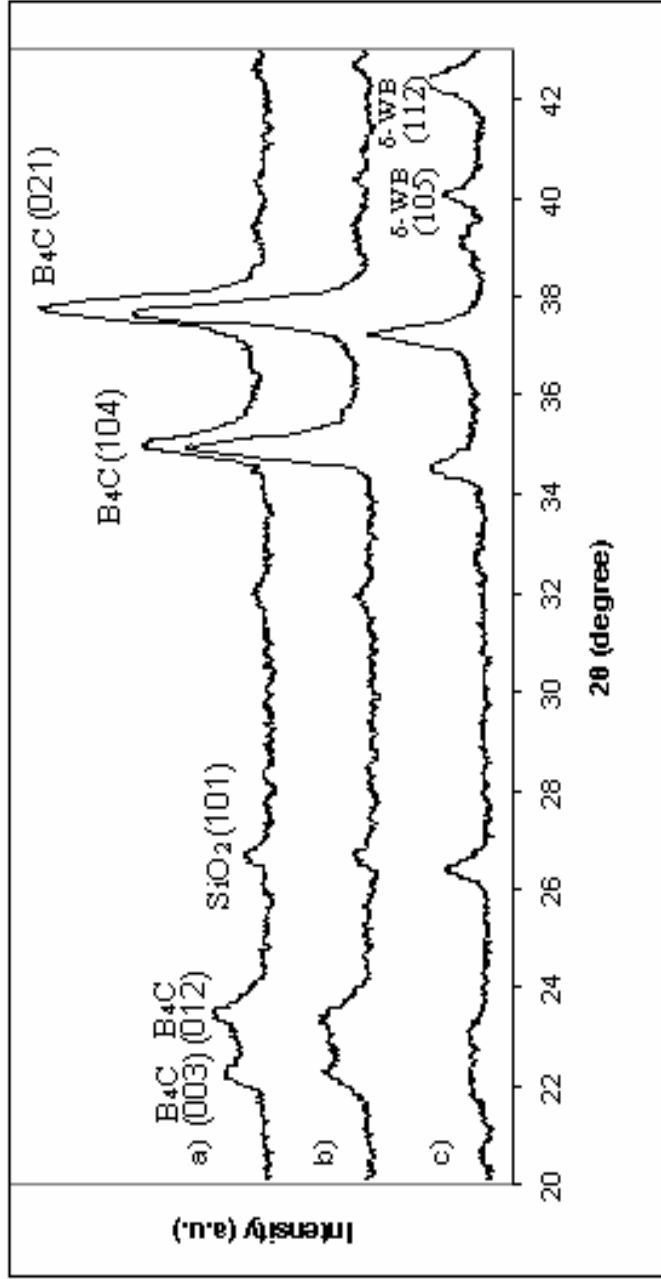


Figure 3.58 X-ray diffraction patterns of the samples produced at different substrate temperatures under atmospheric conditions with initial boron trichloride to methane molar ratio of 4.0 and with a temperature of; a) 1300°C, b) 1200°C, c) 1100°C

corresponding 2θ values for boron carbide and for some other potential impurities in the products are listed in Appendix B.

In the unusual structure of the rhombohedral boron carbide, 5-fold boron icosahedra are linked directly through covalent bonds and also by a chain of three atoms located on the principal body diagonal of the rhombohedron, as shown in Figure 1.1. 12-atom containing boron icosahedra together with the 3 atom diagonal chain builds up a 15-atom unit cell [21]. The change of the stoichiometry of our products with temperature change is possibly due to the replacement of one carbon atom with one boron atom in the C-B-C icosahedral chain, leading B-B-C structure, at lower temperatures.

The occurrence of (101) SiO_2 reflections are expected because the samples were made powder in a pestle made of quartz, which may possibly be scraped into the powder by harder boron carbide particles. The presence of δ -WB is observed only at 1100°C with the characteristic (105) and (112) reflections. This is a very meaningful observation concerning the above discussion. At lower temperatures, boron contents of the films are higher and more boron atoms could have chance to diffuse through the substrate surface, forming tungsten boride phases at the interface.

3.5.3. Scanning Electron Microscopy (SEM) Results

The temperature of the substrate surface is an important parameter influencing the morphology of the products. It is well known that, the deposits are better crystallized and the crystal grain size increases when the temperature increases [10]. The surface morphologies of the films observed in the jet stagnation region were characterized by SEM

(JOEL JSM-6400). Figure 3.59 shows the SEM images of the samples produced at three different temperatures. At 1100°C, a few micron size pyramidal crystal facets are seen.

At 1200°C, the grain size increases substantially up to around 5 micrometer. At this temperature the surface of the pyramidal geometry is covered by tiny and uniform grains, which could be an indication of a second nucleation and growth mechanism. At 1300°C, the surface is covered by 10 to 40 micron size crystals having perfect 5-fold icosahedral symmetry (Figure 3.59c). This is a very striking observation because such large crystals having 5-fold symmetry are rare in previous studies and in nature due to the lack of long-range translational symmetry for those crystals [22]. It is known that, if the extremities of a single crystal are permitted to grow without any external constraint, the crystal will assume a regular geometric shape having flat faces, and its shape is indicative of the crystal system. The basic icosahedral units of B₄C structure (Figure 1.1) could act as nuclei to build up large micrometer scale icosahedral crystals with 5-fold symmetry [22]. The mechanical properties of boron carbides consisting of such massive icosahedral crystals could be improved further because of high degree of symmetry observed. Quite a number of massive 5-fold icosahedral crystals with a grain sizes larger than 30 micrometer can easily be seen in Figure 3.59c.

3.5.4 Effect of Deposition Temperature on the Hardness of Boron Carbide

Boron carbide is an important ceramic material because of its high hardness and strength. In general, such mechanical properties are

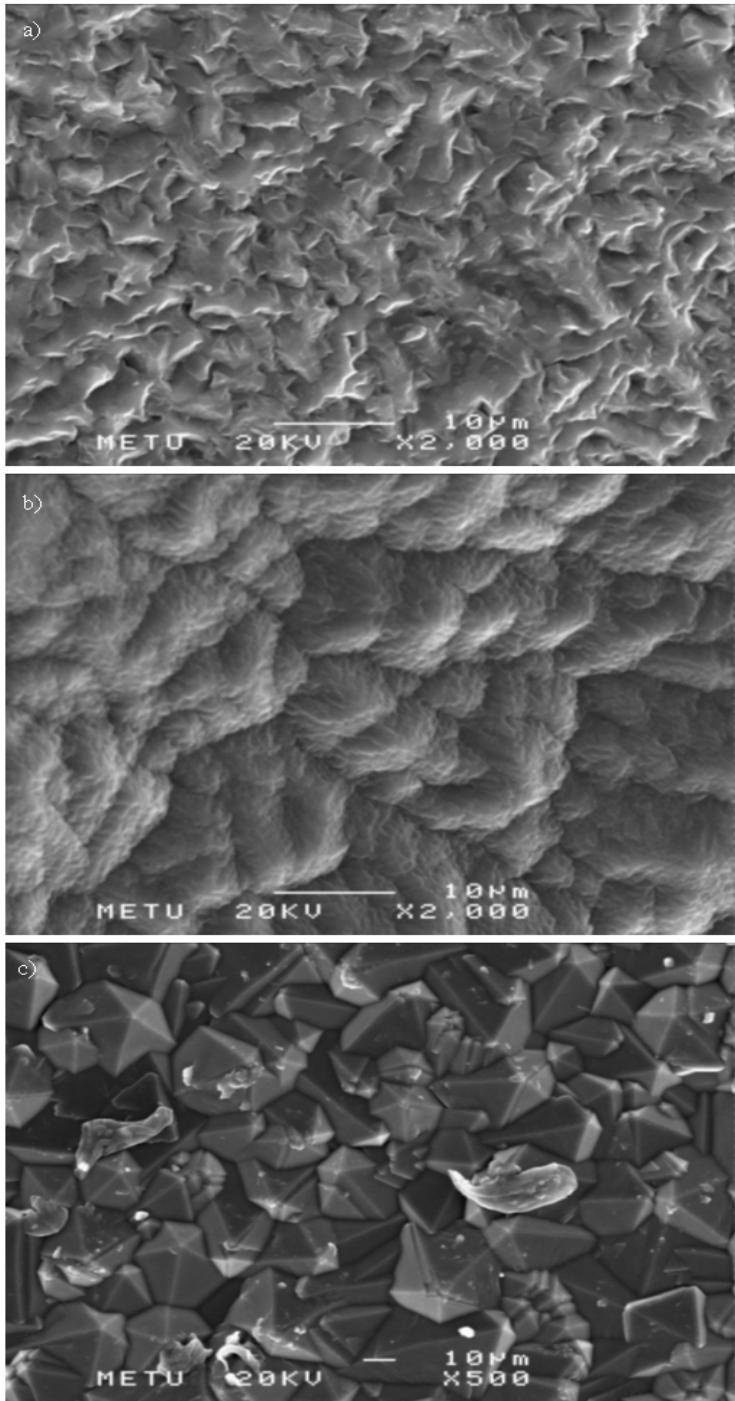


Figure 3.59 SEM images of the samples produced at different temperatures ($P=1$ atm., $y_{\text{CH}_4}/y_{\text{BCl}_3}=0.25$ in hydrogen at reactor inlet) a) 1100°C ; b) 1200°C ; c) 1300°C

highly dependent upon the chemical composition and microstructure. In the previous sections, the effect of temperature on the chemical composition and microstructure of the deposited boron carbide was investigated. In this section, the effect of deposition temperature on hardness of boron carbide will be discussed. The hardness values of boron carbides produced by different methods are widely scattered. Conventional high temperature B₄C production methods usually result in impurities, among them graphite, or free carbon, are the most observed ones. Such impurities are believed to be the main reason behind the widely scattered hardness values. On the other hand, because of its extremely high hardness values, the sample preparation for hardness measurements of boron carbide is very difficult. This is another reason for highly scattered hardness results, and the comparisons between them are difficult [23].

Vickers hardness measurement method is a standard method to determine the hardness of materials, which has extremely hard surfaces like boron carbide. In this study, the hardness measurements were carried out using a microhardness tester (Instron Tukon 2100B) having a diamond pyramid indenter. Surfaces of the specimens should be flat and polished, for any microhardness measurement method. For that reason, boron carbide samples were first polished prior to the hardness analyses.

The samples were first buried into a bakelite mould, and then coarse polishing was made using SiC sandpapers. However, since the hardness of the B₄C samples were greater than SiC, fine polishing of the surfaces was not possible. The reason for SiC treatment was basically to remove excess bakelite material to have a flat surface for

diamond polishing. Diamond paste having 3 μm particle sizes was used for fine polishing in a Metkon-Gripo polisher. After diamond treatment, boron carbide surfaces were well polished and flat for the microhardness analyses. The indenter employed in Vickers test is a square based pyramid with an apex angle of 136° (Figure 3.60). The diamond indenter is pressed into the surface of the material with a 9.8 N load. The size of the indentation on the substrate surface is measured with an optical microscope.

The hardness value (Vickers number, HV) is calculated using the following expression,

$$\text{HV} = 1.854 (F/D^2) \quad (3.45)$$

where F is the force applied in kilograms-force and D^2 is the area of indentation in mm^2 .

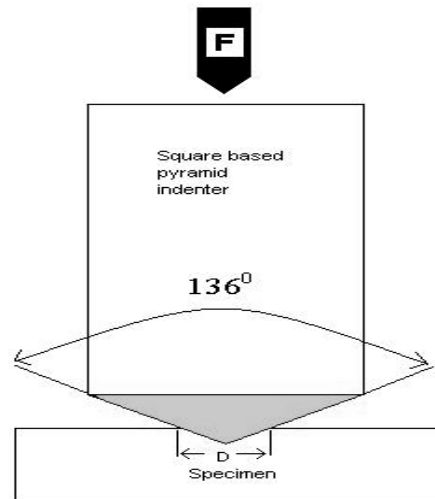


Figure 3.60 Vickers Hardness Test

Hardness measurements were carried out for three different B₄C samples produced at 1100, 1200 and 1300°C, and the results are depicted in Table 3.5. There is an increasing trend in the hardness value with temperature rise. This is an highly expected result, such that, as it was explained in the previous sections, temperature has strong influence on both chemical composition and microstructure. With an increase in temperature, B/C ratio of the boron carbide deposits decreases, due to the entrance of more carbon atom into the structure at higher temperatures. In CVD synthesized boron carbide, hardness values increase with increasing carbon content within the phase homogeneity range [23, 24]. We can conclude that the hardness increase with temperature is resulted from both, increase of bound-carbon content (not free graphite) and evolution in the microstructure of boron carbide with temperature. Especially, at 1300°C, the formation of large icosahedral B₄C crystals is believed to be one of the main reasons for the very high hardness value observed.

Table 3.5. Effect of temperature on Vickers Hardness of Boron Carbide

| Temperature (°C) | Vickers Hardness (kg/mm²) |
|-------------------------|---|
| 1100 | 3850 |
| 1200 | 4085 |
| 1300 | 4750 |

CHAPTER 4

CONCLUSIONS AND RECOMMENDATIONS

The deposition of β -rhombohedral boron carbide on tungsten substrate was achieved by a relatively simple process. Boron carbide deposition was accompanied by the formation of a by-product, dichloroborane in the gas phase, which was proven by FTIR spectrophotometer. The formation of BHCl_2 was attributed mainly to the gas phase reactions within the thin thermal boundary layer next to the substrate surface. In all of the conducted experiments, the rate of boron carbide formation reaction was always lower than that of the dichloroborane formation reaction. Both rates increase with an increase in the inlet molar fraction of boron trichloride, although the B_4C formation rate stabilizes at high BCl_3 inlet concentrations. This implies that the boron carbide formation reaction may be surface reaction limited at that temperature. All the collected kinetic data was fit in an Arrhenius type of a model equation and the activation energy was found to be 56.1kJoule/mol. Exponents of methane and boron trichloride were 0.64 and 0.34, respectively, implying a complex reaction mechanism. The observed correlation coefficient value after the nonlinear regression analysis was 0.95, which actually needs to be improved by assigning more realistic rate equations that are usually applied for

catalytic reactions. This was possible only by a detailed kinetic modeling study.

In the kinetic modelling study, large number of reaction mechanisms were proposed, and among them only the ones considering the molecular adsorption of boron carbide on the substrate surface gave reasonable fits. In the proposed model which best fits the experimental data, hydrogen and methane are adsorbed dissociatively and adsorbed boron trichloride is reduced by adsorbed methane to form an intermediate BC molecule on the substrate surface. This intermediate is reacted in successive series reactions including adsorbed boron trichloride and adsorbed hydrogen to produce finally stoichiometric B₄C phase. The simultaneous fit of the experimental data to the model expression gave good fits for the boron carbide and dichloroborane formation reactions with the high correlation coefficient values.

The temperature of the substrate was found to have a great effect on the film morphology and microstructure. XPS analysis shows the existence of chemical states attributed to the boron carbide phase, together with the existence of oxy-boron carbide species. The carbon concentration of the products decreased with a decrease in the substrate temperature, which was attributed to the replacement of one carbon atom with one boron atom in the C-B-C icosahedral chain, leading B-B-C structure, at lower temperatures. The change of surface morphology with temperature was investigated and the production of huge icosahedral boron carbide crystals having 5-fold symmetry at a substrate temperature of 1300°C was accomplished. Deposition temperature was also found to have great effect on micro-hardness of the products, which was attributed to the dependence of

microstructure and chemical composition of the products on the deposition temperature.

The dual impinging jet reactor configuration that was utilised in this study is a powerful tool to investigate the reaction kinetics including complex surface reactions. However, the mass-production of boron carbide on different substrates will require higher capacity industrial reactors. For that reason, the kinetic data presented in this study should be utilised in the process of designing industrial size reactors. The design and fabrication of a pilot scale lab-to-fab reactor should be considered to scale-up the process, to increase the commercial potential, and to attract industrial attention.

REFERENCES

1. Ali O. Sezer, J.I. Brand, *Materials Science and Engineering*, **B79**(2001), 191.
2. Zenghu Han, Geyang Li, Jiawan Tian, Mingyuan Gu, *Materials Letters*, **57**(2002), 899.
3. J.C. Oliveria, M.N. Oliviera, O. Conde, *Surface and Coatings Technology*, **80**(1996), 100.
4. D.R.Tallant, T.L.Aselage, A.N. Campbell, D.Emin, *Journal of Non-Crystalline Solids*, **106**(1988), 370.
5. Rointan F. Bunshah, *Handbook of Hard Coatings*; Noyes Publications, 2000.
6. U.Cansson, J.O.Carlsson, B.Stridh, S.Söderberg, M.Olsson, *Thin Solid Films*, **172**(1989), 81.
7. A.A. Cochran and J.B. Stephenson, *Metallurgical Transactions*, **1**(1970), 2875.
8. K. Ploog, *Journal of Crystal Growth*, **24/25**(1974), 197.
9. U. Casson and J.O. Carlsson, *Thin Solid Films*, **124**(1985), 95.
10. L.G.Vandenbulcke, *Ind. Eng. Chem.*, **24**(1985), 568.

11. Y.M. Grigor'ev, V.A. Shugaev, A.S. Mukas'yan, N.G. Samoilenko, A.A. Shiryaev, *Russian Journal of Inorganic Chemistry*, **35**(1991), 1089.
12. S.V.Desphande, E. Güleri, S.J. Harris and A.M. Weiner, *Applied Physics Letters*, **65**(1994), 1757.
13. O.Conde, A.J. Silvestre, J.C. Oliviera, *Surface and Coatings Technology*, **125**(2000), 141.
14. S.N.Dilek, H.Ö.Özbelge, N.A. Sezgi, T.Doğu, *Industrial & Engineering Chemistry Research*, **40**(2001), 751.
15. Sezgi N.A., Doğu T., Özbelge H. Ö., 'Kinetics of Boron Fiber Formation', *PhD Thesis, Chemical Engineering Department, Middle East Technical University, 1996*.
16. Hooke R, Jeeves TA., *J. of the ACM*, **8**(1961), 212-229.
17. Sezgi N.A., Dogu T., Ozbelge H.O., (1999). *Chemical Engineering Science*, **54**(1999), 3297.
18. W. J. Pan, J. Sun, H. Ling, N. Xu, Z. F. Ying, J. D. Wu, *Applied Surface Science*, **218**(2003) 297.
19. L. G. Jacobsohn, R. K. Schulze, M. E. H. Maia da Costa, M. Nastasi, *Surface Science*, **572**(2004) 418
20. Selected Powder Diffraction Data for Education and Training Search Manual; International Centre for Diffraction Data, USA, Volume 1/ Volume2, 1988.

21. H. O. Pierson, Handbook of Refractory Carbides and Nitrides: Properties, Characteristics, Processing, and Applications; Noyes Publications, Park Ridge N.J., 1996.
22. B. Wei, R. Vajtai, Y. J. Jung, F. Banhart, G. Ramanath, M. Ajayan, *The Journal of Physical Chemistry*, **106**(2002) 5807.
23. F. Thevenot, *Journal of the European Ceramic Society*, **6**(1990), 205.
24. K. Niihara, A. Nakahira, T. Hirai, *Journal of the American Ceramic Society*, **67**(1984), C13.
25. J. Rey, G. Male, P. Kapsa, J. L. Loubet, *Proc. 7th Eur. Conference CVD*, France, 1989.
26. H. Martin, 'Heat and Mass Transfer between Impinging Gas Jets and Solid Surfaces', in *Advances in Heat Transfer*, Vol. 13, Academic Press, New York, 1977.
27. K. S. Raju, E. U. Schlünder, *Heat and Mass Transfer*, **10**(1977), 131.
28. K. R. Hammond, *Introduction to the Statistical Method*, Knopf Publications, New York, 1962.
29. M. Michaelidis, and R. Pollard, *J. Electrochem. Soc.*, *Solid State Science and Technology*, **131**(1984), 860.

APPENDIX A

FTIR CALIBRATION METHODS

A.1 Calibration of Methane

Before starting calibration experiments, the system was purged with helium in order to remove the impurities, e.g. moisture, oxygen, water vapor, inside the gas cell of FTIR. After that, helium was closed and hydrogen and methane gases were opened at 1 bar. The desired methane concentration in the gas mixture was adjusted using mass flow controllers, keeping the total gas flow rate at 200 mL/min, which is the condition that will be applied during the actual experiments.

The FTIR spectra of the gas mixture passing through the experimental system were taken occasionally, until the peak heights or areas were fixed. When the peak areas or heights were fixed, that values and the corresponding methane concentrations were recorded. The same procedure was applied for different methane compositions and the calibration curve for methane was plotted using the methane composition versus corresponding FTIR peak heights (Figure A-1). The relation between mole fraction of methane and the peak height was found as;

$$y_{\text{CH}_4} = 10.305H_{\text{CH}_4}^2 + 0.2794H_{\text{CH}_4} + 6 \times 10^{-5} \quad (\text{A-1})$$

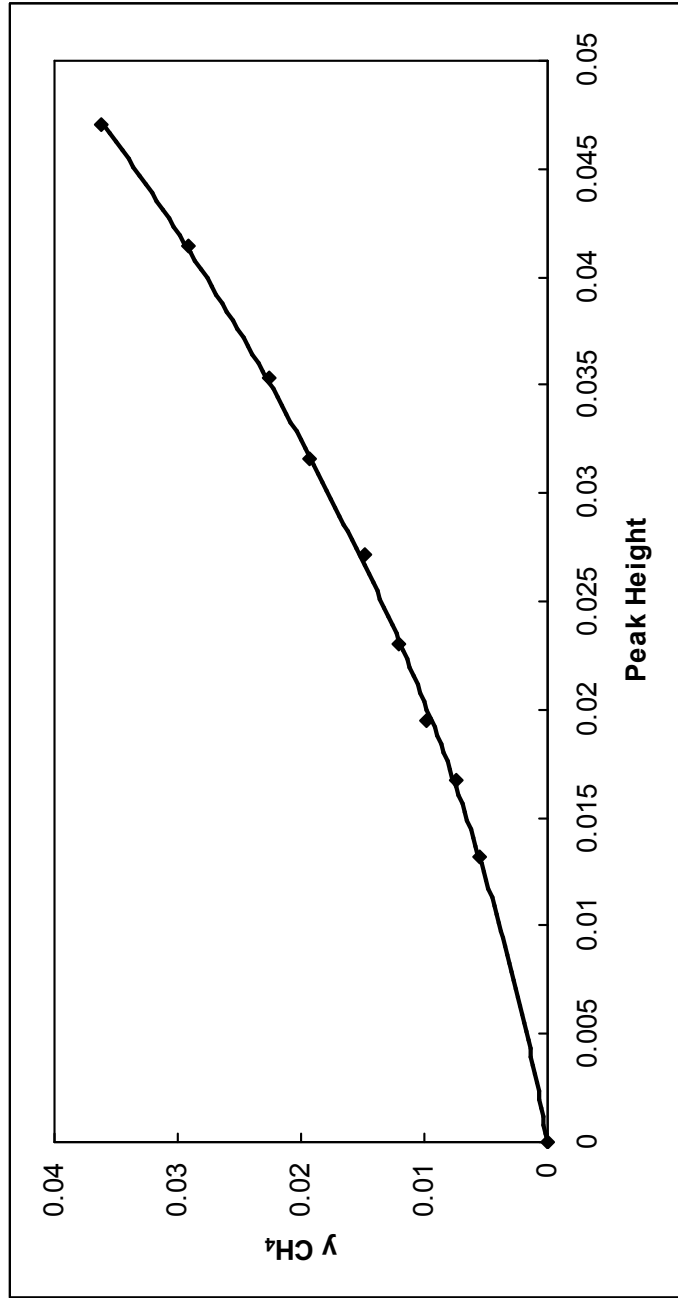


Figure A-1 FTIR Calibration Curve for Methane (Wavenumber: 3183 cm⁻¹)

A.2 Calibration of Boron Trichloride

The actual experimental set-up was used for the calibration of BCl_3 , with the addition of a U tube between the outlet of FTIR and soap bubble meter. Boiling point of boron trichloride at 1 atmosphere pressure is 13.2°C . This physical property of BCl_3 was utilised in the calibration experiments. The aim was to condense boron trichloride inside the U-tube, which was placed into liquid nitrogen bath. In order to condense all of the BCl_3 passing through U-tube, the heat transfer surface area between BCl_3 and liquid nitrogen was increased by filling U-tube with broken glasses.

First of all, the gas mixture containing boron trichloride and hydrogen was passed through the original experimental system. The U-tube was weighted before the calibration experiments. The flowrate of boron trichloride was adjusted by using a needle valve and the FTIR spectra had been taken until the peak area and height reached a constant value. When the desired BCl_3 concentration was obtained, the gaseous mixture was passed through U-tube by using a three-way valve for a measured period of time. At the end of the experiment, the U-tube was weighted. By using the weight difference of U-tube (eqn.A-2), before and after the experiment and the time of the gas flow through the U-tube, mole fraction of BCl_3 was determined (eqn.A-3).

$$W_{\text{BCl}_3} = W_{\text{Utubet=t}} - W_{\text{Utubet=0}} \quad (\text{A-2})$$

$$y_{\text{BCl}_3} = (W_{\text{BCl}_3} * 22400) / (M_{\text{BCl}_3} * V_T * t) \quad (\text{A-3})$$

$$t: \text{min. } W_{\text{BCl}_3}: \text{gram } V_T: \text{cm}^3/\text{min.}$$

The same procedure was repeated for several values of boron trichloride concentrations and the calibration curve was plotted (Figure A-2). The relation between mole fraction of BCl_3 and the peak area is formulated as;

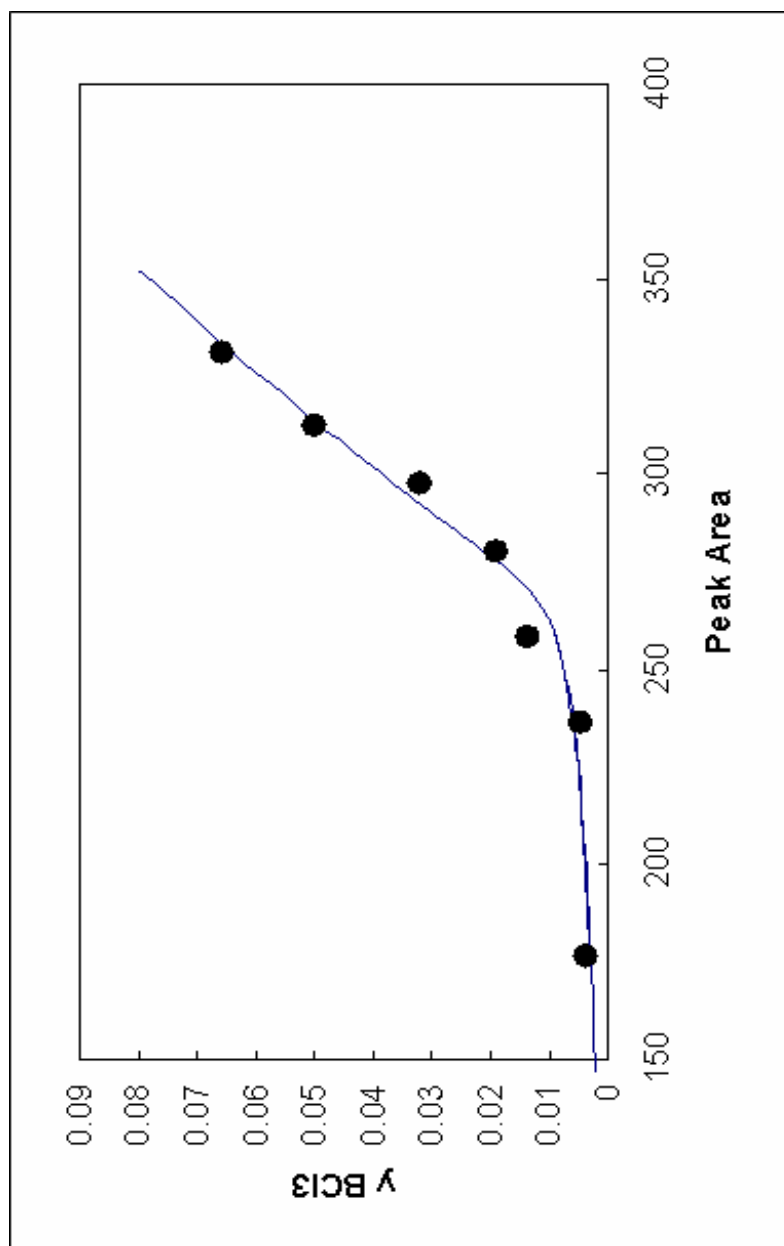


Figure A-2 FTIR Calibration Curve for Boron Trichloride (Wavenumber: 1040-920 cm^{-1})

$$y_{\text{BCl}_3} = \frac{(0.5097 \times 10^{-3} + 0.454 \times 10^{-6} \times A_{\text{BCl}_3})}{(1 - 0.5977 \times 10^{-2} \times A_{\text{BCl}_3} + 0.9023 \times 10^{-5} \times A_{\text{BCl}_3}^2)} \quad (\text{A-4})$$

A.3 Calibration of Hydrogen Chloride

In the calibration experiments of hydrogen chloride gas, helium was used as carrier gas instead of hydrogen. Calibration experiments were carried out using the actual experimental set up, except that methane gas tube was replaced with that of hydrogen chloride. The flowrate of HCl was controlled by means of a rotameter. Before starting the calibration experiments, the system was purged with helium in order to remove impurities. After that, the flowrates of HCl and helium was adjusted, keeping the total volumetric flow rate constant at 200 mL/min. The peak height of HCl was read during the experiments at the same wavenumber. At the end, peak heights of HCl corresponding to different HCl concentrations was plotted (Figure A-3). Equation A-5 gives the relation between mole fraction of HCl and the peak height at a given wavenumber.

$$y_{\text{HCl}} = -1.2754 \times H_{\text{HCl}}^3 + 0.8281 \times H_{\text{HCl}}^2 + 0.0409 \times H_{\text{HCl}} \quad (\text{A.5})$$

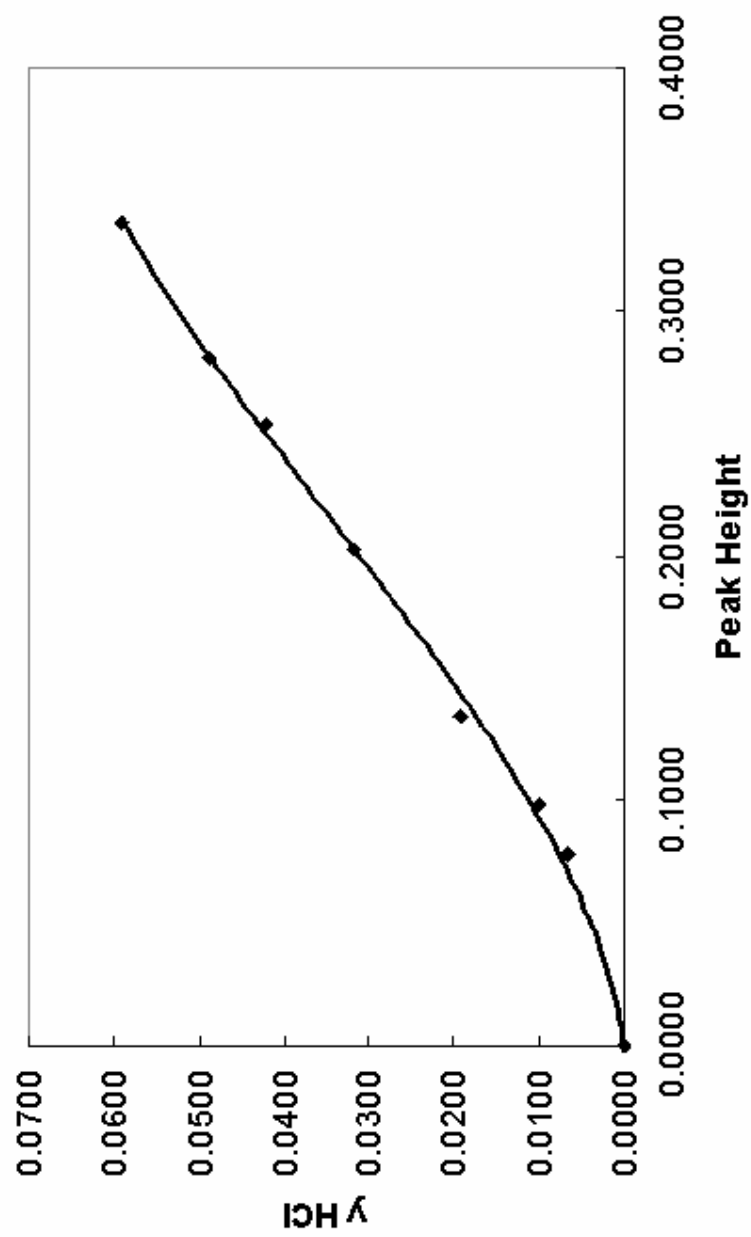


Figure A-3 FTIR Calibration Curve for Hydrochloric Acid (Wavenumber: 2789 cm^{-1})

APPENDIX B

X-RAY DIFFRACTION DATA

Table B.1 XRD Data for Boron Carbide[17]

| B ₄ C Boron Carbide Rad. CuKα ₁ λ= 1.540598 | | |
|--|--------|-------|
| Int | d Å | 2θ |
| 100 | 2.377 | 37.82 |
| 64 | 2.565 | 34.95 |
| 49 | 3.783 | 23.50 |
| 21 | 4.033 | 22.02 |
| 14 | 4.499 | 19.72 |
| 13 | 1.4605 | 63.66 |
| 12 | 1.3995 | 66.79 |
| 11 | 2.803 | 31.90 |
| 11 | 1.712 | 53.48 |
| 10 | 1.4423 | 64.56 |
| 9 | 1.5004 | 61.78 |
| 8 | 1.3369 | 70.37 |
| 8 | 1.3128 | 71.85 |
| 7 | 1.3228 | 71.23 |
| 6 | 1.2571 | 75.58 |
| 4 | 2.3 | 39.13 |
| 4 | 1.8127 | 50.29 |
| 4 | 1.1887 | 80.78 |
| 3 | 1.2605 | 75.34 |
| 2 | 1.6261 | 56.55 |
| 2 | 1.2820 | 73.86 |
| 1 | 1.8906 | 48.09 |
| 1 | 1.5674 | 58.87 |
| 1 | 1.2112 | 78.99 |
| 1 | 1.2065 | 79.35 |

Table B.2 XRD Data for Boron [17]

| B Boron Rad. CuKα λ= 1.541800 | | |
|--|--------|-------|
| Int | d Å | 2θ |
| 45 | 4.2500 | 20.88 |
| 100 | 4.0700 | 21.82 |
| 20 | 3.5440 | 25.11 |
| 70 | 2.5450 | 35.24 |
| 10 | 2.4790 | 36.21 |
| 4 | 2.1800 | 41.38 |
| 4 | 2.1320 | 42.36 |
| 55 | 2.1130 | 42.76 |
| Lt2 | 2.0290 | 44.62 |
| 4 | 1.6660 | 55.08 |
| 8 | 1.6340 | 56.25 |
| 8 | 1.6030 | 57.44 |
| 8 | 1.4820 | 62.63 |
| 15 | 1.4380 | 64.78 |
| 8 | 1.4240 | 65.50 |
| 4 | 1.4030 | 66.60 |
| 8 | 1.3760 | 68.09 |
| 10 | 1.3590 | 69.06 |
| 15 | 1.3460 | 69.82 |
| 12 | 1.2680 | 74.82 |
| 2 | 1.2300 | 77.55 |
| Lt2 | 1.1990 | 79.95 |
| 4 | 1.1780 | 81.67 |
| Lt2 | 1.1610 | 83.13 |
| Lt2 | 1.1250 | 86.43 |

Table B.3 XRD Data for α -Tungsten Carbide [17]

| α -W ₂ C Tungsten Carbide Rad. CuK α ₁ $\lambda = 1.540598$ | | |
|--|--------|------------|
| Int | d Å | 2 θ |
| 100 | 2.2757 | 39.57 |
| 25 | 2.596 | 34.52 |
| 22 | 2.3643 | 38.03 |
| 17 | 1.7478 | 52.30 |
| 14 | 1.4986 | 61.86 |
| 14 | 1.3469 | 69.77 |
| 12 | 1.2657 | 74.98 |
| 10 | 1.2514 | 75.98 |
| 3 | 1.1377 | 85.23 |
| 2 | 1.2975 | 72.84 |
| 2 | 1.1821 | 81.33 |

Table B.4 XRD Data for Tungsten Carbide [17]

| WC Tungsten Carbide Rad. Cu $\lambda = 1.540560$ | | |
|--|-------|------------|
| Int | d Å | 2 θ |
| 100 | 2.518 | 35.63 |
| 100 | 1.884 | 48.27 |
| 45 | 2.84 | 31.47 |
| 30 | 1.236 | 77.10 |
| 25 | 1.294 | 73.06 |
| 20 | 1.454 | 63.98 |
| 20 | 1.151 | 84.01 |
| 14 | 1.259 | 75.44 |
| 6 | 1.42 | 65.70 |

Table B.5 XRD Data for Tungsten [17]

| W Tungsten Rad. CuK α ₁ $\lambda = 1.540500$ | | |
|---|--------|------------|
| Int | d Å | 2 θ |
| 100 | 2.238 | 40.26 |
| 23 | 1.292 | 73.19 |
| 18 | 0.8459 | 131.17 |
| 15 | 1.582 | 58.27 |
| 11 | 1.0008 | 100.64 |
| 8 | 1.1188 | 87.02 |
| 4 | 0.9137 | 114.92 |
| 2 | 0.7912 | 153.57 |

Table B.6 XRD Data for α -Tungsten Carbide [17]

| C Carbon (Diamond-3C) Rad. CuK α ₁ $\lambda = 1.540500$ | | |
|--|--------|------------|
| Int | d Å | 2 θ |
| 100 | 2.0600 | 43.92 |
| 25 | 1.2610 | 75.30 |
| 16 | 1.0754 | 91.50 |
| 8 | 0.8916 | 119.53 |
| 16 | 0.8182 | 140.59 |

Table B.7 XRD Data for Carbon (Diamond) [17]

| C Carbon (Diamond-3C) Rad. CuK α_1 $\lambda=$ 1.540500 | | |
|--|--------|------------|
| Int | d Å | 2 θ |
| 100 | 2.0600 | 43.92 |
| 25 | 1.2610 | 75.30 |
| 16 | 1.0754 | 91.50 |
| 8 | 0.8916 | 119.53 |
| 16 | 0.8182 | 140.59 |

Table B.8 XRD Data for Carbon (Graphite) [17]

| C Carbon (Graphite-2H) Rad. CuK α $\lambda=$ 1.541800 | | |
|---|--------|------------|
| Int | d Å | 2 θ |
| 100 | 3.3600 | 26.53 |
| 10 | 2.1300 | 42.44 |
| 50 | 2.0300 | 44.64 |
| 5 | 1.8000 | 50.72 |
| 80 | 1.6780 | 54.70 |
| 10 | 1.5440 | 59.91 |
| 30 | 1.2320 | 77.47 |
| 50 | 1.1580 | 83.47 |
| 5 | 1.1380 | 85.28 |

Table B.9 XRD Data for Silicon Oxide [17]

| SiO ₂ Silicon Oxide Rad. CuK α_1 $\lambda=$ 1.540598 | | |
|---|--------|------------|
| Int | d Å | 2 θ |
| 100 | 3.342 | 26.65 |
| 22 | 4.257 | 20.85 |
| 14 | 1.8179 | 50.14 |
| 9 | 1.5418 | 59.95 |
| 8 | 2.457 | 36.54 |
| 8 | 2.282 | 39.46 |
| 8 | 1.3718 | 68.32 |
| 7 | 1.3752 | 68.13 |
| 6 | 2.127 | 42.46 |
| 6 | 1.382 | 67.75 |
| 4 | 2.237 | 40.28 |
| 4 | 1.9792 | 45.81 |
| 4 | 1.6719 | 54.87 |
| 3 | 1.1843 | 81.15 |
| 3 | 1.1804 | 81.47 |
| 2 | 1.6591 | 55.33 |
| 2 | 1.288 | 73.46 |
| 2 | 1.2558 | 75.67 |
| 2 | 1.1999 | 79.88 |
| 1 | 1.8021 | 50.61 |
| 1 | 1.6082 | 57.24 |
| 1 | 1.4536 | 64.00 |
| 1 | 1.4189 | 65.76 |
| 1 | 1.2285 | 77.66 |
| 1 | 1.1978 | 80.05 |

Table B.10 XRD Data for Silicon Carbide [17]

| SiC Silicon Carbide Rad. CuK α $\lambda=$ 1.541780 | | |
|--|--------|------------|
| Int | d Å | 2 θ |
| 100 | 2.52 | 35.63 |
| 35 | 1.5411 | 60.03 |
| 25 | 1.314 | 71.84 |
| 20 | 2.18 | 41.42 |
| 5 | 1.2583 | 75.56 |
| 5 | 1.0893 | 90.10 |

Table B.11 XRD Data for α -Silicon Carbide [17]

| α -SiC Silicon Carbide Rad. CuK α_1 $\lambda=$ 1.540560 | | |
|--|-------|------------|
| Int | d Å | 2 θ |
| 100 | 2.511 | 35.73 |
| 40 | 2.621 | 34.18 |
| 40 | 1.311 | 71.97 |
| 35 | 1.537 | 60.15 |
| 20 | 2.352 | 38.23 |
| 15 | 1.418 | 65.81 |
| 15 | 1.286 | 73.59 |
| 15 | 1.087 | 90.25 |
| 10 | 2.174 | 41.50 |
| 7 | 1.256 | 75.65 |
| 7 | 1.042 | 95.33 |

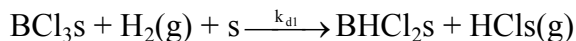
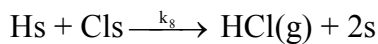
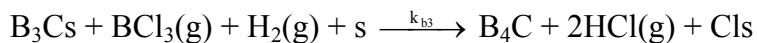
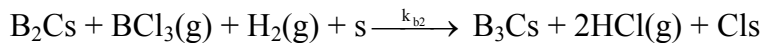
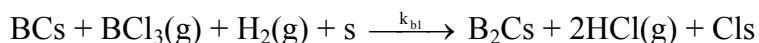
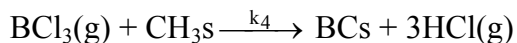
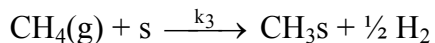
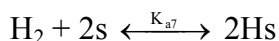
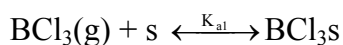
APPENDIX C

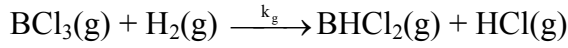
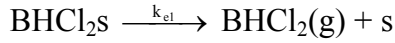
DERIVATIONS OF RATE LAWS FROM PROPOSED MECHANISMS

In this section, the derivations of the rate laws for the production rates of boron carbide and dichloroborane for Model 7 are given. The derivations for the other models were done in the similar manner.

Model 7

The elementary reaction steps proposed for this mechanism as follows:





The rate limiting step was selected to be step 7, which is a surface reaction step, in which boron carbide was formed on the solid surface. The rate of boron carbide and dichloroborane formation reactions can be written as follows considering the rate limiting step:

$$R_{\text{B}_4\text{C}} = k_{b3} f_{\text{B}_3\text{C}} P_{\text{BCl}_3} P_{\text{H}_2} f_v \quad \text{C.1}$$

$$R_{\text{BHCl}_2} = k_{e1} f_{\text{BHCl}_2} + k_g P_{\text{BCl}_3} P_{\text{H}_2} \quad \text{C.2}$$

The fractions of the surface occupied by boron trichloride, methane and hydrogen are;

$$f_{\text{BCl}_3} = K_{a1} P_{\text{BCl}_3} f_v \quad \text{C.3}$$

$$f_{\text{CH}_3} = \frac{k_3}{k_4} \frac{P_{\text{CH}_4}}{P_{\text{BCl}_3}} f_v \quad \text{C.4}$$

$$f_{\text{H}} = \sqrt{K_{a7} P_{\text{H}_2}} f_v \quad \text{C.5}$$

In equations C1 and C2, the term f_v , which defines the fraction of unoccupied substrate surface, is calculated as follows;

$$1 = f_v + f_{\text{H}} + f_{\text{BCl}_3} + f_{\text{CH}_3} \quad \text{C.6}$$

$$1 = K_{a1} P_{\text{BCl}_3} f_v + \frac{k_3}{k_4} \frac{P_{\text{CH}_4}}{P_{\text{BCl}_3}} f_v + \sqrt{K_{a7} P_{\text{H}_2}} f_v \quad \text{C.7}$$

$$\Rightarrow f_v = \frac{1}{1 + K_{a1} P_{\text{BCl}_3} + \frac{k_3}{k_4} \frac{P_{\text{CH}_4}}{P_{\text{BCl}_3}} + \sqrt{K_{a7} P_{\text{H}_2}}} \quad \text{C.8}$$

where total number of substrate surface sites is taken as 1.

The terms $f_{\text{B}_3\text{C}}$ ve f_{BHCl_2} are written for the fractions of surface occupied by the unstable intermediates B_3C and BHCl_2 , respectively. Those terms were calculated using steady-state approximation,

considering that the fraction of surface covered by intermediates are small. Accordingly;

$$f_{\text{BHCl}_2} = \frac{k_9}{k_{10}} K_1 P_{\text{BCl}_3} f_v P_{\text{H}_2} \quad (\text{C.9}) \quad \text{and} \quad f_{\text{B}_3\text{C}} = \frac{k_3 P_{\text{CH}_4}}{k_7 P_{\text{H}_2}} \quad (\text{C.10})$$

All of those calculated adsorption terms are placed in equations C1 and C2, and finally the rate laws are derived in terms of the partial pressures of the reaction gases, which are in this case methane, boron trichloride and hydrogen.

The rate laws are;

$$R_{\text{B}_4\text{C}} = \frac{k_3 P_{\text{CH}_4} P_{\text{BCl}_3}}{1 + K_{a1} P_{\text{BCl}_3} + \frac{k_3 P_{\text{CH}_4}}{k_4 P_{\text{BCl}_3}} + (K_{a7} P_{\text{H}_2})^{1/2}} \quad (\text{C.11})$$

$$R_{\text{BHCl}_2} = \frac{k_{d1} K_{a1} P_{\text{H}_2} P_{\text{BCl}_3}}{1 + K_{a1} P_{\text{BCl}_3} + \frac{k_3 P_{\text{CH}_4}}{k_4 P_{\text{BCl}_3}} (K_{a7} P_{\text{H}_2})^{1/2}} + k_g P_{\text{BCl}_3} P_{\text{H}_2} \quad (\text{C.12})$$

APPENDIX D

RAW DATA

Table D.1 Raw Data for the Experiment BCL3B

| Run | Duration | y_{BCl_3} | y_{CH_4} | y_{H_2} | y_{HCl} | y_{BHCl_2} | Temperature ($^{\circ}\text{C}$) |
|-----|----------|--------------------|-------------------|------------------|------------------|---------------------|------------------------------------|
| 1 | 0 | 0.1181 | 0.0195 | 0.8624 | 0.0000 | 0.0000 | 1150 |
| 2 | 5 | 0.0885 | 0.0198 | 0.8330 | 0.0275 | 0.0309 | 1147 |
| 3 | 10 | 0.0240 | 0.0171 | 0.7635 | 0.1108 | 0.0836 | 1146 |
| 4 | 15 | 0.0195 | 0.0168 | 0.7585 | 0.1173 | 0.0867 | 1152 |
| 5 | 20 | 0.0210 | 0.0165 | 0.7594 | 0.1179 | 0.0839 | 1150 |
| 6 | 25 | 0.0270 | 0.0167 | 0.7657 | 0.1106 | 0.0789 | 1148 |
| 7 | 30 | 0.0277 | 0.0166 | 0.7662 | 0.1106 | 0.0777 | 1147 |
| 8 | 35 | 0.0276 | 0.0166 | 0.7661 | 0.1107 | 0.0778 | 1146 |
| 9 | 42 | 0.0270 | 0.0165 | 0.7653 | 0.1120 | 0.0780 | 1150 |
| 10 | 47 | 0.0276 | 0.0164 | 0.7658 | 0.1121 | 0.0770 | 1145 |

Table D.2 Raw Data for the Experiment BCI3D

| Spectrum no | Duration | y_{BCl_3} | y_{CH_4} | y_{H_2} | y_{HCl} | y_{BHCl_2} | Temperature ($^{\circ}\text{C}$) |
|-------------|----------|--------------------|-------------------|------------------|------------------|---------------------|------------------------------------|
| 1 | 0 | 0.0894 | 0.01997 | 0.8906 | 0.0000 | 0.0000 | 1150 |
| 2 | 5 | 0.0183 | 0.0177 | 0.8148 | 0.0872 | 0.0615 | 1155 |
| 3 | 10 | 0.0164 | 0.0170 | 0.8115 | 0.0941 | 0.0604 | 1146 |
| 4 | 15 | 0.0148 | 0.0174 | 0.8107 | 0.0928 | 0.0637 | 1151 |
| 5 | 20 | 0.0145 | 0.0168 | 0.8092 | 0.0974 | 0.0615 | 1150 |
| 6 | 25 | 0.0145 | 0.0165 | 0.8086 | 0.0995 | 0.0602 | 1152 |
| 7 | 35 | 0.0141 | 0.0168 | 0.8088 | 0.0977 | 0.0619 | 1149 |
| 8 | 45 | 0.0144 | 0.0169 | 0.8093 | 0.0967 | 0.0620 | 1150 |
| 9 | 55 | 0.0143 | 0.0167 | 0.8088 | 0.0983 | 0.0612 | 1150 |
| 10 | 63 | 0.0144 | 0.0169 | 0.8093 | 0.0967 | 0.0620 | 1145 |

Table D.3 Raw Data for Experiment BC13F

| Spectrum no | Duration | y_{BCl_3} | y_{CH_4} | y_{H_2} | y_{HCl} | y_{BHCl_2} | Temperature ($^{\circ}\text{C}$) |
|-------------|----------|--------------------|-------------------|------------------|------------------|---------------------|------------------------------------|
| 1 | 0 | 0.0761 | 0.0195 | 0.9044 | 0.0000 | 0.0000 | 1150 |
| 2 | 13 | 0.0173 | 0.0188 | 0.8441 | 0.0638 | 0.0559 | 1150 |
| 3 | 17 | 0.0165 | 0.0183 | 0.8422 | 0.0682 | 0.0546 | 1151 |
| 4 | 25 | 0.0155 | 0.0181 | 0.8408 | 0.0706 | 0.0548 | 1145 |
| 5 | 30 | 0.0152 | 0.0178 | 0.8398 | 0.0731 | 0.0538 | 1147 |
| 6 | 35 | 0.0144 | 0.0175 | 0.8384 | 0.0760 | 0.0534 | 1150 |
| 7 | 40 | 0.0147 | 0.0174 | 0.8384 | 0.0765 | 0.0526 | 1150 |
| 8 | 46 | 0.0141 | 0.0163 | 0.8355 | 0.0849 | 0.0487 | 1155 |
| 9 | 50 | 0.0142 | 0.0165 | 0.8360 | 0.0834 | 0.0494 | 1152 |
| 10 | 54 | 0.014067 | 0.01662 | 0.8361 | 0.0827 | 0.0500 | 1150 |

Table D.4 Raw Data for Experiment BC13C

| Spectrum no | Duration | y_{BCl_3} | y_{CH_4} | y_{H_2} | y_{HCl} | y_{BHCl_2} | Temperature ($^{\circ}\text{C}$) |
|-------------|----------|--------------------|-------------------|------------------|------------------|---------------------|------------------------------------|
| 1 | 0 | 0.0411 | 0.01989 | 0.9390 | 0.0000 | 0.0000 | 1150 |
| 2 | 5 | 0.0180 | 0.0186 | 0.9127 | 0.0326 | 0.0180 | 1149 |
| 3 | 15 | 0.0165 | 0.0183 | 0.9105 | 0.0363 | 0.0183 | 1154 |
| 4 | 25 | 0.0164 | 0.0178 | 0.9091 | 0.0401 | 0.0164 | 1150 |
| 5 | 35 | 0.0161 | 0.0177 | 0.9086 | 0.0411 | 0.0163 | 1145 |
| 6 | 45 | 0.0157 | 0.0181 | 0.9092 | 0.0386 | 0.0183 | 1140 |
| 7 | 50 | 0.0156 | 0.0177 | 0.9081 | 0.0416 | 0.0168 | 1153 |
| 8 | 55 | 0.0155 | 0.0178 | 0.9082 | 0.0410 | 0.0173 | 1150 |
| 9 | 60 | 0.0156 | 0.0178 | 0.9083 | 0.0409 | 0.0172 | 1155 |
| 10 | 63 | 0.01557 | 0.0177 | 0.9081 | 0.0417 | 0.0169 | 1152 |

Table D.5 Raw Data for Experiment BC13G

| Spectrum no | Duration | y_{BCl_3} | y_{CH_4} | y_{H_2} | y_{HCl} | y_{BHCl_2} | Temperature ($^{\circ}\text{C}$) |
|-------------|----------|--------------------|-------------------|------------------|------------------|---------------------|------------------------------------|
| 1 | 0 | 0.0302 | 0.0203 | 0.9496 | 0.0000 | 0.0000 | 1150 |
| 2 | 5 | 0.0155 | 0.0191 | 0.9319 | 0.0233 | 0.0101 | 1147 |
| 3 | 10 | 0.0151 | 0.0188 | 0.9308 | 0.0259 | 0.0094 | 1150 |
| 4 | 20 | 0.0142 | 0.0185 | 0.9291 | 0.0290 | 0.0091 | 1151 |
| 5 | 35 | 0.0136 | 0.0187 | 0.9290 | 0.0281 | 0.0105 | 1150 |
| 6 | 45 | 0.0136 | 0.0184 | 0.9283 | 0.0304 | 0.0093 | 1150 |
| 7 | 54 | 0.0137 | 0.0184 | 0.9284 | 0.0303 | 0.0091 | 1153 |

Table D.6 Raw Data for Experiment BC13E

| Spectrum no | Duration | y_{BCl_3} | y_{CH_4} | y_{H_2} | y_{HCl} | y_{BHCl_2} | Temperature ($^{\circ}\text{C}$) |
|-------------|----------|--------------------|-------------------|------------------|------------------|---------------------|------------------------------------|
| 1 | 0 | 0.0229 | 0.0198 | 0.9573 | 0.0000 | 0.0000 | 1150 |
| 2 | 5 | 0.0155 | 0.0191 | 0.9482 | 0.0124 | 0.0047 | 1150 |
| 3 | 10 | 0.0122 | 0.0189 | 0.9441 | 0.0178 | 0.0070 | 1151 |
| 4 | 20 | 0.0109 | 0.0182 | 0.9412 | 0.0238 | 0.0058 | 1150 |
| 5 | 35 | 0.0112 | 0.0188 | 0.9430 | 0.0191 | 0.0078 | 1155 |
| 6 | 40 | 0.0108 | 0.0183 | 0.9414 | 0.0230 | 0.0064 | 1151 |
| 7 | 43 | 0.0109 | 0.0182 | 0.9411 | 0.0240 | 0.0057 | 1150 |

Table D.7 Raw Data for Experiment CH4D

| Spectrum no | Duration | y_{BCl_3} | y_{CH_4} | y_{H_2} | y_{HCl} | y_{BHCl_2} | Temperature ($^{\circ}\text{C}$) |
|-------------|----------|--------------------|-------------------|------------------|------------------|---------------------|------------------------------------|
| 1 | 0 | 0.084 | 0.0423 | 0.8737 | 0.0000 | 0.0000 | 1150 |
| 2 | 10 | 0.0585 | 0.0421 | 0.8478 | 0.0269 | 0.0247 | 1143 |
| 3 | 15 | 0.0510 | 0.0403 | 0.8367 | 0.0466 | 0.0253 | 1160 |
| 4 | 25 | 0.0450 | 0.0399 | 0.8299 | 0.0553 | 0.0297 | 1150 |
| 5 | 35 | 0.0451 | 0.0393 | 0.8288 | 0.0592 | 0.0273 | 1145 |
| 6 | 45 | 0.0421 | 0.0386 | 0.8244 | 0.0669 | 0.0275 | 1143 |
| 7 | 50 | 0.0360 | 0.0378 | 0.8168 | 0.0784 | 0.0304 | 1151 |
| 8 | 55 | 0.0314 | 0.0372 | 0.8111 | 0.0870 | 0.0326 | 1140 |
| 9 | 60 | 0.0318 | 0.0374 | 0.8119 | 0.0852 | 0.0330 | 1155 |
| 10 | 62 | 0.0314 | 0.0372 | 0.8111 | 0.0870 | 0.0326 | 1150 |

Table D.8 Raw Data for Experiment CH4B

| Spectrum no | Duration | y_{BCl_3} | y_{CH_4} | y_{H_2} | y_{HCl} | y_{BHCl_2} | Temperature ($^{\circ}\text{C}$) |
|-------------|----------|--------------------|-------------------|------------------|------------------|---------------------|------------------------------------|
| 1 | 0 | 0.0840 | 0.0387 | 0.8773 | 0.0000 | 0.0000 | 1158 |
| 2 | 10 | 0.0455 | 0.0372 | 0.8358 | 0.0488 | 0.0326 | 1144 |
| 3 | 15 | 0.0435 | 0.0363 | 0.8319 | 0.0569 | 0.0311 | 1160 |
| 4 | 25 | 0.0480 | 0.0343 | 0.8323 | 0.0661 | 0.0188 | 1158 |
| 5 | 35 | 0.0311 | 0.0351 | 0.8172 | 0.0774 | 0.0387 | 1175 |
| 6 | 45 | 0.0377 | 0.0350 | 0.8236 | 0.0715 | 0.0317 | 1163 |
| 7 | 50 | 0.0341 | 0.0344 | 0.8188 | 0.0792 | 0.0329 | 1159 |
| 8 | 55 | 0.0351 | 0.0338 | 0.8186 | 0.0823 | 0.0296 | 1148 |
| 9 | 60 | 0.0355 | 0.0340 | 0.8194 | 0.0805 | 0.0300 | 1150 |
| 10 | 62 | 0.0350 | 0.0342 | 0.8193 | 0.0796 | 0.0313 | 1157 |

Table D.9 Raw Data for the Experiment CH4E

| Spectrum no | Duration | y_{BCl_3} | y_{CH_4} | y_{H_2} | y_{HCl} | y_{BHCl_2} | Temperature ($^{\circ}\text{C}$) |
|-------------|----------|--------------------|-------------------|------------------|------------------|---------------------|------------------------------------|
| 1 | 0 | 0.0840 | 0.0309 | 0.8851 | 0.0000 | 0.0000 | 1150 |
| 2 | 5 | 0.0645 | 0.0308 | 0.8654 | 0.0202 | 0.0191 | 1148 |
| 3 | 10 | 0.0510 | 0.0305 | 0.8513 | 0.0358 | 0.0314 | 1180 |
| 4 | 20 | 0.0434 | 0.0294 | 0.8414 | 0.0511 | 0.0346 | 1140 |
| 5 | 30 | 0.0505 | 0.0294 | 0.8484 | 0.0440 | 0.0275 | 1150 |
| 6 | 40 | 0.0388 | 0.0279 | 0.8337 | 0.0661 | 0.0332 | 1165 |
| 7 | 50 | 0.0405 | 0.0288 | 0.8372 | 0.0581 | 0.0351 | 1150 |
| 8 | 55 | 0.0357 | 0.0282 | 0.8312 | 0.0671 | 0.0374 | 1148 |
| 9 | 60 | 0.0377 | 0.0272 | 0.8311 | 0.0721 | 0.0314 | 1150 |
| 10 | 66 | 0.0376 | 0.027 | 0.8306 | 0.0736 | 0.0307 | 1152 |

Table D.10 Raw Data for the Experiment CH4F

| Spectrum no | Duration | y_{BCl_3} | y_{CH_4} | y_{H_2} | y_{HCl} | y_{BHCl_2} | Temperature ($^{\circ}\text{C}$) |
|-------------|----------|--------------------|-------------------|------------------|------------------|---------------------|------------------------------------|
| 1 | 0 | 0.0840 | 0.0241 | 0.8919 | 0.0000 | 0.0000 | 1145 |
| 2 | 10 | 0.0585 | 0.0240 | 0.8662 | 0.0262 | 0.0251 | 1150 |
| 3 | 15 | 0.0405 | 0.0222 | 0.8443 | 0.0570 | 0.0357 | 1150 |
| 4 | 25 | 0.0381 | 0.0220 | 0.8415 | 0.0608 | 0.0373 | 1148 |
| 5 | 35 | 0.0380 | 0.0219 | 0.8412 | 0.0616 | 0.0370 | 1150 |
| 6 | 45 | 0.0377 | 0.0213 | 0.8396 | 0.0662 | 0.0348 | 1147 |
| 7 | 50 | 0.0370 | 0.0209 | 0.8381 | 0.0697 | 0.0339 | 1151 |
| 8 | 55 | 0.0376 | 0.0204 | 0.8376 | 0.0727 | 0.0312 | 1147 |
| 9 | 60 | 0.0377 | 0.0202 | 0.8373 | 0.0738 | 0.0304 | 1150 |
| 10 | 66 | 0.0376 | 0.0203 | 0.8373 | 0.0737 | 0.0306 | 1152 |

Table D.11 Raw Data for the Experiment CH4A

| Spectrum no | Duration | y_{BCl_3} | y_{CH_4} | y_{H_2} | y_{HCl} | y_{BHCl_2} | Temperature ($^{\circ}\text{C}$) |
|-------------|----------|--------------------|-------------------|------------------|------------------|---------------------|------------------------------------|
| 1 | 0 | 0.0840 | 0.0188 | 0.8973 | 0.0000 | 0.0000 | 1150 |
| 2 | 10 | 0.0728 | 0.0186 | 0.8858 | 0.0121 | 0.0107 | 1140 |
| 3 | 15 | 0.0405 | 0.0165 | 0.8488 | 0.0597 | 0.0342 | 1150 |
| 4 | 25 | 0.0359 | 0.0168 | 0.8449 | 0.0621 | 0.0400 | 1150 |
| 5 | 35 | 0.0405 | 0.0162 | 0.8482 | 0.0619 | 0.0329 | 1049 |
| 6 | 45 | 0.0399 | 0.0157 | 0.8465 | 0.0661 | 0.0314 | 1050 |
| 7 | 50 | 0.0397 | 0.0153 | 0.8454 | 0.0692 | 0.0300 | 1044 |
| 8 | 55 | 0.0388 | 0.0152 | 0.8443 | 0.0708 | 0.0305 | 1054 |
| 9 | 60 | 0.0399 | 0.0155 | 0.8461 | 0.0675 | 0.0306 | 1044 |
| 10 | 66 | 0.0393 | 0.0153 | 0.8450 | 0.0696 | 0.0304 | 1055 |

Table D.12 Raw Data for the Experiment TEA

| Spectrum no | Duration | y_{BCl_3} | y_{CH_4} | y_{H_2} | y_{HCl} | y_{BHCl_2} | Temperature ($^{\circ}\text{C}$) |
|-------------|----------|--------------------|-------------------|------------------|------------------|---------------------|------------------------------------|
| 1 | 0 | 0.08412 | 0.02085 | 0.8950 | 0.0000 | 0.0000 | 1000 |
| 2 | 10 | 0.0510 | 0.0198 | 0.8596 | 0.0407 | 0.0288 | 1003 |
| 3 | 15 | 0.0420 | 0.0197 | 0.8504 | 0.0504 | 0.0374 | 1000 |
| 4 | 25 | 0.0366 | 0.0201 | 0.8459 | 0.0529 | 0.0444 | 1004 |
| 5 | 30 | 0.0375 | 0.0199 | 0.8464 | 0.0534 | 0.0427 | 1002 |
| 6 | 35 | 0.0330 | 0.0195 | 0.8410 | 0.0608 | 0.0455 | 1000 |
| 7 | 40 | 0.0285 | 0.0193 | 0.8361 | 0.0667 | 0.0492 | 1001 |
| 8 | 45 | 0.0301 | 0.0195 | 0.8382 | 0.0634 | 0.0485 | 1000 |
| 9 | 50 | 0.0288 | 0.0194 | 0.8367 | 0.0654 | 0.0495 | 1000 |
| 10 | 58 | 0.02865 | 0.01953 | 0.8367 | 0.0649 | 0.0500 | 998 |

Table D.13 Raw Data for the Experiment TEB

| Spectrum no | Duration | y_{BCl_3} | y_{CH_4} | y_{H_2} | y_{HCl} | y_{BHCl_2} | Temperature ($^{\circ}\text{C}$) |
|-------------|----------|--------------------|-------------------|------------------|------------------|---------------------|------------------------------------|
| 1 | 0 | 0.0828 | 0.0212 | 0.8961 | 0.0000 | 0.0000 | 1120 |
| 2 | 5 | 0.0436 | 0.0204 | 0.8553 | 0.0446 | 0.0361 | 1105 |
| 3 | 15 | 0.0328 | 0.0201 | 0.8438 | 0.0575 | 0.0456 | 1120 |
| 4 | 20 | 0.0223 | 0.0198 | 0.8327 | 0.0701 | 0.0549 | 1078 |
| 5 | 25 | 0.0228 | 0.0190 | 0.8315 | 0.0753 | 0.0510 | 1100 |
| 6 | 30 | 0.0233 | 0.0188 | 0.8316 | 0.0762 | 0.0497 | 1100 |
| 7 | 35 | 0.0243 | 0.0191 | 0.8332 | 0.0731 | 0.0500 | 1115 |
| 8 | 40 | 0.0211 | 0.0187 | 0.8292 | 0.0791 | 0.0515 | 1120 |
| 9 | 45 | 0.0217 | 0.0189 | 0.8302 | 0.0771 | 0.0517 | 1110 |
| 10 | 48 | 0.0217 | 0.0189 | 0.8302 | 0.0771 | 0.0517 | 1100 |

Table D.14 Raw Data for the Experiment TEC

| Spectrum no | Duration | y_{BCl_3} | y_{CH_4} | y_{H_2} | y_{HCl} | y_{BHCl_2} | Temperature ($^{\circ}\text{C}$) |
|-------------|----------|--------------------|-------------------|------------------|------------------|---------------------|------------------------------------|
| 1 | 0 | 0.0804 | 0.0206 | 0.8991 | 0.0000 | 0.0000 | 1204 |
| 2 | 5 | 0.0711 | 0.0200 | 0.8855 | 0.0134 | 0.0070 | 1205 |
| 3 | 10 | 0.0566 | 0.0181 | 0.8668 | 0.0414 | 0.0139 | 1210 |
| 4 | 20 | 0.0180 | 0.0176 | 0.8274 | 0.0834 | 0.0501 | 1200 |
| 5 | 25 | 0.0171 | 0.0176 | 0.8265 | 0.0843 | 0.0510 | 1200 |
| 6 | 30 | 0.0159 | 0.0175 | 0.8251 | 0.0862 | 0.0517 | 1220 |
| 7 | 35 | 0.0161 | 0.0173 | 0.8249 | 0.0874 | 0.0507 | 1215 |
| 8 | 46 | 0.0160 | 0.0173 | 0.8249 | 0.0873 | 0.0510 | 1200 |

Table D.15 Raw Data for the Experiment TED

| Spectrum no | Duration | y_{BCl_3} | y_{CH_4} | y_{H_2} | y_{HCl} | y_{BHCl_2} | Temperature ($^{\circ}\text{C}$) |
|-------------|----------|--------------------|-------------------|------------------|------------------|---------------------|------------------------------------|
| 1 | 0 | 0.0815 | 0.0203 | 0.8982 | 0.0000 | 0.0000 | 130 |
| 2 | 5 | 0.0322 | 0.0171 | 0.8399 | 0.0723 | 0.0360 | 1315 |
| 3 | 10 | 0.0301 | 0.0162 | 0.8358 | 0.0808 | 0.0343 | 1300 |
| 4 | 15 | 0.0122 | 0.0160 | 0.8177 | 0.0999 | 0.0512 | 1299 |
| 5 | 20 | 0.0117 | 0.0159 | 0.8169 | 0.1015 | 0.0510 | 1303 |
| 6 | 25 | 0.0118 | 0.0159 | 0.8171 | 0.1010 | 0.0511 | 1300 |
| 7 | 28 | 0.0117 | 0.0159 | 0.8170 | 0.1014 | 0.0510 | 1298 |

Table D.16 Raw Data for the Experiment TEE

| Spectrum no | Duration | y_{BCl_3} | y_{CH_4} | y_{H_2} | y_{HCl} | y_{BHCl_2} | Temperature ($^{\circ}\text{C}$) |
|-------------|----------|--------------------|-------------------|------------------|------------------|---------------------|------------------------------------|
| 1 | 0 | 0.0801 | 0.0206 | 0.8993 | 0.0000 | 0.0000 | 1150 |
| 2 | 10 | 0.0365 | 0.0200 | 0.8536 | 0.0504 | 0.0397 | 1155 |
| 3 | 20 | 0.0277 | 0.0181 | 0.8447 | 0.0599 | 0.0481 | 1140 |
| 4 | 30 | 0.0248 | 0.0176 | 0.8418 | 0.0628 | 0.0510 | 1150 |
| 5 | 40 | 0.0221 | 0.0176 | 0.8371 | 0.0719 | 0.0499 | 1160 |
| 6 | 50 | 0.0233 | 0.0175 | 0.8394 | 0.0672 | 0.0508 | 1150 |
| 7 | 60 | 0.0217 | 0.0173 | 0.8371 | 0.0710 | 0.0512 | 1155 |
| 8 | 68 | 0.0217 | 0.0173 | 0.8370 | 0.0713 | 0.0509 | 1150 |

Table D.17 Raw Data for the Experiment TEF

| Spectrum no | Duration | y_{BCl_3} | y_{CH_4} | y_{H_2} | y_{HCl} | y_{BHCl_2} | Temperature ($^{\circ}\text{C}$) |
|-------------|----------|--------------------|-------------------|------------------|------------------|---------------------|------------------------------------|
| 1 | 0 | 0.0815 | 0.0207 | 0.8979 | 0.0000 | 0.0000 | 1400 |
| 2 | 5 | 0.0615 | 0.0206 | 0.8777 | 0.0207 | 0.0195 | 1415 |
| 3 | 10 | 0.0367 | 0.0193 | 0.8500 | 0.0548 | 0.0390 | 1420 |
| 4 | 15 | 0.0311 | 0.0192 | 0.8443 | 0.0611 | 0.0441 | 1418 |
| 5 | 20 | 0.0267 | 0.0183 | 0.8379 | 0.0719 | 0.0448 | 1400 |
| 6 | 25 | 0.0234 | 0.0191 | 0.8364 | 0.0695 | 0.0514 | 1390 |
| 7 | 30 | 0.0222 | 0.0191 | 0.8352 | 0.0707 | 0.0526 | 1395 |
| 8 | 35 | 0.0217 | 0.0189 | 0.8343 | 0.0726 | 0.0523 | 1410 |
| 9 | 40 | 0.0218 | 0.0189 | 0.8344 | 0.0725 | 0.0522 | 1400 |
| 10 | 43 | 0.0217 | 0.0189 | 0.8342 | 0.0726 | 0.0523 | 1405 |

APPENDIX E

HEAT AND MASS TRANSFER CALCULATIONS AROUND THE TUNGSTEN FILAMENT

Impinging jet devices are usually utilised in some special applications in order to improve the convection heat and/or mass transfer coefficients. In this section, some empirical correlations together with the well known energy equation will be utilised to carry out heat transfer calculations around the heated tungsten filament. To solve the heat transfer problem in our study, the required variables were the gas flow rate, the nozzle diameter, and the distance between the nozzle and the substrate surface. The empirical correlations utilised in the following discussion are based extensively on the review paper by Holger Martin [26].

E.1 Calculation of Heat Dissipated From the Substrate Surface

The phenomena of jet-impingement on a solid uniform surface is usually characterised by separating the flow pattern into three regions (see Figure E.1). The first region is the free jet region in which the conditions are unaffected by the jet impingement. This region starts at the nozzle exit and extends up to the stagnation zone. At the nozzle

exit, the velocity profile is uniform, however, with increasing distance from the exit, momentum exchange between the jet and ambient causes the free boundary of the jet to broaden. In the impingement zone flow is influenced by the substrate surface and decelerated in the z direction and accelerated in the x direction. However, since the ambient is stationary, the momentum change does not allow for continuous acceleration, and the stagnation zone is transformed to the decelerating wall jet region. With increasing x , velocity component parallel to the surface increases from zero to some maximum, and subsequently decays to zero. Since substrate temperature is greater than the ambient temperature, convection heat transfer occurs in both the stagnation and wall jet regions.

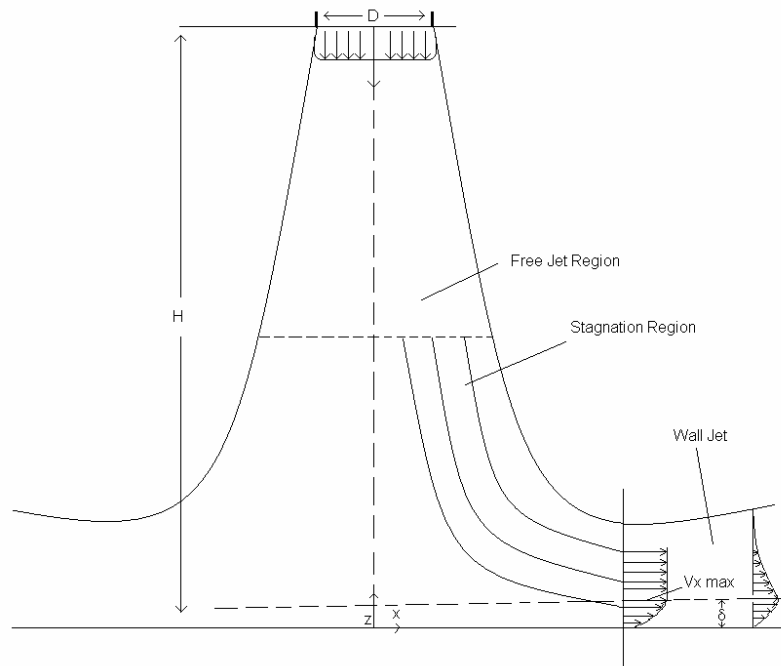


Figure E.1 Schematic representation of jet impingement on the flat surface

According to the Newton's Law of Cooling, the heat dissipation due to the convection is expressed as,

$$q'' = h(T_s - T_c) \quad (E.1)$$

Martin [26] performed an extensive research on the convection heat transfer for impinging jets. The recommended correlation for single round nozzle is,

$$Nu = f(Re, Pr, r/D_h, H/D_h) \quad (E.2)$$

$$\frac{\overline{Nu}}{Pr^{0.42}} = G(r/D, H/D)F_1(Re) \quad (E.3)$$

The ranges of validity of equation E.3 are,

$$2 \leq H/D \leq 12$$

$$2.5 \leq r/D \leq 7.5$$

Since the experiments were carried out in excess hydrogen, the calculations were carried out using the physical properties of hydrogen gas at 1 atm., and at the mean temperature.

Physical properties (Hydrogen gas @ 1 atm.):

$$T_m = (1150+50)/2 = 600 \text{ } ^\circ\text{C}$$

$$\rho = 0.0281 \text{ kg/m}^3$$

$$\mu = 1.83 \times 10^{-5} \text{ Ns/m}^2$$

$$\alpha = 963.03 \times 10^{-6} \text{ m}^2/\text{s}$$

$$k = 399.42 \times 10^{-3} \text{ W/m-K}$$

$$\overline{C_p} = 14.782 \text{ kJ/kg-K}$$

$$Pr = \frac{C_p \mu}{k} = 0.67$$

Characteristic length is the hydraulic diameter of the nozzle D_h , which is defined as, $4A_c/p = D_h$, where A_c is the cross-sectional area of the nozzle. For circular nozzles, the characteristic length is the nozzle diameter, D .

$$Nu = \frac{\bar{h}D_h}{k} \quad (E.4) \quad Re = \frac{V_c D_h}{\nu} \quad (E.5)$$

In an our typical experiment:

$$H = 5 \times 10^{-3} \text{m}$$

$$x = 1.5 \times 10^{-2} \text{m}$$

$$D_h = 1 \times 10^{-3} \text{m}$$

$$Re = \frac{V_c D_h}{\nu} = \frac{1 \times 10^{-3} \text{m} \cdot 2.12 \text{m/s}}{6.51 \times 10^{-4} \text{m}^2/\text{s}} = 3.25$$

The functions F_1 and G are,

$$F_1 = 2 Re^{1/2} (1 + 0.005 Re^{0.55})^{1/2} \quad (E.6)$$

$$G = \frac{D}{r} \frac{1 - 1.1 D/r}{1 + 0.1 (H/D - 6) D/r} \quad (E.7)$$

$$F_1(Re) = 2 Re^{1/2} (1 + 0.005 Re^{0.55})^{1/2} = 2(18.9)^{1/2} (1 + 0.005(18.9)^{0.55})^{1/2} = 3.62$$

$$G = \frac{D}{r} \frac{1 - 1.1 D/r}{1 + 0.1 (H/D - 6) D/r} = 0.0622$$

Thus Equation E.3 gives,

$$\rightarrow \frac{\bar{Nu}}{Pr^{0.42}} = 0.0622 \times 3.62 = 0.225$$

$$\rightarrow \frac{\bar{Nu}}{0.67^{0.42}} = 0.225 \quad \rightarrow \bar{Nu} = 0.190 = \frac{\bar{h}L}{k}$$

$$\rightarrow \bar{h} = 5.07 \text{ W/K-m}^2$$

$$q = A * \bar{h} * (T - T^\infty) = (3 \times 10^{-3} \times 1.5 \times 10^{-2}) \text{ m}^2 \times 5.07 \text{ W/m}^2\text{-K} \times (1150 - 40) \text{ K}$$

| |
|-------------------|
| q = 0.25 W |
|-------------------|

This low flux is confirmed by the small difference in exit and entrance temperature of the reaction mixture through the reactor.

E.2 Temperature profile around the filament

The temperature profile determination in any flow system requires simultaneous solution of energy, mass (equation of continuity), and momentum (Navier-Stokes equations of motion) equations. For complicated geometries like impinging jet, the solution requires computer aided methods, like finite difference analysis. Here, the analysis is much simplified by using empirical correlations for the velocity components, which then, are used in energy equation to find the temperature profile. It was assumed that the velocity components are not affected by the temperature variations (the low flux value found in the previous section verifies this assumption), considering the extremely short residence time of the gas jet within the reactor.

The 2-dimensional energy equation is,

$$V_x \frac{\partial T}{\partial x} + V_z \frac{\partial T}{\partial z} = \alpha \frac{\partial^2 T}{\partial z^2} + \frac{\nu}{C_p} \left(\frac{\partial V_x}{\partial z} \right)^2 \quad (\text{E.8})$$

The valid equation for the velocity on the jet axis for the whole free jet region can be calculated following Schlunder [27] for the axisymmetric free jets,

$$\frac{V(0,z)}{V_D} = \left[1 - \exp \left[- \left(\frac{D/z}{\sqrt{2C}} \right)^2 \right] \right]^{1/2} \quad (\text{E.9})$$

where the constant C is defined as,

$C = 0.127(4D/z_k)$ and it has a value about 0.1, slightly depending on the shape of the nozzle and the exit Reynolds number [27].

z_k is the core length which is the distance from the nozzle exit where the pressure head on the z axis has fallen to 95% of its maximum value. Core lengths of around four slot widths can be expected for a single round nozzle [27].

The stagnation flow begins relatively close to the surface [26]. For single round nozzles the limiting distance is about 1.2 times the nozzle diameter. Exact analytical solutions of the Navier-Stokes equation of motion are known for the idealized limiting case of infinitely extended plane and axisymmetric laminar stagnation flows. They are typical boundary layer flows, the velocity components of flow outside the boundary layer are given by,

$$V_z = -2*a_R*z \quad (E.10)$$

$$V_x = a_R*x \quad (E.11)$$

Where a_R is a constant, which means that velocity components are linearly proportional to the distance from the stagnation point.

The boundary layer thickness is defined as the distance from the surface where lateral component reaches 99% of the velocity (V_x) defined above,

$$\delta = 1.95 (V/a_R)^{1/2} \quad (\text{for stagnation flow}) \quad (E.12)$$

For real stagnation flows due to impinging jets, the constant a_R can be written as [26];

$$a_R = (v_D/D)(1.04-0.034H/D)$$

$$\rightarrow \delta = D*1.95 / \text{Re}^{1/2} * (1.04-0.034*H/D)^{-1/2}$$

$$\rightarrow \delta \approx 5*10^{-4} \text{ m} = 0.5 \text{ mm}$$

This value of heat transfer boundary layer thickness enables us to make an educated guess for the thickness (or the volume) through which the gas phase reaction is possible. If the temperature profile is assumed to be linear in heat transfer boundary layer then,

$$-\frac{dT}{dz} = \frac{(1150 - 40)}{0.5} = -2200 \text{ K/mm} \quad (E.13)$$

The lowest temperature at which the reaction can take place can be assumed as 300⁰C.

$$T=1150-2220z=300$$

$$z=850/2220=0.38\text{mm}$$

that means the reaction can possibly take place within 0.38 mm thick gas film next to the substrate surface.

This result allows us to express the dichloroborane formation reaction (which takes place in the gas phase) rate on per unit area basis as was done in Section 3.2.1.

Following the above discussion, z and x components of the gas velocity in the stagnation zone were found as,

$$V_x = a_R * x = 1827 * x \text{ [m/s]} \quad (\text{E.14})$$

$$V_z = -2 * a_R * z = -3654 * z \text{ [m/s]} \quad (\text{E.15})$$

Then these velocity components were inserted in energy equation and the equation was solved using bottom boundary condition as the temperature of the substrate surface (1150 °C), and the top boundary condition as the reactor outlet temperature (40 °C) (this outlet temperature was observed when the substrate surface temperature was set to 1150 °C during any experimental run).

The algebraic calculations were carried out using a Matlab code, and the results are summarised in a single 2-D Matlab graphical output plot (Figure E.2).

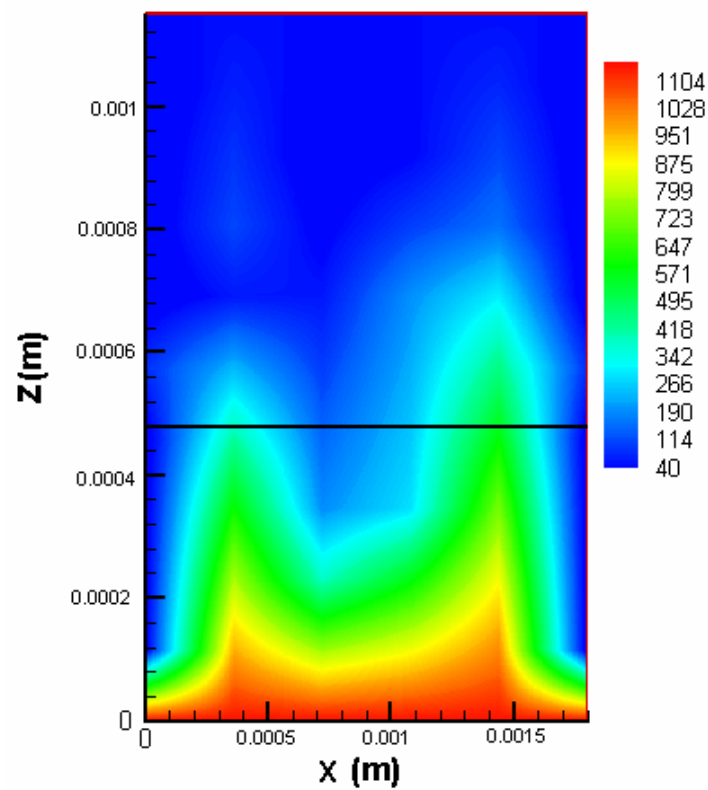


Figure E.2 Temperature profile in the vicinity of the heated substrate surface at 1150 °C (x: distance along the surface; z: distance from the surface)

E.3 Comparison of Diffusion Effects Over the Substrate Surface Between the Impinging Jet and Parallel Flow Conditions

The detailed kinetic study carried out in this study was based on the assumption that the mass transfer limitation on the reaction kinetics were minimized. The best way to check the validity of this assumption is to compare the mass transfer boundary layer thicknesses in the case of jet impingement and the mass transfer coefficient with a parallel flow system.

In section E.1, the boundary layer thickness was calculated for the case of impinging jet geometry utilized in this study. In order to predict the mass transfer boundary layer thickness the following correlation was utilized,

$$\delta_c = \delta / Sc^{1/3}$$

$$(\delta_c)_1 = 0.5 * 10^{-3} / 1.67^{1/3} = 4.2 * 10^{-4} \text{m}$$

For the calculation of boundary layer thickness for parallel flow conditions, the flow geometry was assumed to be the flat plate in parallel flow. The Reynolds number for parallel flow over the substrate surface can be calculated as,

$$Re = \frac{V_\infty L}{\nu} = \frac{2.12 \times 3 \times 10^{-2}}{6.51 \times 10^{-4}} = 98 \text{ (Laminar flow for entire surface)}$$

Therefore for the boundary layer thickness,

$$\delta = \frac{5x}{\sqrt{Re_x}} = \frac{5 * 3 * 10^{-2}}{\sqrt{98}} = 0.015 \text{m}$$

$$\delta_c = \delta / Sc^{1/3}$$

$$(\delta_c)_2 = 0.015 / 1.67^{1/3} = 1.26 * 10^{-2} \text{m}$$

Hence, it was observed that the mass transfer boundary layer thickness decreased almost 30 folds, in the presence of impinging jet system.

APPENDIX F

REPRODUCIBILITY CALCULATIONS

Reproducibility experiment is important to test the reliability of the experimental data. For that purpose, three experiments were repeated on separate days, with nearly the same experimental conditions (Table F.1). Having exactly the same conditions at the start of the experiments were impossible because of the control limitations. The final compositions of the reactor effluent streams for the separate runs were the measure of the reproducibility. From the final composition of the reactor effluent, the rates of the boron carbide and dichloroborane formation reactions were calculated and a statistical analysis was done. In the statistical analysis, the aim is to calculate the confidence intervals for both boron carbide and dichloroborane formation rates.

In order to calculate confidence interval (ω) for the situations where sample size is small and the population standard deviation is not known, students-t methodology is employed, for which;

$$\omega = \bar{X} \pm \frac{tS}{\sqrt{N}}$$

where \bar{X} is the sample mean and S is the sample standard deviation;

Table F.1 Experimental Conditions for the Reproducibility Experiments

| Y_{CH_4O} | Y_{BCl_3O} | Y_{H_2O} | R_{B_4C} | R_{BHCl_2} |
|-------------|--------------|------------|------------|--------------|
| 0.0208 | 0.0921 | 0.8871 | 3.81E-05 | 0.000511 |
| 0.0206 | 0.0894 | 0.8899 | 3.98E-05 | 0.000483 |
| 0.0207 | 0.0881 | 0.8912 | 4.06E-05 | 0.000461 |

$$\bar{X} = \frac{\sum_{i=1}^N x_i}{N} \quad S = \sqrt{\frac{\sum_{i=1}^N (x_i - \bar{x})^2}{N-1}}$$

The t-distribution has one parameter which is called the degrees of freedom (ν) where;

$$\nu = N-1$$

For the large degrees of freedom values, the t-distribution approaches to the normal distribution. For any given values of the degrees of freedom, the t values are tabulated as a function of confidence levels [28].

For the three experimental runs given in Table F.1, the degrees of freedom is 2. Using the t-distribution table [28], the value of t was found to be 2.92 for 95% confidence limit.

Accordingly, the confidence intervals for the boron carbide and dichloroborane formation rates were found as $\pm 4.1\%$, and $\pm 5.2\%$, respectively for 95% of confidence limits.

APPENDIX G

COMPARISON BETWEEN EQUILIBRIUM CONVERSIONS AND THE EXPERIMENTALLY OBSERVED CONVERSIONS

In order to find out the extent through which reaction system approaches equilibrium for the two overall formation reactions of boron carbide and dichloroborane, the equilibrium constants of these two reactions (K_{p1} and K_{p2} , respectively) were compared with the experimentally observed conversion values (Y_1 and Y_2 , respectively) at different substrate temperatures.

Y_1 and Y_2 values were calculated using the molar fractions of reactor outlet gases.

$$Y_1 = \frac{P_{\text{HCl}}^3}{P_{\text{BCl}_3} P_{\text{H}_2} P_{\text{CH}_4}^{1/4}} \quad (\text{G.1})$$

$$Y_2 = \frac{P_{\text{BHCl}_2} P_{\text{HCl}}}{P_{\text{BCl}_3} P_{\text{H}_2}} \quad (\text{G.2})$$

The mole fractions of each species at the reactor effluent were already explained by equations 3.9 through 3.13, hence equations G.1 and G.2 becomes,

$$Y_1 = \frac{(3X_1 + X_2)^3 y_{\text{BCl}_3}^2}{\left(1 + \frac{1}{4} y_{\text{BCl}_3} X_1\right)^{3/4} (1 - X_1 - X_2) (y_{\text{H}_2\text{O}} - y_{\text{BCl}_3} (X_1 + X_2)) (y_{\text{CH}_4} - \frac{1}{4} y_{\text{BCl}_3} X_1)^{1/4}}$$

$$Y_2 = \frac{(3X_1 + X_2) y_{\text{BCl}_3} X_2}{(1 - X_1 - X_2) (y_{\text{H}_2\text{O}} - y_{\text{BCl}_3} (X_1 + X_2))}$$

Y_1 and Y_2 values were calculated using the reactor outlet gas compositions for the experiments carried out at different temperatures.

The temperature dependent equilibrium constants of the boron carbide formation reaction was calculated using well known van't Hoff equation,

$$\frac{d\ln K_p}{dT} = \frac{\Delta H_{\text{rxn}}}{RT^2} \quad (\text{G.3})$$

where,

$$\Delta H_{\text{rxn}} = \Delta H_{298} + \int_{298}^T \Delta C_p dT \quad (\text{G.4})$$

Hence integration of equation G.3 gives K_p values at the desired temperatures. The specific heats and heat of formation values for the reactants and products are tabulated in Table G.1.

Table G.1 Thermodynamic Properties of Reactants and Products

| Substance | C_p (J/mol K= $a+bT+cT^2+dT^3$) (T in K) | | | | ΔH_f° (J/mole) (298 K & 1 atm) |
|----------------------|--|----------|-----------|-----------|--|
| | a | b | c | d | |
| BCl_3 | 32.61 | 0.139 | -1.46E-04 | 5.44E-08 | -4.03E+05 |
| H_2 | 27.14 | 9.27E-03 | -1.38E-05 | 7.65E-09 | - |
| B_4C | 95.999 | 2.32E-02 | -4.10E-07 | -8.14E-11 | -6.27E+04 |
| HCl | 30.67 | -0.0072 | 1.25E-05 | -3.90E-09 | -9.24E+04 |

The same procedure can be applied for dichloroborane formation reaction, however, the temperature dependence of equilibrium constant of dichloroborane (K_{p2}) is readily available in the literature [29].

$$K_{p2} = \exp\left(17.51 - \frac{0.81 \times 10^{-4}}{T} - 2.08 \ln T + 0.94 \times 10^{-3} T - 0.07 \times 10^{-6}\right)$$

Temperature dependence of the values of equilibrium constants K_{p1} and K_{p2} , in comparison with the Y_1 and Y_2 values is given in Figure G.1. As can be seen clearly from the figure, magnitudes of Y_1 and Y_2 values are much smaller than the equilibrium constants. This observation indicates that in impinging jet reactor, both reactions are far from equilibrium.

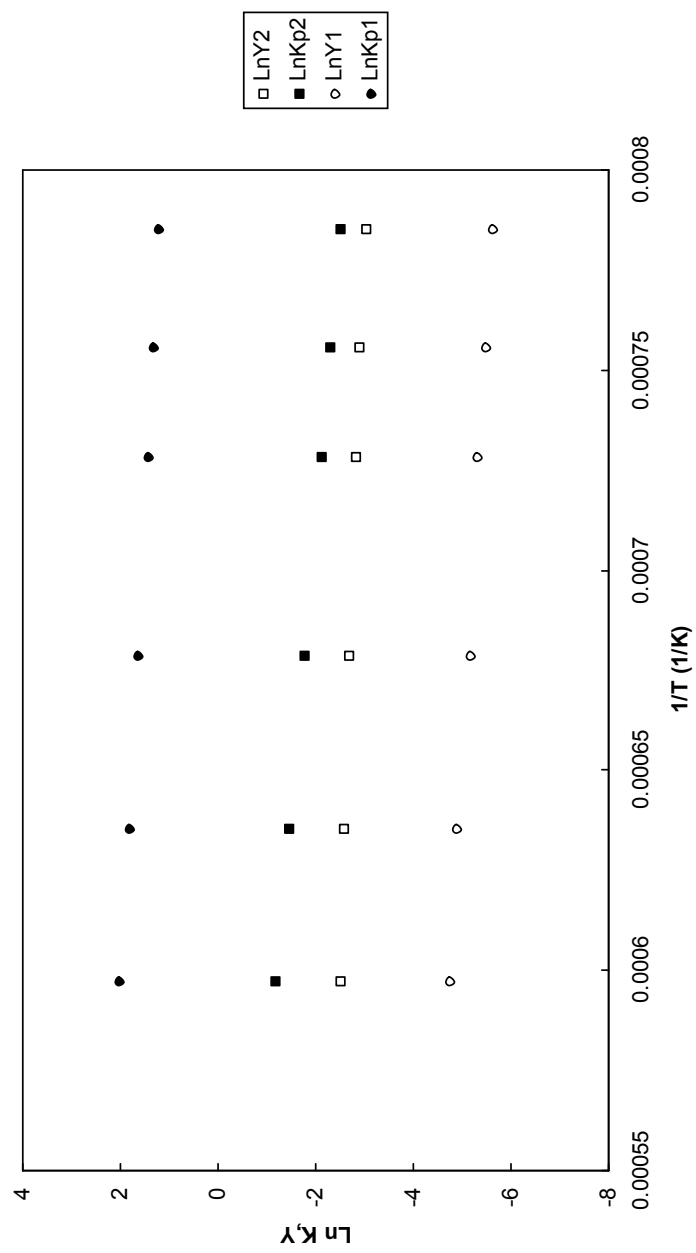


Figure G.1 Temperature dependence of chemical equilibrium constants for boron carbide and dichloroborane formation reactions

CIRRICULUM VITAE

NAME

Mustafa Karaman

ADRESS

Department of Chemical Engineering, Middle East Technical
University (METU),

06531, Çankaya, Ankara

Phone: 90-312-210 43 53

Fax : 90-312-210 26 00

e-mail : kamustaf@metu.edu.tr

web: www.che.metu.edu.tr/~mkaraman/

DATE & PLACE OF BIRTH

Jan 14, 1980, Adana, Turkey

CITIZENSHIP

Turkish

LANGUAGES

English, read and speak

EDUCATION

Ph.D., Chemical Engineering, METU, (2002-2007)

B.Sc., Chemical Engineering, METU, (1997-2002)

High School, Adana Borsa High School, (1994-1997)

PROFESSIONAL EXPERIENCE

Research & Teaching Assistant

Chemical Engineering, METU [September 2002 - To date]

INTEREST AREAS

- Reaction Engineering
- Thin Film Synthesis and Characterization
- Advanced materials

ACADEMIC EXPERIENCES

- Assistantship to some undergraduate courses namely, Heat and Mass Transfer Operations, Fluid Mechanics, Thermodynamics, Chemical Engineering Laboratory, Introduction to Computers and FORTRAN Programming, and assistantship to a graduate course namely, Transport Phenomena
- Attended to ‘Defence Technologies Congress’ in Ankara, Turkey on June 2004
- Attended to ‘6th National Meeting of Chemical Engineering’ in İzmir, Turkey on Sep 2004
- Attended to ‘1st National Workshop on Boron’ in Ankara, Turkey on April 2005
- Attended to ‘2005 Materials Research Society Fall Meeting’ in Boston, USA on November 2005
- Visiting Studentship in Massachusetts Institute of Technology, Boston, USA between March, 2006 and April, 2005.
- Attended to ‘Sommer Symposium Series 1’ in Ankara, Turkey on May 2007

PUBLICATIONS

1. Karaman M., Özbelge H.Ö., Sezgi N.A., Doğu T., ‘Kimyasal Buhar Biriktirme Yöntemi İle Bor Karbür Üretimi’, 1. Ulusal Bor Çalıştayı Bildiriler Kitabı, 28-29 Nisan 2005, Ankara
2. Karaman M., Özbelge H.Ö., Sezgi N.A., Doğu T., ‘Mechanism And Characterization Studies on Boron Carbides Deposited by Chemical Vapor Deposition Technique’, Proceedings of Materials for

Direct Thermal to Electric Energy Conversion, MRS (Materials Research Society) Fall Meeting 2005, Boston USA Karaman M., Özbelge H.Ö, Sezgi N.A., Doğu T., ‘Kinetic Investigation of Chemical Vapor Deposition of B₄C on Tungsten Substrate’, AICHE Journal, 52, 12, 4161-4166, 2006.

3. Karaman M., Özbelge H.Ö, Sezgi N.A., Doğu T., ‘Mechanism studies on CVD of boron carbide from a gas mixture of BCl₃, CH₄ and H₂ in a dual impinging jet reactor’, Chemical Engineering Science, under review.

RESEARCH PROJECTS

1. H.Önder Özbelge and Mustafa Karaman ‘Chemical Vapor Deposition of Boron Carbide’, Project code: Misag-217, TUBITAK (The Scientific and Technological Council of Turkey), Ankara, 2002-2006.

2. H.Önder Özbelge and Mustafa Karaman ‘Kinetic Studies on CVD of Boron Carbides’, Project code: BAP-08-DPT2002K120510-İM-5, DPT (State Planning Organization of Turkey), Ankara, 2002-2007.

COMPUTER RELATED SKILLS

Programming Languages: FORTRAN 77/90

Operating Systems: Windows 9X/2000/XP

Commercial and Research Software Packages: Visio, SigmaStat, Statistica, Mathcad, Chemcad, Mathematica, Microsoft Office (Word, Excel, PowerPoint, Frontpage)